Actuation Efficiency and Work Flow in piezoelectrically Driven Linear and Non-linear Systems

by

Yong Shi

B. Eng., National University of Defense Technology, P. R. China (1985)

Submitted to the Department of Aeronautics and Astronautics
in partial fulfillment of the requirements for the degree of

Master of Science

at the

MASSACHUSETTS INSTITUTE OF TECHNOLOGY

June 2001

© Massachusetts Institute of Technology 2001. All rights reserved.

The author hereby grants to MASSACHUSETTS INSTITUTE OF TECHNOLOGY
permission to reproduce and
to distribute copies of this thesis document in whole or in part.
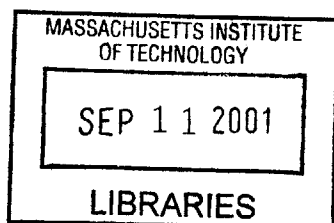
Signature of Author . . . .

Department of Aeronautics and Astronautics
2 May 2001

Certified by . . . .

Nesbitt W. Hagood, IV
Associate Professor, Thesis Supervisor
Thesis Supervisor

Accepted by . . . .

Wallace E. Vander Velde
Professor of Aeronautics and Astronautics
Chair, Committee on Graduate Students

AERO

Actuation Efficiency and Work Flow in piezoelectrically Driven Linear and Non-linear Systems

by

Yong Shi

Submitted to the Department of Aeronautics and Astronautics
on 2 May 2001, in partial fulfillment of the
requirements for the degree of
Master of Science

Abstract

It is generally believed that the maximum actuation efficiency of piezoelectrically driven systems is a quarter of the material coupling coefficient squared. This maximum value is reached when the stiffness ratio of structure and piezo stack equals to one. However, previous study indicts that load coupling has significant influence on the work flow and actuation efficiency in the systems. Theoretical coupled analysis of such systems has shown that the actuation efficiency is the highest at the stiffness ratio larger than one and this maximum value is much higher than that predicted by the uncoupled analysis when coupling coefficient is relatively high. Moreover, for non-linear systems, the actuation efficiency can be twice as high as that of linear systems. The objectives of this research is to verify the theoretical coupled analysis experimentally and explore the possibility for the mechanical work to be done into the environment. To do this, a testing facility has been designed and built with programmable impedances and closed loop test capability. However, the feedback control method is not fast enough in determining the voltage for the driving stack which has limited the test frequency. Meanwhile, the original mechanical design can not guarantee the accurate measurement of mechanical work. Renovation on the existing tester has been made and feed forward open loop test methodology has been used utilizing a Force-Voltage model developed from Ritz Formulation. Linear test results correlate very well with the theoretical prediction. Two non-linear functions have been chosen for non-linear tests. The results have shown that the actuation efficiency of non-linear systems is much higher than that of linear systems. The actuation efficiency of system simulated by non-linear function 1 is about 200% that of linear systems and the work output of this system is about 254% that of the linear systems. These test results exactly proved out the theoretical prediction of non-linear loading systems. The capability of modeling and testing of non-conservative thermodynamic cycles have also been demonstrated which make it possible to take advantage of the mechanical work out of the systems.

Thesis Supervisor: Nesbitt W. Hagood, IV
Title: Associate Professor, Thesis Supervisor

Acknowledgements

It is with heartfelt gratitude that I dedicate this thesis to all those who have played a role in the successful completion of my research. I would like to thank Ching-Yu Lin, David Roberson, Mauro Atlalla, Chris Dunn, Viresh Wickramasinghe, Timothy Glenn as well as all my lab-mates and roommates who are always ready to help me in every expect from the tester design, test setup, data acquisition and handling, signal analysis and the using of different equipment or instrument and software in the lab, just to mention a few. Their sincere helps make my research a lot easier and my working at AMSL a wonderful memory.

I am also very grateful to my Chinese friends here and I would also like to thank my family—my parents, my wife, my brother and sisters. I am very grateful to my parents who love me and worry about me all the time. My special thanks go to my wife Zhihong. It is her love which actually makes all this becoming true. I still remember all the sufferings in the past two years, the pain from legs and the pain from research. She is always standing by my side taking care of me and encouraging me. There is no word which could express my love and thanks to her. I would also like to dedicate this thesis to my son-Caleb who will come to this word very soon.

Nomenclature

α	Stiffness ratio, load stiffness divided by material stiffnes
A	Cross-sectional area of the material
A_{p1}	Cross-sectional area of the piezoelectric material, or the sample stack
A_{p2}	Cross-sectional area of the driving stack
A_s	Cross-sectional area of the structure
C_{p1}^S	Capacitance of the system under constant strain
c_{33}^E	Young's modulus of the active material in the "three-three" direction under constant electric field
c_0	Linear part of the Young's modulus of non-linear loads
c_s	Young's modulus of the structure
c_x	Non-linear part of the Young's modulus of non-linear loads
δ	Variation operator
d	Derivative operator
D_3	Electric displacement in the active material in the "three" direction
d_{33}	Electromechanical coupling term of the active material in the "three-three" direction
ε_0	Dielectric constant of free space
ε_{33}^S	Dielectric constant of the active material in the "three-three" direction under constant strain
ε_{33}^T	Dielectric constant of the active material in the "three-three" direction under constant stress

E_3	Electric field in the active material in the "three" direction
e_t	Electromechanical coupling of active materials
e_{33}	Electromechanical coupling of active materials in the "three-three" direction
f_1	Generalized force vector of the active material of the sample stack
f_2	Generalized force vector of the driving stack
F_{bl}	Blocked the force of the active material
F_{linear}	Blocked the force of the active material
F_{linear}	Linear Load
$F_{non-linear1}$	Non-linear load 1
$F_{non-linear2}$	Non-linear load 2
f_s	Generalized force vector of the structure
K_{p1}^E	Stiffness of the active material under constant electric field
k_s	Stiffness of the structure
k_{33}	Material coupling coefficient of the active material
l	Length of material or structure
l_{p1}	Length of active material
l_s	Length of structure
η	Actuation efficiency of systems
$\eta_{\max}$	Maximum actuation efficiency of systems
N	Number of layers in piezoelectric stack
θ_1	Electromechanical coupling of the active material
θ_2	Electromechanical coupling of the driving stack
Q_1	Charge vector of the active material
Q_2	Charge vector of the driving stack
S_3	Strain in "three" direction of the active material
s_{33}^E	Elastic constant of the active material in the "three-three" direction under constant electric field

s_{33}^D	Elastic constant of the active material in the "three-three" direction at open circuit
T_3	Elastic constant of the active material in the "three-three" direction at open circuit
t_l	Thickness of the stack layers
V_0	Initial voltage to the sample stack
V_1	Voltage applied to the active material or the sample stack during testing
V_2	Voltage applied to the driving stack
V_f	Final voltage to the sample stack
V_{max}	Maximum voltage applied during tests
V_{p1}	Volume of the active material or the sample stack
W_E	Electric Work
W_M	Mechanical work
W_{in}	Work into the system
W_{out}	Work out of the system
x_0	Initial displacement
x	Displacement of the system
x_1	Displacement of the active materials
x_2	Displacement of the driving stack
x_{free} or x_f	Free displacement of the system
Ψ_E	Electric mode shape
Ψ_M	Mechanical mode shape

Contents

List of Figures

13

List of Tables

Chapter 1

Introduction

1.1 Motivation

Recently piezoelectric actuators have been extensively used for different applications, such as, precise positioning[Karl, 2000] and [Roberts, 1999], vibration suppression[Hagood, 1991] and [Binghamand, 1999], and ultrasonic motors [Bar-Cohen, 1999] and [Frank, 1999, spie]. Moreover, their special characteristics have also made them popular in micro-systems as well as in optical device applications [Varadan, 2000, spie]. However, to use these actuators efficiently, it is necessary to evaluate and understand the material response, energy flow and actuation efficiency in the system at working conditions.

Piezoelectric materials have been initially developed for sensors applications initially which focus on low power properties. For example, the linear material model is valid for low electric field. These properties are not appropriate for the applications of actuators which are used at high frequency, high electric field, and high mechanical loads. Furthermore, standard assumptions about the efficiency of piezoelectrically driven systems neglect the electromechanical coupling in the system. These pending problems also necessitate the study of work flow and actuation efficiency in such systems.

1.2 Objective

The objective of this research is to closely examine the work input, work output and actuation efficiency in a fully coupled system. Different expressions such as material coupling coefficient, device coupling coefficient, and efficiency of coupling elements have been used traditionally to describe the systems. Actuation efficiency, which is a thermodynamic efficiency expression defined by the ratio of mechanical work out and electrical work in, may best describe coupled systems.

Previous theoretical analysis [Malinda1, 1999] has shown that the actuation efficiency of one dimensional linear systems reaches the highest when the stiffness ratio of the structure and the active material is larger than one. This peak value of actuation efficiency is much higher than the prediction of the coupling element efficiency of Hall [Hall, 1996]when the coupling coefficient is relatively high. However, for active materials working against non-linear loads, it is possible to significantly increase the actuation efficiency in the systems. So another objective of this research is to validate the theoretical derivation and verify the analysis results experimentally, then to explore the possibility for the mechanical work out of the system to be done to the environment.

1.3 Previous Work

1.3.1 Material Coupling Coefficient.

Much work has been done in the area of material characterization of actuators and the efficiency analysis of the systems. However, people tend to use different expressions to describe and compare the efficiency of systems according to their specific application and interests. Material coupling coefficient has long been regarded as a measure of the capability of active materials transduce mechanical work to electrical work and vice versa. Material coupling coefficient k_{33} is defined as [IEEE,1978]

$$k_{33}^2 = \frac{W_{out}}{W_{in}} = \frac{d_{33}^2}{s_{33}^E \varepsilon_{33}^T} \tag{1.1}$$

However, material coupling coefficient only describes the interaction of the mechanical and electrical states in the active materials itself. The conditions under which the material cou-

pling coefficient is derived are idealized work conditions. The interaction or coupling between the active materials and the structures, which are driven by the interrelation of force and displacement as well as that of charge and voltage, have all been neglected. Materials coupling coefficient itself is not an accurate measure of actuation efficiency of systems.

1.3.2 Berlincount's Work

Berlincourt [Berlincount, 1971] found out that boundary conditions, times and orders at which mechanical load and electrical load were applied could also change the efficiency of the systems. He defined an effective coupling factor after he studied the differences in efficiency of a few different cycles. By using these different loading cycles, he changed the amount of energy extracted from the systems. For example, he claimed that one of the loading cycles increased the effective coupling factor of PZT-4 to 0.81 while the material coupling coefficient of this material is only 0.70. He also showed the influence of boundary conditions on efficiency. The effective coupling factor of a thin disk with clamped edges was increased to 0.68 compared to the material coupling coefficient of 0.50. He then examined the efficiency of the systems under ideal linear or non-linear loads assuming one-time energy conversion, which was associated with polarization or depolarization of active materials. The mechanical work of the systems using such non-linear loads doubled that using linear loads. However, the effective coupling factor Berlincourt defined still focused on the information obtained from the material coupling coefficient, and it did not include the information of the structures that the active materials worked against. The study of the one-time conversion process considered the dependence on the structures which the active materials worked against, but the complete depolarization of the active materials assumed made it difficult to apply this theory to real cyclic operation.

1.3.3 Lesieutre and Davis' Work

Lesieutre and Davis [Lesieutre, 1997]defined a device coupling coefficient when they studied the changes of material coupling coefficient of a bender device, which composed of two piezoelectric wafers bonded to a substrate with a destabilizing preload on both ends. They still used the same work cycle as used by the material coupling coefficient. By means of simplifying the Rayleigh-Ritz formulation presented by Hagood, Chung and Von Flotow[Hagood, 1990], they

destabilized the matrix relation to describe the system. Then, they assumed the proper mechanical and electrical mode shapes and found out the corresponding stiffness, capacitance and electromechanical coupling of the bender without preload. They also discussed the influence of the axial preload on the stiffness of the bender. Finally, they defined the apparent actuation efficiency and proper actuation efficiency. The apparent actuation efficiency did not include the work done by preload, while the proper actuation efficiency included it. They claimed that the work by preload could not be considered a steady-state source of energy in the system, so the proper actuation efficiency expression was correct. Although the device coupling coefficient still looked at the energy conversion of the active materials, it included the effect of the external load. It described the actuation efficiency of a special coupled systems with distributed elements and could hardly be applied to general cases.

1.3.4 Spangler and Hall's Work

When studying the discrete actuation systems for helicopter rotor control, Spangler and Hall and later Hall and Prechtl [Hall, 1996] defined an impedance matched efficiency expression. This expression came from the mathematical study of the linear material load line and linear structure load line on a stress-strain diagram. The intersection of the two lines was the stress-strain state for a specific load or electric field condition. The area under the material load line represented the maximum energy for mechanical work in the active materials, while the area under the structure load line represented the total strain energy in the structure. They found out that at most one quarter of the actuation stain energy could be usefully applied to actuating a control surface.

$$\eta_{\max} = \frac{W_{M\max}}{W_{Esystem}} = \frac{1}{4}\frac{W_{Msystem}}{W_{Esystem}} = \frac{1}{4}k_{33}^2 \tag{1.2}$$

This mathematical optimum occurred at the impedance matched conditions when the stiffness ratio of the structure and the actuator is one. This impedance matched efficiency served well in their research, however, they did not take into account the effect of the load, which the systems worked against, had on the Electrical work into the systems. Therefore, this efficiency expression is still not a true thermodynamic actuation efficiency for the systems studied.

1.3.5 Giurgiutiu's Work

Giurgiutiu et al [Giurgiutiu, 1997] studied this effect in 1994. They assumed active materials such as piezo actuators behaved like electrical capacitors. Under non-load conditions, the electrical work stored was

$$E^*_{elec} = \frac{1}{2}CV^2 \tag{1.3}$$

This is actually the W_{in} in 1.1. However, when external load was applied onto the active materials, the electrical energy stored inside changed. Giurgiutiu et al modulated their capacitances under external load by the stiffness ration of structures and the active materials. They found the resulting electrical work to be

$$E_{elec} = (1 - k^2\frac{r}{1+r}) * (\frac{1}{2}CV^2) = (1 - k^2\frac{r}{1+r})E^*_{elec} \tag{1.4}$$

Where r is the stiffness ratio of structures and active materials. In 1997, Giurgiutiu et al tried to find the actuation efficiency of a system where a PZT actuator operating against a mechanical load under static and dynamic conditions. For the static case, they found the mechanical work out to be

$$E_{out} = \frac{r}{(1+r)^2}E^*_{mech} \tag{1.5}$$

Where E^*_{mech} is actually the ideal work out resulting from electromechanical conversion, i.e. the W_{out} in 1.1. They also found mathematically that E_{out} had a maximum value at $r = 1$.

$$E_{out-max} = \frac{1}{4}E^*_{mech} \tag{1.6}$$

When finding the actuation efficiency of the systems, instead of using the ratio of 1.5 to 1.4, they used the ratio of 1.6 to 1.4 which resulted in

$$\eta = \frac{1}{4}\frac{k^2}{1 - k^2\frac{r}{r+1}} \tag{1.7}$$

Where k^2 is actually $k^2_{33} = \frac{W_{out}}{W_{in}}$ in 1.1. This expression actually has an implied condition which is $r = 1$, so it is not the correct expression. However, they seemed to have used the correct expression to find the maximum value for the actuation efficiency of the system. Actually this

has been verified mathematically. Giurgiutiu et al also extended their work to dynamic analysis for a similar case, but they did not experimentally verify their analytical results for both static and dynamic cases.

1.3.6 C. L. Davis' Work

Davis et al [Davis, 1999] used a different approach than that used by Giurgiutiu to estimate the actuation efficiency of structurally integrated active materials. They converted the one dimensional linear constitutive equation of piezo element into a set of two equations in the frequency domain. Then, they found the complex electrical power consumed by the piezo element and the mechanical power delivered to the mechanical load. They defined their actuation efficiency of the system as the ratio of this mechanical energy to this electrical energy. Their expression was in the frequency domain expressed as

$$\eta = k^2 \frac{\alpha}{(1+\alpha) * [1 + (1 - k^2) * \alpha]} \tag{1.8}$$

Where α here is the ratio of the mechanical load impedance to the effective mechanical impedance of the piezo element. In a static one-dimensional case, α is actually r as defined in 1.4, and k is actually k_{33} as in 1.1. After a simple algebraic operation, we can rewrite equation 1.8 as:

$$\eta = \frac{\frac{\alpha}{(1+\alpha)^2} k^2}{1 - k^2 \frac{\alpha}{1+\alpha}} \tag{1.9}$$

Actuation efficiency expressed by Equation 1.9 is exactly the same as the expression of Giurgiutiu if we use the ratio of 1.5 to 1.4 in their study. Davis et al also extended their work into dynamic analysis, however, like Giurgiutiu et al, they did not experimentally verify their work either.

1.3.7 M. Mitrovic's Work

M. Mitrovic et al [Mitrovic, 1999] conducted a series of experiments to understand the behavior of piezoelectric materials under electrical, mechanical, and combined electromechanical loading conditions. They evaluated parameters such as strain output, permittivity, mechanical stiffness, energy density and material coupling coefficient as a function of mechanical preload and

electrical field applied. Unlike the work discussed above, their work was mainly experimental. They tested five different commercially available piezoelectric stack actuators and found the stiffness dependence on preload and applied electrical field. They also found out that piezo-electric coefficients and the energy density delivered by the actuator initially increased when mechanical preload was applied, however, higher preload had the adverse effect on the stacks' response. The tests were conducted on a 22 kip Instron 8516 servo-hydraulic test frame. The mechanical loading frequency was from 0.1 Hz to 40 Hz, while the electrical load frequency was only 0.1 Hz and 1 Hz. Although they tried to determine the optimum conditions under which the piezo actuators could be operated and did found some interesting results in mechanical power delivered from the actuators and electrical power delivered to the actuators, they did not discuss the actuation efficiency of the systems as a whole. In addition, they did not theoretically analyze the systems and did not make any prediction as explanations for the test results.

1.3.8   Lutz and Hagood's Work

Lutz and Hagood [Malinda, 1999] studied the actuation efficiency and work flow both analytically and experimentally. They were also able to extend their work for the systems where piezo actuators working against not only linear loads but also non-linear loads. They used a different approach than those used by Giurgiutiu or Davis and studied this problem almost at the same time. The method they utilized was the Rayleigh-Ritz formulation presented by Hagood, Chung and Von Flotow[Hagood, 1990], simplified for quasi-static analysis. They found out that load coupling had significant influence on the work flow and actuation efficiency of the systems. For linear loading systems, their analysis has shown that the actuation efficiency is the highest when the stiffness ratio is larger than one. This maximum value is much higher than that predicted by the uncoupled analysis when the material coupling coefficient is relatively high, while for non-linear loading systems, actuation efficiency can be twice as high as that of the linear systems. The analytical results for linear systems actually agree very well with those found by Giurgiutiu [Giurgiutiu, 1997] and Davis [Davis, 1999]. The equation for linear systems in [Malinda, 1999] has typos. To verify the analytical results, a testing facility was designed and built to measure the actual work input, work output, and actuation efficiency of a discrete actuator working against both linear and non-linear loads. The testing facility was

designed for load application with programmable impedances and closed loop testing capability at frequency up to 1 kHz compared to the maximum testing frequency of 40 Hz for an Instron testing machine. However, due to some mechanical and control problems, it was difficult to measure mechanical and electrical work accurately. Not much valid experimental data was obtained, and further exploration was needed.

1.4 Approach

The work discussed in this thesis is a follow-up of Malinda and Hagood's work. For the purpose of mathematically verifying the theories derived by them and also for the completeness of this document, the expressions for work input, work output and actuation efficiency will be derived again using the Rayleigh-Ritz formulation presented by Hagood, Chung and Von Flotow [Hagood, 1990] at the beginning, and will be compared to those derived previously. General expressions will be derived first in terms of the actuating voltage of the piezo actuators and then applied to the chosen linear and non-linear cases. Due to the difficulty in finding the close form solution for the displacement of the actuators in terms of the applied voltage to them, expressions for the work and actuation efficiency in terms of displacement of the piezo actuators will also be derived. The results predicted by the theoretical analysis for linear and non-linear systems will be compared and contrasted.

Then, experimental data from previous work will be studied and summarized, so as to find out the remaining problems. Methods used to determine the material properties such as stiffness, capacitance, electromechanical and coupling terms as well as the methods for measuring mechanical work and electrical work will all be examined. Proper renovation and validation on the existing test facility will be made to guarantee accurate measurements. For the linear and non-linear actuation tests, the feed back control methodology will also be checked, and improvements will be made accordingly.

For the convenience of comparing with the test results obtained before, the same Sumitomo stack actuator, as used by Lutz, will still be used as the test sample. The experimental data from linear and non-linear tests will be compared with the theoretical prediction, and an expansion of this work to non-conservative systems will be discussed.

1.5 Organization of the Document

This document is organized in the same way as the problem is approached.

Chapter 2 presents the theoretical derivation of the mechanical work, electrical work, and actuation efficiency for linear and non-linear systems. It begins by defining work terms and actuation efficiency as well as the constitutive relation for piezo active materials, followed by the mathematical derivation using the Rayleigh-Ritz formulation mention above. Then it shows the application of the general expressions to both linear and non-linear cases in terms of either voltage to the active material or the displacement of it during the actuation tests. The analytical results for linear and non-linear systems are compared and discussed at the end.

Chapter 3 presents the redesign of the important mechanical part of the tester and the validation of the test methods. It summarizes the previous test results and some insights on the remaining problems first followed by discussing the test results from the laser vibrometer, which reveals the serious bending effect of the sample during tests. After that, possible improvements based on the tests and previous analysis has are discussed, and the new design of the load transfer device is exhibited too. Finally, it shows the validation test results made on the new test facility. These tests include calibration of force, displacement, stiffness, and capacitance measurement which guarantee the correct measurement of mechanical and electrical work.

Chapter 4 presents the test results and their correlation with theoretical prediction. It begins by discussing the problem of the former feed back control test methodology and presents the proposed feed forward method. Then, it displays the derived Voltage-Force model using the Rayleigh-Ritz formulation for the simulated actuator-structure-actuator system. Afterwards, linear test results are presented first and compared with the theoretical prediction and the data found in the literature. For the non-linear tests, the two non-linear functions chosen are analyzed and the driving voltage for the sample is determined, then the determination of voltage for the driving stack is shown using the established Voltage-Force model. The non-linear test results are compared with the theoretical prediction and linear test results.

Chapter 5 discusses the possibility for mechanical work to be done on the environment. The linear and non-linear tests discussed above are all for conservative systems. This chapter shows that the net work in these systems is zero. To take advantage of the mechanical work from the actuator, proper thermodynamic cycle should be chosen so that the net work in the system is

not zero. Possible thermodynamic cycles used in other applications is presented as a reference. The out of phase actuation of the driving stack and the sample stack at the same frequency is demonstrated to be such a thermodynamic cycle. The experimental results are also compared with the analytical results at the end.

Chapter 6 concludes the document and the research. It highlights the important test and analytical results in the research and their correlation with each other. The possibility for the mechanical work to be done on the environment is also emphasized. Then recommendations for future work in this area are presented, and recommendation are made to extand the application of piezo actuators and take further advantage of them.

Chapter 2

Analysis of the Work Flow and Actuation Efficiency of Electromechanically Coupled Systems

The system analyzed and the method used in this research are essentially the same as those used by Malinda and Hagood. The purpose to include this part of work is for the completeness of this document and a verification of the previous work. In addition, Malinda just found a close form solution for linear systems in terms of the applied voltage to the active materials, while for non-linear systems she had to rely on numerical results for work input and output. This is not convenient because the independent variable in her expression is voltage to the sample stack, however, there is no close form expression for the displacement of the active materials in terms of the applied voltage for non-linear cases, which can be seen from the compatibility equation derived later. To derive a close form expression, we should choose displacement of the active materials as the independent variable.

The system studied is a generalized system comprised of an electromechanically coupled core with a generalized energy input, working against a generalized load which has some defined linear or non-linear relation. The coupled core could be a variety of systems such
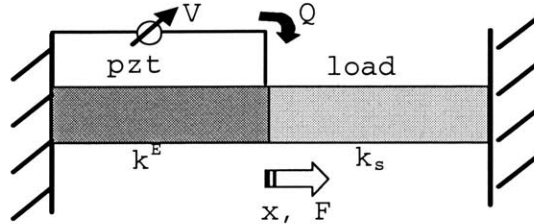
Figure 2-1: Piezoelectrically Driven One Dimensional Model

as a discrete actuator and the magnification mechanism, a mechanically coupled system or a hydraulic actuation system. The input into the system could be any generalized work pair like charge and voltage or current and voltage. The output of the system could be another work pair like displacement and force or strain and stress.

The generalized expression will be derived first, then applied to linear or non-linear cases for discrete piezo actuator systems. In order to compare and discuss different systems, it is necessary to define work input, work output and actuation efficiency in the beginning.

2.1   Definition of Work Terms

The system which will be studied has been shown in Figure 2-1. Work input is defined as the electrical work, while work output is defined as the mechanical work. The actuation efficiency is then a true thermodynamical efficiency defined as the ratio of mechanical work to electrical work. Each of the work terms is defined below.

2.1.1 Mechanical Work

The mechanical work of a system is described as the integral of force times the derivative of displacement:

$$W_M = \int_{x_0}^{x_f} F\,dx \tag{2.1}$$

Or it can be defined in terms of stress and strain as:

$$W_M = \int_{Vol} \int_s T\,ds \cdot dVol \tag{2.2}$$

2.1.2 Electrical Work

Electrical work of a system is defined in the same way as mechanical work is defined. It is the integral of voltage times the derivative of charge:

$$W_E = \int_{Q_0}^{Q_f} V\,dQ \tag{2.3}$$

Or it can be defined in terms of electrical field and electrical displacement as

$$W_E = \int_{Vol} \int_D E\,dD \cdot dVol \tag{2.4}$$

2.1.3 Actuation Efficiency

As being discussed in the previous chapter, the material coupling coefficient is not a good measure to describe the efficiency of a device or a system, while actuation efficiency is a viable metric. It is defined as the work out of the system divided by the work into the system when working over a typical operation cycle. As mentioned before, work input is defined as the electrical work, while work out is defined as the mechanical work. Therefore, actuation efficiency is expressed as

$$\eta = \frac{W_{out}}{W_{in}} = \frac{W_M}{W_E} \tag{2.5}$$
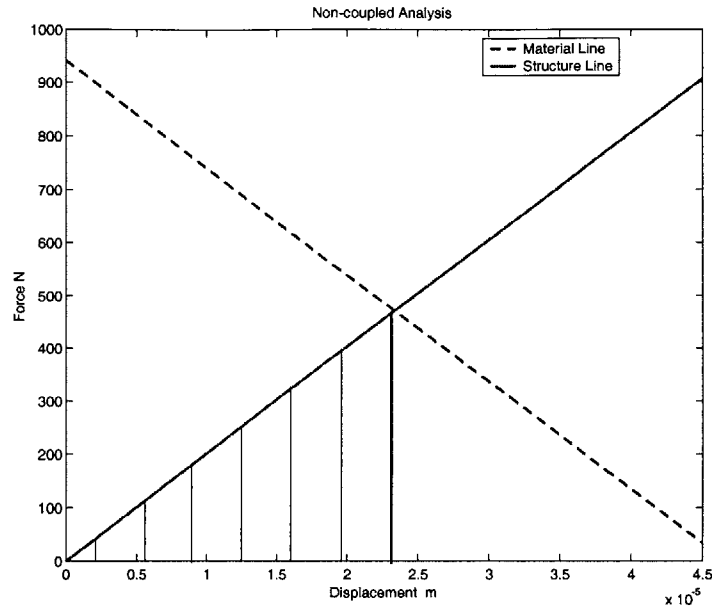
Figure 2-2: Material and Structure Loading Line for the Linear Systems

2.2 Linear and Non-linear Systems

The motivation for looking into non-linear systems comes from the diagram showing the intersection of a material load line and a structure load line on a force-displacement diagram, shown in figure 2-2.

The area under the structure load line from the origin to the intersection is the actual mechanical work of the system. The area under the material load line is the total amount of energy available to do mechanical work. So if a structure load line, such as a curve, can encompass more area under the material load line before it intersect with the structure load line, it is possible that more mechanical work can be done on the structure. Thus, the actuation efficiency of the system will be increased. Such curves do exist and we can call them non-linear loading functions, while the corresponding systems called non-linear systems. Two sample non-linear loading functions are shown in Fig. 2-3. They are essentially the same functions defined by Malinda for the purpose of comparison and discussion.

Linear loading function:

$$\frac{F_{linear}}{F_{bl}} = \frac{x}{x_{free}} \tag{2.6}$$

29
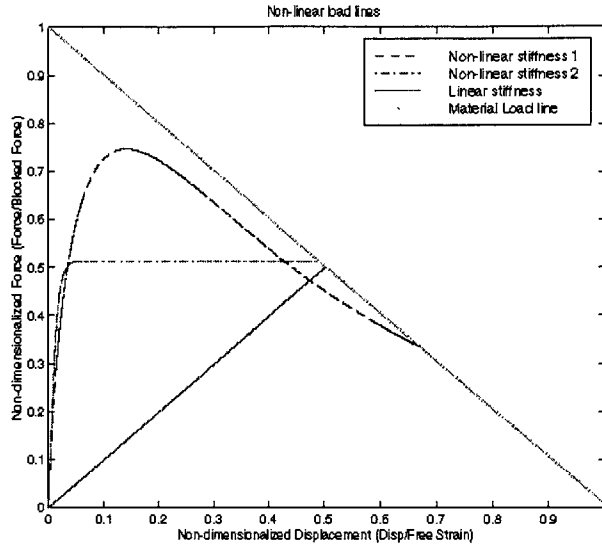
Figure 2-3: Comparison of Linear and Non-linear Functions

Non-linear loading function 1:

$$\frac{F_{non-linear1}}{F_{bl}} = \frac{x}{x_{free}} \left(41 \exp^{-5.45\left(\frac{x}{x_{free}}\right)^{\frac{1}{2}}} \right) \tag{2.7}$$

Non-linear loading function 2:

$$\frac{F_{non-linear2}}{F_{bl}} = \frac{1}{2} \left(\tanh \left(66\frac{x}{x_{free}} \right) \right) \tag{2.8}$$

2.3 General Analysis

The object we are going to study here is a piezo actuator. The linear constitutive equations of the piezoelectric are presented first, then the general actuator and sensor equations derived by Hagood et al [Hagood, 1990] are introduced. The work terms are derived using the actuator and sensor equations and then applied to one dimensional linear and non-linear cases.

30

2.3.1 Linear Constitutive Equations

For small stresses and electric fields, piezoelectric materials follow a linear set of governing equations which describe the electrical and mechanical interaction of the materials. The equation can be expressed as

$$\left\{ \begin{array}{c} S \\ D \end{array} \right\} = \left[\begin{array}{cc} s^D & d_t \\ d & \varepsilon^T \end{array} \right] \left\{ \begin{array}{c} T \\ E \end{array} \right\} \tag{2.9}$$

These equations have four system states: T, the stress in six directions; E, the electric field in three directions; S, the strain in six directions; D, the electric displacement in three directions. The materials constitutive relation is a nine by nine matrix. This matrix can be reduced using either plain stress, plain strain assumptions, or by assuming one dimensional relations. Most of the work in this document will be using one dimensional relations, which is a two by two matrix.

2.3.2 Governing Equations for the coupled systems

The governing equations for the piezo active materials are the simplified actuator equation and sensor equation for quasi-static cases, which can be expressed as [Hagood, 1990]

$$\left[\begin{array}{cc} K_{p1}^E & -\theta_1 \\ \theta_1 & C_{p1}^S \end{array} \right] \left\{ \begin{array}{c} x_1 \\ V_1 \end{array} \right\} = \left\{ \begin{array}{c} f_1 \\ Q_1 \end{array} \right\} \tag{2.10}$$

Where K_{p1}^E is the stiffness matrix for the active materials; θ_1 is the electromechanical coupling terms; C_{p1}^S is the capacitance of the active materials under constant strain and x_1, V_1, f_1 and Q_1 are the displacement, voltage, force and charge vector respectively. Dynamic terms are neglected since the tests were done quasistatically.

For the non-piezoelectric structure, force-displacement relation can be written as:

$$f_s = k_s x_s \tag{2.11}$$

Where k_s is the stiffness of the structure and can be either linear or non-linear with respect to x_s, the displacement of the structure.

31

2.3.3 Compatibility and Equilibrium

The states of the structure and active material are related by compatibility and equilibrium requirements.

Force equilibrium:

$$f_1 = f_s \tag{2.12}$$

Compatibility:

$$x_1 = -x_s = x \tag{2.13}$$

From equation 2.10 we have

$$K_{p1}^E x_1 - \theta_1 V_1 = f_1 \tag{2.14}$$

Substitute equation 2.12 and equation 4.21, we have

$$x = \frac{\theta_1 V_1}{k_s + K_{p1}^E} \tag{2.15}$$

This is an implicit relationship between V_1 and x. which is automatically satisfied during the test. Therefore, this equation can be used to determine displacement of the active material when a voltage is applied or for an expected displacement, the required voltage can be determined by solving this equation iteratively.

2.3.4 Electrical Work

Electrical work is defined in equation 2.3.

From equation 2.10:

$$Q_1 = \theta_1^T x + C_{p1}^S V_1 \tag{2.16}$$

Substitute equation 2.15 into 4.18, we have

$$Q_1 = \theta_1^T \frac{\theta_1 V_1}{k_s + K_{p1}^E} + C_{p1}^S V_1 = \left(\frac{\theta_1^T \theta_1}{k_s + K_{p1}^E} + C_{p1}^S \right) V_1 \tag{2.17}$$

Then the variation of Q_1 in terms of V_1 can be expressed as

$$\delta Q_1 = \left[\frac{\theta_1^T \theta_1}{k_s + K_{p1}^E} + C_{p1}^S - \frac{\theta_1^T \theta_1 V_1}{(k_s + K_{p1}^E)^2} \frac{dk_s}{dx} \frac{dx}{dV_1} \right] \delta V_1 \tag{2.18}$$

Substitute equation 2.18 into equation 2.3, we have the electrical work expressed as

$$W_E = \int_{V_0}^{V_f} \left[\frac{\theta_1^T \theta_1 V_1}{k_s + K_{p1}^E} + C_{p1}^S V_1 - \frac{\theta_1^T \theta_1 V_1^2}{(k_s + K_{p1}^E)^2} \frac{dk_s}{dx} \frac{dx}{dV_1} \right] \delta V_1 \tag{2.19}$$

2.3.5 Mechanical Work

Mechanical work is defined in equation 2.1, where

$$F = k_s x \tag{2.20}$$

Finding the variation of x using equation 2.15, we have

$$\delta x = \left[\frac{\theta_1}{k_s + K_{p1}^E} - \frac{\theta_1 V_1}{(k_s + K_{p1}^E)^2} \frac{dk_s}{dx} \frac{dx}{dV_1} \right] \delta V_1 \tag{2.21}$$

Substitute equation 2.20 and equation 2.21 into 2.1, we will have the mechanical work expressed as

$$W_M = \int_{V_0}^{V_f} \frac{k_s \theta_1^T \theta_1 V_1}{(k_s + K_{p1}^E)^2} \left[1 - \frac{V_1}{k_s + K_{p1}^E} \frac{dk_s}{dx} \frac{dx}{dV_1} \right] \delta V_1 \tag{2.22}$$

2.3.6 Actuation Efficiency

The actuation efficiency of the system is defined in equation 2.5, which is simply the ratio of equation 2.22 to equation 2.19.

2.4 One Dimensional Linear Systems

2.4.1 Expressions for Linear Systems

The systems discussed here has been shown in Fig. 2-1. For linear systems,

$$\frac{dk_s}{dx} = 0 \tag{2.23}$$

And assume $V_0 = 0$ and $V_f = V_1$, equation 2.19 and equation 2.22 can be simplified and expressed as

$$W_E = \frac{1}{2}V_1^2\left(\frac{\theta_1^T\theta_1}{k_s + K_{p1}^E} + C_{p1}^S\right) \tag{2.24}$$

$$W_M = \frac{1}{2}V_1^2\frac{k_s\theta_1^T\theta_1}{(k_s + C_{p1}^S)^2} \tag{2.25}$$

2.4.2 Constitutive Equations

The central axis of the actuator and structure is regarded as the 3-direction of the systems. Linear material relations is used and constitutive equations 2.9 is simplified for one dimensional cases. The one dimensional constitutive equations in 3-direction can be written as

$$\left\{\begin{array}{c} S_3 \\ D_3 \end{array}\right\} = \left[\begin{array}{cc} s_{33}^E & d_{33} \\ d_{33} & \varepsilon_{33}^T \end{array}\right]\left\{\begin{array}{c} T_3 \\ E_3 \end{array}\right\} \tag{2.26}$$

This equation can be rewritten to have strain as the free variable, then

$$\left\{\begin{array}{c} T_3 \\ D_3 \end{array}\right\} = \left[\begin{array}{cc} c_{33}^E & -e_{33} \\ e_{33} & \varepsilon_{33}^S \end{array}\right]\left\{\begin{array}{c} S_3 \\ E_3 \end{array}\right\} \tag{2.27}$$

From equation 2.26 and equation 2.27 we can find the following relations

$$c_{33}^E = \frac{1}{s_{33}^E} \tag{2.28}$$

$$e_{33} = d_{33}c_{33}^E \tag{2.29}$$

34

$$\varepsilon_{33}^S = \varepsilon_{33}^T - d_{33}^2 c_{33}^E \tag{2.30}$$

2.4.3   Finding the Constants in Work Expressions

To find the constants in the work expressions, i.e. equation 2.24 and equation 2.25, The Ritz method is used. Electrical and mechanical mode shapes , which satisfy the prescribed voltage boundary conditions and the geometric boundary conditions of this specific problem respectively are assumed as

$$\Psi_E = \frac{x}{l_{p1}} \tag{2.31}$$

$$\Psi_M = \frac{x}{l_{p1}} \tag{2.32}$$

The assumed mode shapes can be used to find C_{p1}^S, K_{p1}^E and θ_1 using the equation developed by Hagood et al [Hagood, 1990]

$$
\begin{aligned}
K_{p1}^E &= \int_{V_{p1}} N_x^T c^E N_x dV_{p1} \\
&= \int_{V_{p1}} \frac{1}{l_{p1}} c_{33}^E \frac{1}{l_{p1}} dV_{p1} \\
&= \frac{c_{33}^E A_{p1}}{l_{p1}}
\end{aligned}
\tag{2.33}
$$

$$
\begin{aligned}
\theta_1 &= \int_{V_{p1}} N_x^T e_t N_v dV_{p1} \\
&= \int_{V_{p1}} \frac{1}{l_{p1}} e_{33} \frac{1}{l_{p1}} dV_{p1} \\
&= \frac{e_{33} A_{p1}}{l_{p1}}
\end{aligned}
\tag{2.34}
$$

$$
\begin{aligned}
C_{p1}^S &= \int_{V_{p1}} N_v^T \varepsilon^S N_v dV_{p1} \\
&= \int_{V_{p1}} \frac{1}{l_{p1}} \varepsilon_{33}^S \frac{1}{l_{p1}} dV_{p1} \\
&= \frac{\varepsilon_{33}^S A_{p1}}{l_{p1}}
\end{aligned}
\tag{2.35}
$$

35

For a one dimensional linear structure, we have

$$k_s = \frac{A_s}{l_s} c_s \tag{2.36}$$

2.4.4 Simplified Expressions for Electrical and Mechanical Work

Assume that the structure and the piezoelectric have the same effective length and the same cross sectional area, then we have

$$A_s = A_{p1} = A \tag{2.37}$$

$$l_s = l_{p1} = l \tag{2.38}$$

Substitute equation 2.33, 2.34, 2.35, 2.36, 2.37 and 2.38 into equation 2.24 and 2.25, we will be able to find the simplified expressions for mechanical work , electric work and actuation efficiency.

Mechanical Work

$$W_M = \frac{1}{2} \frac{A}{l} V_1^2 \frac{c_s e_{33}^2}{(c_{33}^E + c_s)^2} \tag{2.39}$$

Electrical Work

$$W_E = \frac{1}{2} \frac{A}{l} V_1^2 \left(\varepsilon_{33}^S + \frac{e_{33}^2}{c_{33}^E + c_s} \right) \tag{2.40}$$

We can further simplify these two equations by taking advantage of the material coupling coefficient expressed as

$$k_{33}^2 = \frac{d_{33}^2}{s_{33}^E \varepsilon_{33}^T} \tag{2.41}$$

And the relation expressed in equations 2.28, 2.29 and 2.30. Then the mechanical work and electrical work will be

Mechanical Work

$$W_M = \frac{1}{2} \frac{A}{l} V_1^2 \varepsilon_{33}^T k_{33}^2 \frac{\alpha}{(1 + \alpha)^2} \tag{2.42}$$

36

Electrical Work

$$W_E = \frac{1}{2}\frac{A}{l}V_1^2\varepsilon_{33}^T\left(1 - \frac{\alpha}{1+\alpha}k_{33}^2\right)$$ (2.43)

Where

$$\alpha = \frac{c_s}{c_{33}^E} = \frac{k_s}{k_{p1}^E}$$ (2.44)

2.4.5 Actuation Efficiency

Actuation efficiency of the one dimensional linear system can be determined by equation 2.42 and 2.43, which is

$$\eta = \frac{W_{out}}{W_{in}} = \frac{k_{33}^2\frac{\alpha}{(1+\alpha)^2}}{1 - \frac{\alpha}{1+\alpha}k_{33}^2}$$ (2.45)

This expression is exactly the same as which derived by Giurgiutiu [Giurgiutiu, 1997] and Davis [Davis, 1999] respectively, but we use a different approach here.

It can be shown mathematically that equation 2.45 has a peak at

$$\alpha = \frac{1}{\sqrt{1 - k_{33}^2}}$$ (2.46)

And the maximum value is

$$\eta_{\max} = \frac{k_{33}^2}{\left(1 + \sqrt{1 - k_{33}^2}\right)^2}$$ (2.47)

2.4.6 Discussion on Actuation Efficiency

To better understand the expression we have derived here, actuation efficiency is plotted in Fig. 2-4 with the impedance matched system efficiency by Hall and Prechtl, equation 1.2, for comparison.

This figure shows that when material coupling coefficient is small, the actuation efficiency correlates the impedance matched systems efficiency. However, when material coupling coefficient is significantly large, there is a big difference between the two due to higher electromechanical coupling. In addition, the peak value of the actuation efficiency occurs at a stiffness ratio larger than one, while the impedance matched system efficiency always occurs at the impedance matched condition.

Actuation Efficiency from coupled and uncoupled Analysis for linear systems
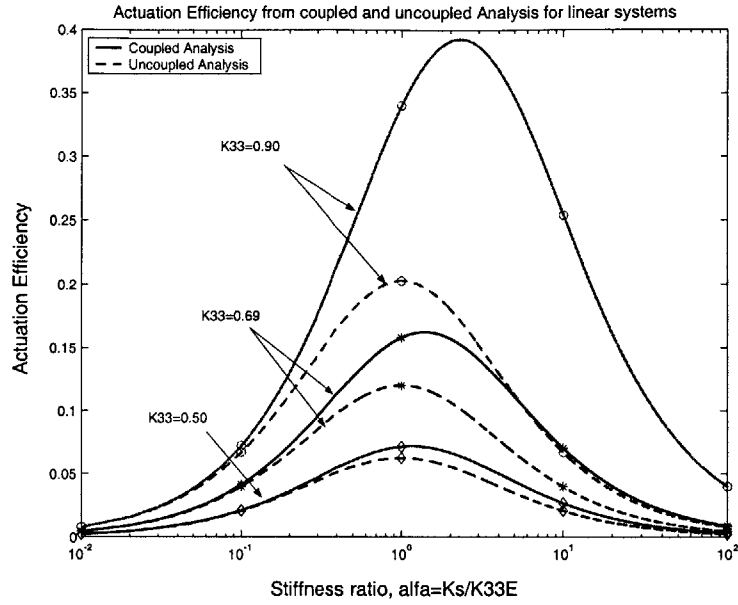
Figure 2-4: Comparison of Actuation Efficiency of Linear Systems with Different k_{33}

The relations of peak actuation efficiency and the corresponding stiffness ratio with the material coupling coefficient is illustrated in Fig.2-5.

2.5 One dimensional Non-linear Systems

2.5.1 General Analysis

In genaral, we can not find a close form solution for mechanical work and electrical work in terms of V_1, the applied voltage to test sample. For the convenience of analysis, we can use equation 2.20 and equation 2.36 to rewrite the non-linear functions, equation 2.7 and 2.8, in the following form:

$$f_s = k_s x = \frac{c_0 c_x A_s}{l_s} x \qquad (2.48)$$

Where c_0 is a constant independent of x, and c_x is the non-linear part of the stiffness.

For nonlinear function 1:

$$c_x = 41 \exp^{-5.45 \left(\frac{x}{x_{free}} \right)^{\frac{1}{2}}} \qquad (2.49)$$

38
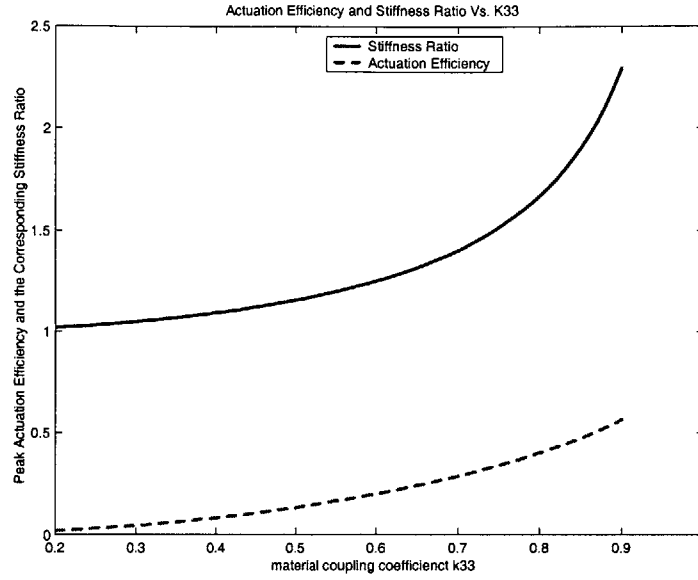
Figure 2-5: Max. Actuation Efficiency vs. k_{33} for 1D Linear Systems

For non-linear function 2:

$$c_x = \frac{1}{2x}\left(\tanh\left(66\frac{x}{x_{free}}\right)\right) \tag{2.50}$$

If we substitute equation 2.49, into equation 2.15, for example, we will have

$$x = \frac{\theta_1 V_1}{\frac{c_0 A_s}{l_s} 41 \exp^{-5.45\left(\frac{x}{x_{free}}\right)^{\frac{1}{2}}} + K_{p1}^E} \tag{2.51}$$

It is obvious that there is no close form solution for x in terms of V_1. Therefore, we can not find close form solutions for mechanical work and electrical work for such non-linear systems by simply substituting equation 2.51 in to equation 2.19 and equation 2.22. To find a close form solution, we need to express mechanical and electrical work in terms of the displacement of the active materials.

2.5.2 Mechanical and electrical Work in terms of Displacement

Electrical and mechanical work is still the same as defined in equation 2.3 and equation 2.1.

39

Mechanical work

$$W_M = \int_{x_0}^{x_f} k_s x dx \qquad (2.52)$$

Electrical work

$$W_E = \int_{Q_0}^{Q_f} V_1 dQ_1 \qquad (2.53)$$

From equation 2.15, we have

$$V_1 = \frac{k_s + K_{p1}^E}{\theta_1} x \qquad (2.54)$$

Substitute equation 2.54 into 4.18, we have

$$Q_1 = \theta_1^T x + C_{p1}^S \frac{k_s + K_{p1}^E}{\theta_1} x \qquad (2.55)$$

Then the variation of Q_1 in terms of x can be expressed as

$$dQ_1 = \left[\theta_1^T + \frac{C_{p1}^S}{\theta_1} \left(k_s + K_{p1}^E \right) + \frac{C_{p1}^S}{\theta_1} \frac{dk_s}{dx} x \right] dx \qquad (2.56)$$

Substitute equation 2.54 and equation 2.56 into equation 2.53, we have

$$W_E = \int_{x_0}^{x_f} \frac{k_s + K_{p1}^E}{\theta_1} x \cdot \left[\theta_1^T + \frac{C_{p1}^S}{\theta_1} \left(k_s + K_{p1}^E \right) + \frac{C_{p1}^S}{\theta_1} \frac{dk_s}{dx} x \right] dx \qquad (2.57)$$

2.5.3   Simplified Expressions for Mechanical and Electrical Work

As we have done for linear systems, we also need to assume mode shapes for the non-linear systems so as to find the material constants in equation 2.52 and equation 2.57. Here we assume the same electrical and mechanical mode shapes as in linear analysis. Therefore, we can simply substitute equation 2.33, 2.34, 2.35, 2.37, 2.38, and $k_s = \frac{c_0 c_x A_s}{l_s}$ from 2.48 into equation 2.52 and 2.57, and obtain

Mechanical work

$$W_M = \frac{c_{33}^E A}{l} \alpha \int_{x_0}^{x_f} c_x x dx \qquad (2.58)$$

40

Electrical work

$$W_E = \frac{c_{33}^E A}{l} \int_{x_0}^{x_f} (1 + \alpha c_x) x dx + \frac{(c_{33}^E)^2 A}{l} \frac{\varepsilon_{33}^S}{e_{33}^2} \int_{x_0}^{x_f} (1 + \alpha c_x)^2 x dx + \tag{2.59}$$

$$+ \frac{c_0 c_{33}^E A}{l} \frac{\varepsilon_{33}^S}{e_{33}^2} \int_{x_0}^{x_f} (1 + \alpha c_x) x^2 \frac{dc_x}{dx} dx \tag{2.60}$$

Again we can further simplify the expression by utilizing equation 2.41, 2.28, 2.29 and 2.30. Then, the final expression for electrical work can be written as

$$W_E = \frac{c_{33}^E A}{l} \int_{x_0}^{x_f} (1 + \alpha c_x) x dx + \frac{c_{33}^E A}{l} \left(\frac{1}{k_{33}^2} - 1 \right) \int_{x_0}^{x_f} (1 + \alpha c_x)^2 x dx + \tag{2.61}$$

$$+ \frac{c_{33}^E A}{l} \alpha \left(\frac{1}{k_{33}^2} - 1 \right) \int_{x_0}^{x_f} (1 + \alpha c_x) x^2 \frac{dc_x}{dx} dx \tag{2.62}$$

Where

$$\alpha = \frac{c_0}{c_{33}^E} \tag{2.63}$$

Now if we substitute equation 2.49 or equation 2.50 into 2.58 and 2.61 respectively, we can obtain the close form solutions for mechanical work and electrical work for these two cases. However, the solutions are very long and it is much easier to evaluate the integrals numerically. Even though, it is still more convenient to use equation 2.58 and equation 2.61 rather than use 2.22 and 2.19.

2.5.4 Actuation Efficiency

Similarly, the actuation efficiency of one dimensional non-linear systems can be found by dividing equation 2.58 with equation 2.61.

2.6 Comparison of Linear and Non-linear Systems

Assume the stiffness of both the active materials are one and the material coupling coefficient is 0.75. Mechanical work, electrical work and actuation efficiency of both the linear and non-linear systems has been shown in Fig. 2-6 and Fig. 2-7.

It is obvious that the work output and actuation efficiency of the non-linear systems is much higher than that of the linear system. For non-linear system 1, the actuation efficiency is almost

41
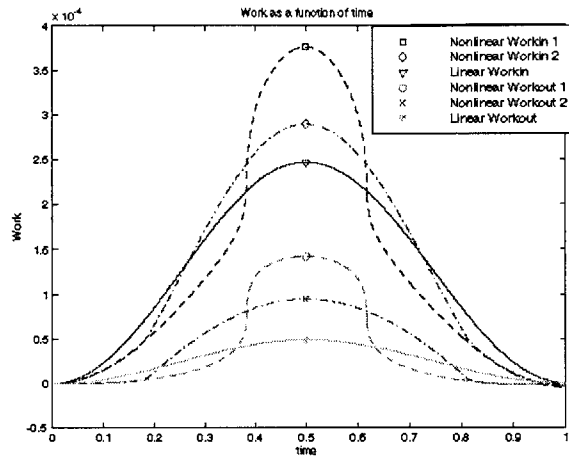
Figure 2-6: Comparison of Electrical and Mechanical Work for 1D Systems
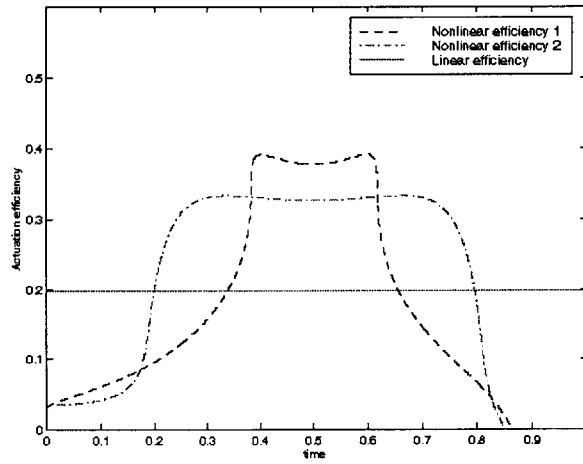
Figure 2-7: Comparison of Actuation Efficiency for 1D systems

42

doubled, while the work output is almost tripled.

2.7 Summary

Equations for the electric work, mechanical work and actuation efficiency for both the one dimensional linear and non-linear systems have been derived.

For linear systems, the analysis has shown that when material coupling coefficient is small, the actuation efficiency correlates the impedance matched systems efficiency. However, when material coupling coefficient is significantly large, there is a big difference between the two due to higher electromechanical coupling. In addition, the peak value of the actuation efficiency occurs when the stiffness ratio is larger than one, while the maximum impedance matched system efficiency always occurs at the impedance matched condition. The maximum actuation efficiency of the linear systems can be increased significantly when the material coupling coefficient of the active materials become large. For a given active materials whose material coupling coefficient is a constant, the stiffness of the structure should be carefully chosen to maximize the actuation efficiency of the system.

It has also been shown theoretically that the work output and actuation efficiency of the non-linear systems is much higher than that of the linear system. For non-linear system 1, the actuation efficiency is almost doubled, while the work output is almost tripled

Chapter 3

Renovation on the Existing Component Testing Facility

A component test facility has already been designed and built previously by Lutz [Malinda1, 1999] in order to verify the theoretical derivation of the mechanical, electrical work and actuation efficiency for both linear and non-linear systems. The picture in Fig. 3-1 shows the compressive component testing machine. However, due to some mechanical problems, force and displacement or the mechanical work from the active materials can not be measured accurately which necessitates a renovation on the tester. For a basis of discussion, the existing component tester is briefly introduced and the remaining problems are discussed, then the new design is presented and validated.

3.1 The existing Component Tester

3.1.1 Design Requirements

The main design requirements for this tester include:

- providing uniaxial testing with load application up to 8900 N and programmable impedances with a force resolution of 100 mN;

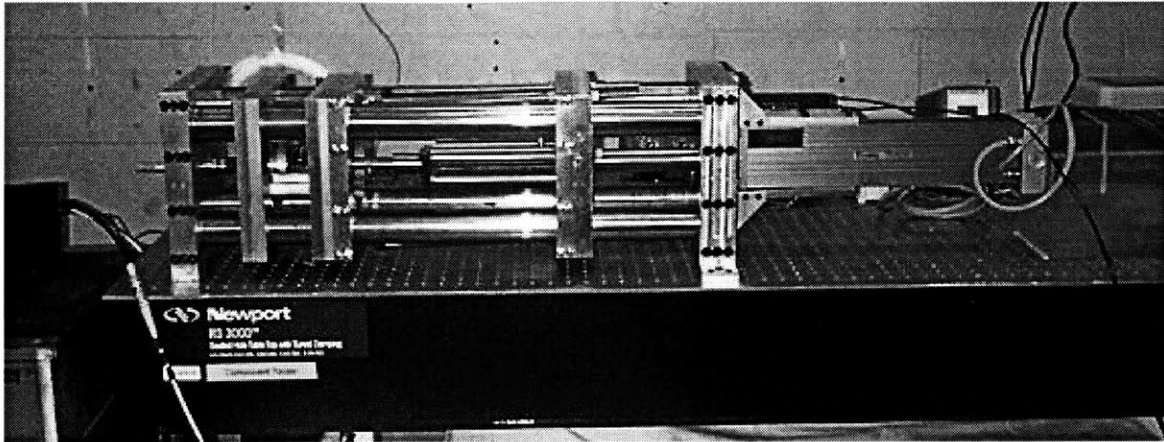- To provide closed-loop testing capabilities at frequencies up to 1 KHz

Figure 3-1: The Original Component Testing Facility

- To provide a testing facility that accommodates samples 0-120 mm long

- To provide the capability to perform 'free strain' and 'blocked force' tests

- To compensate for non-parallelism in the sample faces

- The ability to test most kinds of piezoelectric, electrostrictive, magnetostrictive and shape memory materials

3.1.2 Main Features of the Component Tester

The component tester actually built satisfies some of these requirements, such as loading capability and frequency range. The mechanical part consists of a large scale linear positioning system, which can provide preload to the sample, and two sets of driving piezo stacks, which can be chosen according to the applications. An alignment mechanism has been designed to compensate for the bending effect during the test. All the tests are controlled through the National Instrument/Labview data acquisition system. The feedback control of the systems mentioned above have also been implemented in Labview.

Specifications for some of the key components are listed below for reference:

- Preload: Flexline linear positioner, up to 20 kN.

- Optical displacement sensors: MTI 2000, range 0.127-0.510 mm, resolution 25 μm, frequency up to 20 kHz.

- Entran load cell: 13.35 KN, resolution 4.5 N, frequency up to 700 Hz

- Kistler load cell: 22.250 KN, resolution 4.5 N, frequency up to 3000Hz

- Trek amplifier: Model 609 D-6, output voltage range 0 to ±4 KV, DC or peak AC; output current range 0 to 20 mA, DC or peak AC; voltage monitor ratio 1V/1000 V, accuracy 0.1% of full scale; current monitor ratio 1V/2 mA, accuracy 0.5% of full scale.

- Amplifier for Driving Stack: +800 V, -800 V or ±400 V.; 1 A per channel, 1.5 A peak.

- Driving stacks: Data shown in Table 3.1 below.

	Small Stacks	Large Stacks
Max. Displacement (no load)	78.74 μm	182.88 μm
Stiffness	105.64×10^6 N/m	45.20×10^6 N/m
Capacitance	1.28 μF	3.00 μF
Diameter	30.86 mm	30.86 mm
Overall Length	97.28 mm	184.15 mm

Table 3.1: Driving Stack Parameters

3.2 Previous Test Results

3.2.1 Material Properties Measurement

Material properties of piezo stacks such as open circuit stiffness, short circuit stiffness, dielectric constant and electromechanical coupling terms are required in the theoretical prediction of the mechanical and electrical work and actuation efficiency. The correct measurement of these properties is also a good validation of the methods used for the measurement of basic parameters including displacement, force, current and voltage. These basic parameters are the key parameters for acquiring mechanical and electrical work experimentally.

The test sample chosen is Sumitomo stack MLA-20B. The tested properties measured by Lutz [Malinda1,1999], are listed in Table 3.2 below.

	Units	Ave. Value	Max. Value	Max.Value
Elastic constant	10^{-12} m^2/N	31.3	34.5	27.5
Dielectric Constant	$\varepsilon^T_{33}/\varepsilon_0$	4015	4818	3215
Electromechanical coupling	10^{-12} m/V	785	824	746

Table 3.2: Sumitomo Stack Parameters

Method of Obtaining Value	Coupling Coefficient k^2_{33}	Data Label
Bulk Material	0.72	-
Measured Stack Resonance	0.44	-
max s^E_{33} max ε^T_{33} max d_{33}	0.675	Theory 1
min s^E_{33} min ε^T_{33} min d_{33}	0.843	Theory 2
mean s^E_{33} mean ε^T_{33} mean d_{33}	0.745	Theory 3
max s^E_{33} max ε^T_{33} min d_{33}	0.611	Theory 4
min s^E_{33} min ε^T_{33} max d_{33}	0.932	Theory 5

Figure 3-2: Determination of k_{33} for Sumitomo Stack

From table 3.2, we can see that the material properties actually could not be measure accurately. For this reason, the material coupling coefficient could not be determined accurately either. Different combination of the data listed in Table 3.2 had to be used to find a better estimation of the material coupling coefficient, which is shown in following Fig. 3-2 [Malinda1, 1999].

The k_{33} estimated in this table varies from 0.44 to 0.932 which has a difference of more than 100%. It is obvious that the mechanical work and electrical work can not be predicted accurately.

3.2.2   Linear Test Results

The mechanical work, electrical work and actuation efficiency of the linear tests is shown in Fig. 3-3, Fig. 3-4 and Fig. 3-5 respectively [Malinda1,1999]. Theory 1 to Theory 5 represents the five theoretical predictions using the five different estimated k^2_{33}.
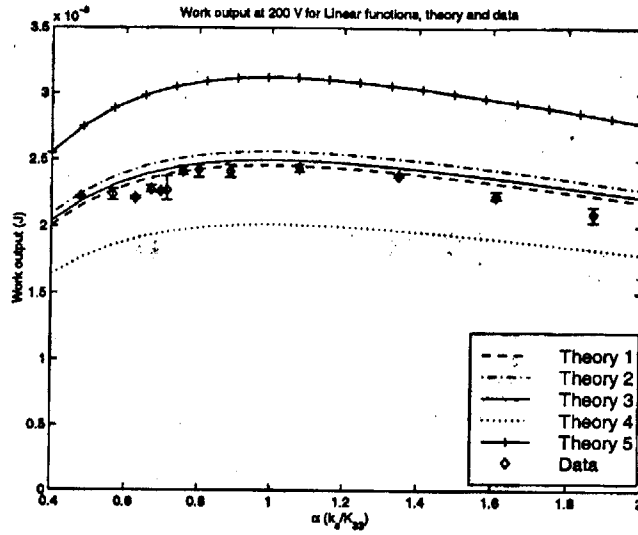
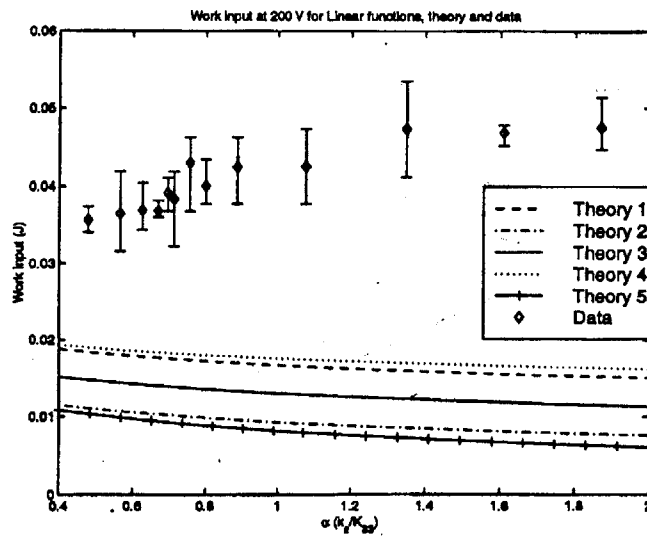Figure 3-3: Mechanical Work vs. Stiffness Ratio α for Linear Systems

Figure 3-4: Electrical Work vs. Stiffness Ratio α for Linear Systems
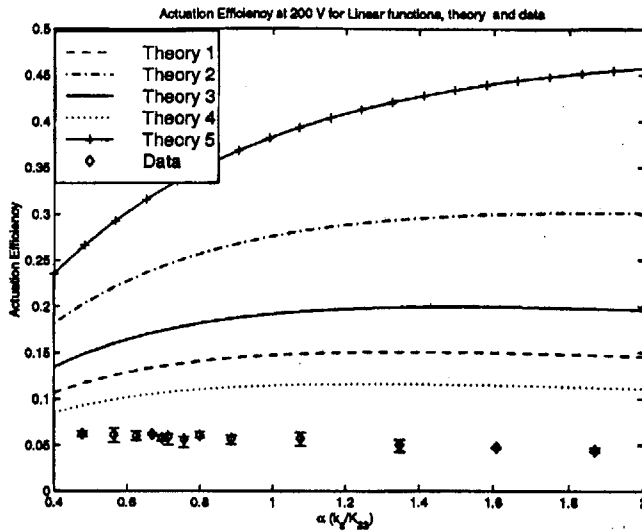
Figure 3-5: Actuation Efficiency vs. Stiffness Ratio α for Linear Systems

3.2.3 Nonlinear Test Results

No much data was obtained for non-linear tests [Malinda1,1999]. The actuation efficiency comparison for linear and non-linear systems is shown in Fig. 3-6.

Form the figures shown above, it is obvious that the experimental data do not match the theoretical prediction.

3.3 Analysis of the Problems

The accurate measurement of electrical and mechanical work is the basis for the comparison of theoretical prediction and experimental data. From previous discussion we know that the theoretical prediction could not be made accurately because of the bad material property data. This actually implies that the mechanical work and electrical work could not be measured accurately either since the basic parameters required are the same, such as current, voltage, displacement and force.
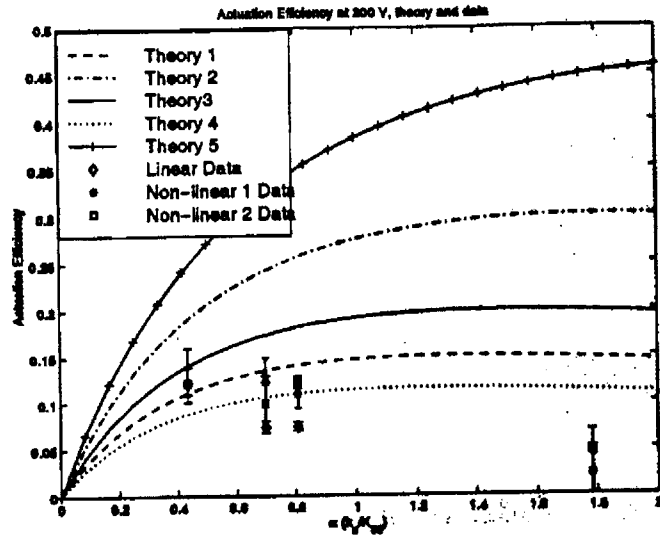
Figure 3-6: Comparison of Actuation Efficiency for Linear and Non-linear Systems

3.3.1 Electrical Work Measurement

The time trace of a representative test is shown in Fig. 3-7. It is obvious that the data is unaccessible, which could be one of the reasons for the mismatch of electrical work from prediction and experiment.

Form this figure, we can also find that the length of the test is 20 seconds, using half a sine wave. The driving frequency of the test is then 1/40 Hz, i.e. 0.025 Hz. The applied voltage to the sample is 200 V, which can also be seen from the figure. The nominal capacitance of the Sumitomo stack MLA-20B is 800 nF at free condition. From these data we can estimate the magnitude of the current in the systems which is:

$$
\begin{aligned}
I &= 2\pi f V F \\
&= 2 \times 3.14 \times 0.025 \times 200 \times 800 \times 10^{-9} \\
&= 0.025 \text{ mA}
\end{aligned}
\tag{3.1}
$$

The current magnitude computed is so small that it is far below the lowest value of an accurate measurement for the current monitor of the Trek amplifier, which is about $0.5\% \times 20 =$
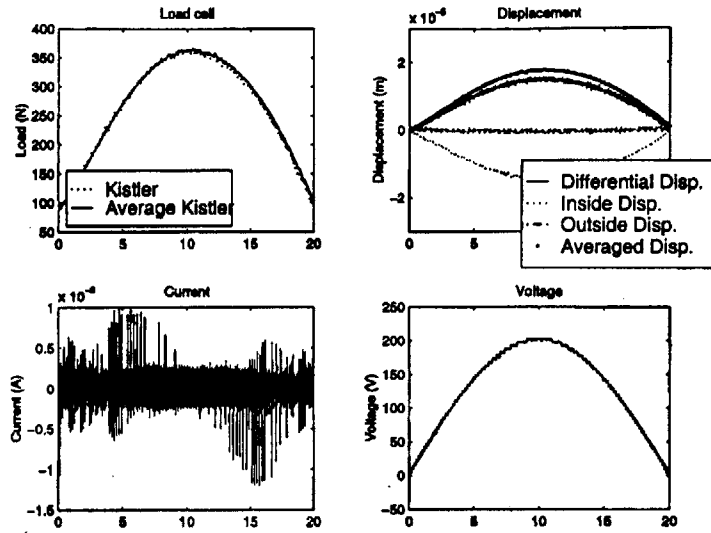
Figure 3-7: Time Trace of from Previous Test

0.1 mA. This value can be found from the specification of the Trek amplifier listed before. The current measurement problem could be solved by simply increasing the test frequency so that the current magnitude is high enough for the current monitor. However, the driving frequency is actually limited by the capability of the control system of the tester. An improvement in the control method should be made to guarantee an better current measurement. This will be demonstrated later in this chapter. The voltage measurement should have no problem and this will be demonstrated later too.

3.3.2 Mechanical Work Measurement

The mechanical work measurement seemed to be a very difficult problem. To get an idea of the displacement and force measurement accuracy, stiffness of an Aluminum bar was measured first.

Aluminum Bar Stiffness Measurement

The Al bar measured has a length of 0.0832 m, diameter of ϕ 0.008 m and the theoretical stiffness of it is 4.229×10^7 N/m. The Aluminum bar was placed on the different locations

51

	Test 1		Test 2		Test 3	
	Align.	No Align.	Align	No Align.	Align	No. Align.
Kis.10^7 N/m	2.3001	2.3110	3.2283	4.5397	2.0136	3.7400
Ent. 10^7 N/m	1.9266	1.9350	2.9663	4.0373	1.6331	2.600

Table 3.3: Al Bar Stiffness Measurement

on the sample plate of the tester. The test were done under two conditions: testing with the alignment mechanism or without the alignment mechanism. When tested with the alignment mechanism, the stiffness of the Al bar should be

$$K = \frac{1}{\frac{1}{K_{measu.}} - \frac{1}{K_{align.}}} \qquad (3.2)$$

The displacement of the Al bar was measured by the MTI Fotonic sensors, and force was measured by both Entran and Kistler load cells. The results are listed in Table 3.3.

It was obvious that the stiffness measured did not match the theoretical value when tested without the alignment mechanism. The alignment mechanism was designed to remove the bending effect during tests, however, the data measured with the alignment mechanism was questionable also. In addition to the Aluminum bar stiffness measurement, several plastic bars were measured and the data was also unaccessible, which has been shown in Fig. 3-8.

This necessitated the accurate stiffness measurement of the alignment mechanism.

Alignment Mechanism Stiffness Measurement

The alignment mechanism is shown Fig. 3-9. It consists of two circular plates connected by a thin bar which is designed to compensate for the un-parallelism of both the test sample and the champing plates.

The stiffness of the alignment mechanism measured was unexpected which showed a stiffness change with respect to the preload applied on it. Fig. 3-10 shows the results.

Cage Assembly

Besides the problem of the alignment mechanism, the cage assembly caused some problems also. The cage assembly was designed and built for two purposes mainly. First the cage provides the capability of transferring load from the driving stacks to the test sample, and the convenience
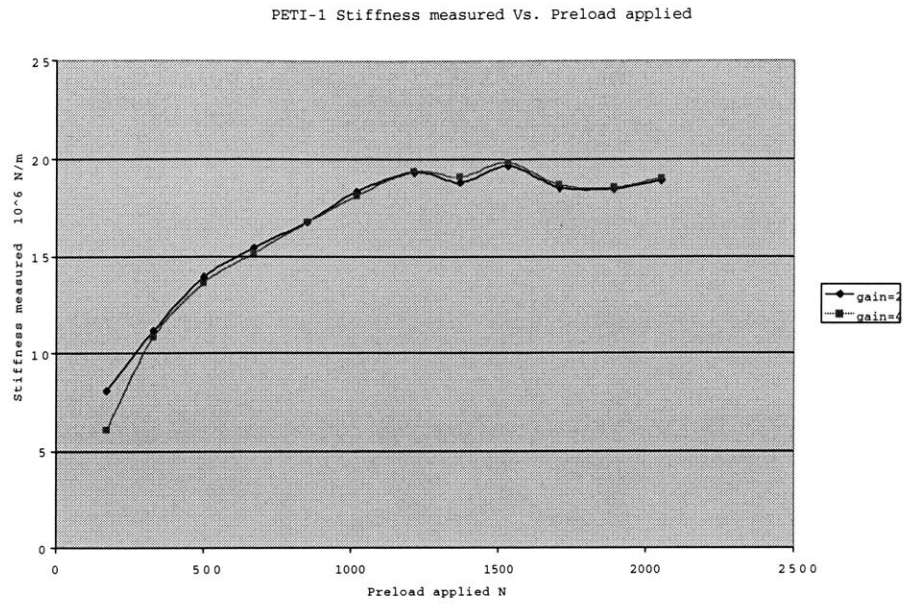
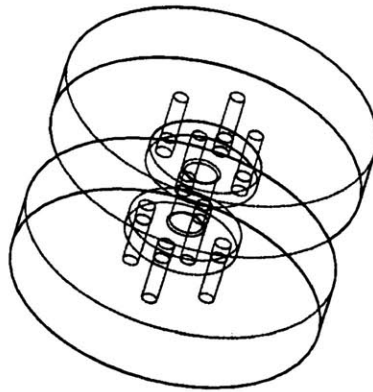Figure 3-8: Stiffness of PETI-1 vs. Applied Preload

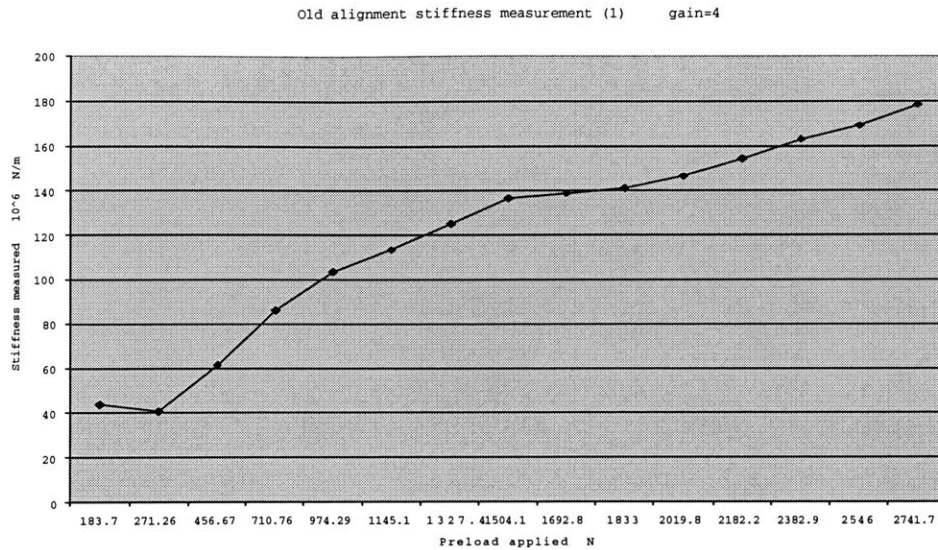Figure 3-9: The Original Alignment Mechanism

53

Figure 3-10: Stiffness of the Alignment Mechanism vs.Preload

for the displacement measurement of the sample. The load was transferred through two thin flextures. Second, the cage provides the protection of the loading and testing systems in case of serious misalignment. This was done by reinforcing the loading and testing systems through this cage mounted on the four rods. A picture of the cage assembly is shown in Fig. 3-11.

It was found, however, the stiffness of the flextures, and the friction between the rods and the bushing of the cage was too high. In addition, test sample was placed on one side of the cage and the load cells for force measurement were all placed on the other side of the cage. This made it very hard to determine the accurate displacement of the sample and the actual load on it.

Other Considerations

In addition to the problems discussed above, the MTI probes caused some problems also. MTI probes were used to measure the displacement of the test sample when it was actuated. However, it was difficult to get repeatable displacement measurements for the same test at the beginning. This turned out to be caused by problems in calibrating the MTI probes, such as finding the peak value. The MTI probes has to be calibrated very carefully.
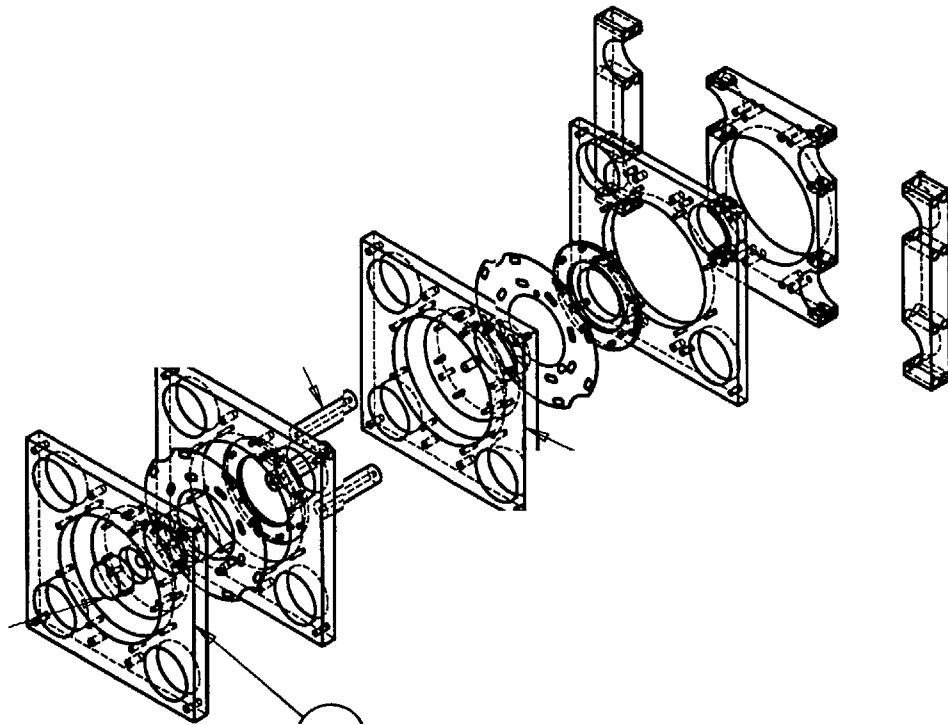
Figure 3-11: The Original Cage System for Load Transfer and Protection

Another remaining problem is the different force measurement from Entan and Kistler load cell as shown in Table 3-3. The measurement from Kistler is very reliable which will be demonstrated later in this chapter. The difference is caused by Entran load cell which is a strain gauge type load cell which needed to be calibrated every time before it is used.

From the discussion above, we can see that the alignment and the load transferring device of the component tester should be improved or replaced. Some modification on the existing cage could not guarantee the improvement of performance, therefore, a new design was made and built to replace the cage assembly.

3.4 Re-design of the Load Transfer Device

3.4.1 Initial design

The objectives of this design was to replace the cage assembly and the alignment mechanism for accurate force and displacement measurements and safe tests. As a result, the alignment mechanism was replaced by the spherical joint connection between different mechanical parts, and the cage assembly was replaced by a linear bearing system. For a protection of the loading system, the bearing system was mounted on a plate which again was mounted on the four rods. A schematic view of this design is shown is Fig. 3-12.

From the figure we can see that the Kistler load cells (load cell1) is on the sample side and Entran load cell (load cell 2) is on the other side of the linear bearing. The connection between different parts are all spherical joints. In addition, the configuration of the loading systems can be changed freely according to request because we have designed and built different connectors.

3.4.2 Vibration Measurement and Improvement on the Design

To validate this new tester configuration, Polytec CLV 100 Laser Vibrometer was used to monitor the transverse vibration of the tester during test. The transverse vibration of different parts of the tester were monitored one by one. The information obtained from the test sample itself seemed to be more important. The transfer function of the test sample, a steel tube with the similar stiffness as the piezo stack, is shown in Fig. 3-13.

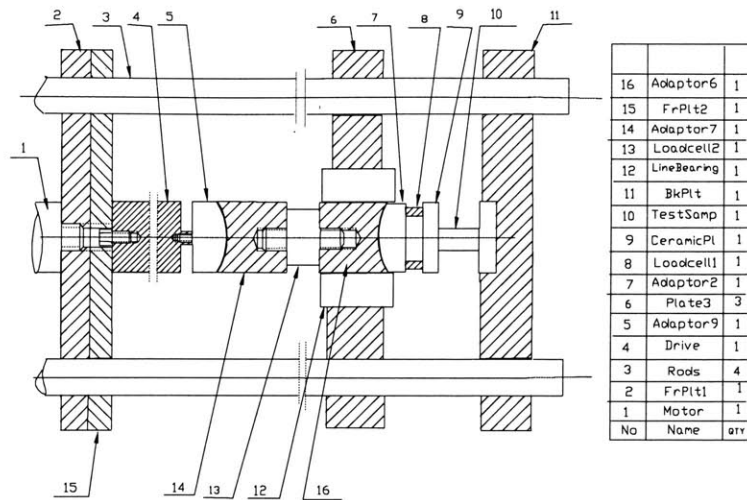From the transfer function we can see the peak at about 400 Hz as well as other peaks.

16	Adaptor6	1
15	FrPlt2	1
14	Adaptor7	1
13	Loadcell2	1
12	LineBearing	1
11	BkPlt	1
10	TestSamp	1
9	CeramicPl	1
8	Loadcell1	1
7	Adaptor2	1
6	Plate3	3
5	Adaptor9	1
4	Drive	1
3	Rods	4
2	FrPlt1	1
1	Motor	1
No	Name	QTY

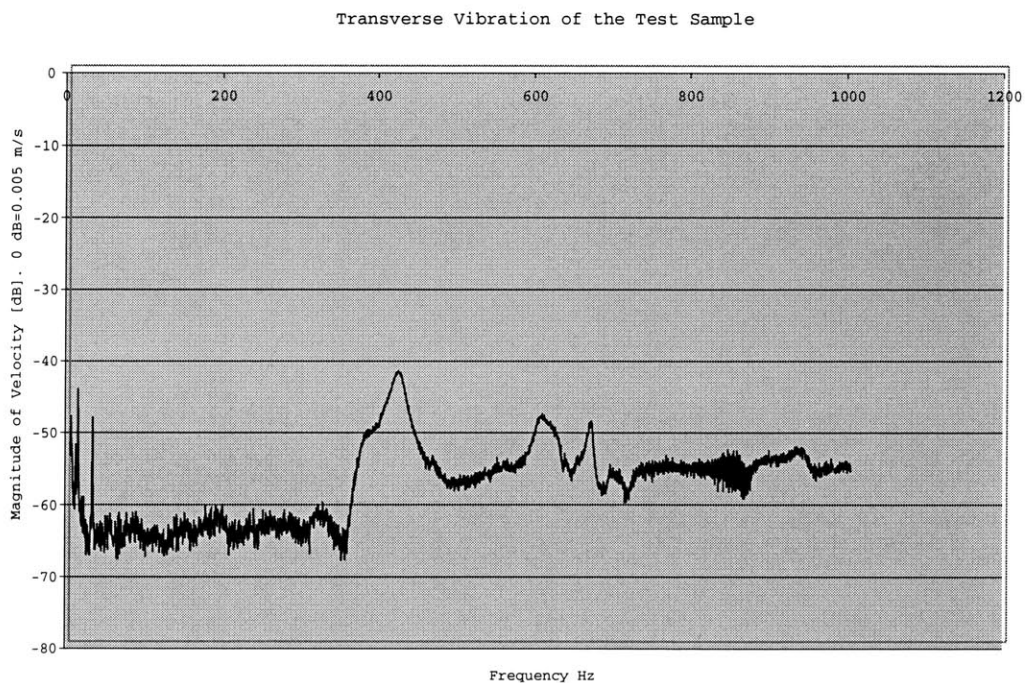Figure 3-12: New Design of the Load Transfer System

Figure 3-13: Transfer Function of the Transverse Velocity of Test Sample to the Input to Drive
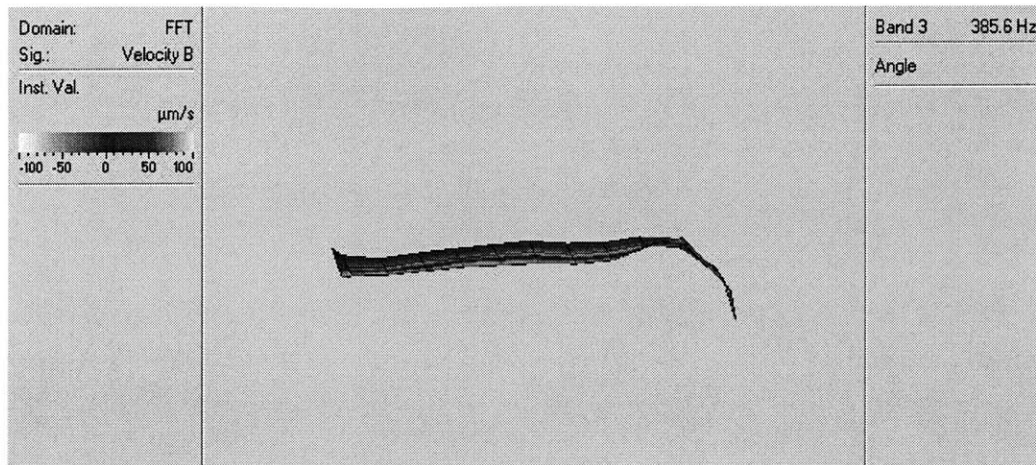
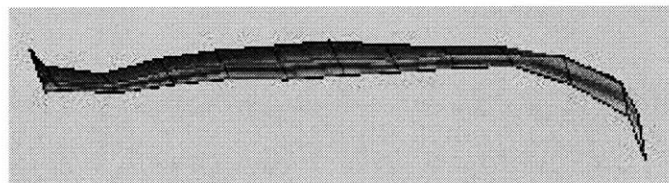Figure 3-14: Transverse Vibraton of Test Sample at Time 1

Figure 3-15: Transverse Vibration at Time 2

Pictures shown in Fig. 3-14 to 3-19 provides information in detail about the transverse vibration of the test sample at this frequency.

Fig. 3-14 shows the picture for the transverse vibration at the peak frequency for a start moment. The transverse vibration is more obvious when check the pictures in a timely order.

From this series of pictures, we could find that the left side of the sample had bad contact with the clamping plate of the tester. The lower left part of the sample vibrated much more severely than that of the upper left part. This means that the misalignment of the sample with the tester was larger than what the spherical joints could compensate for. For this reason, three springs were mounted between the joint and the plate, where the linear bearing was mounted, as shown in Fig. 3-20. The springs could provide enough preload to the sample so that the position of the sample could be adjusted carefully before the driving system pressed on it.

Pictures of the new design are shown in Fig. 3-21 and Fig. 3-22. The improvement seemed
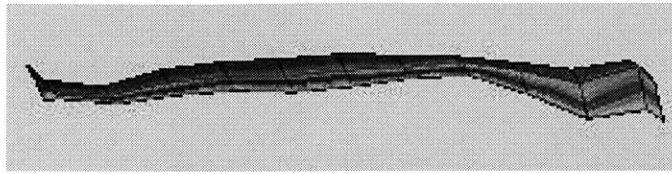
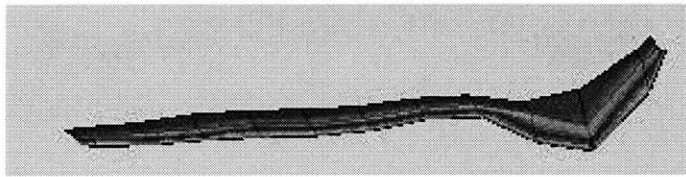Figure 3-16: Transverse Vibration at Time 3

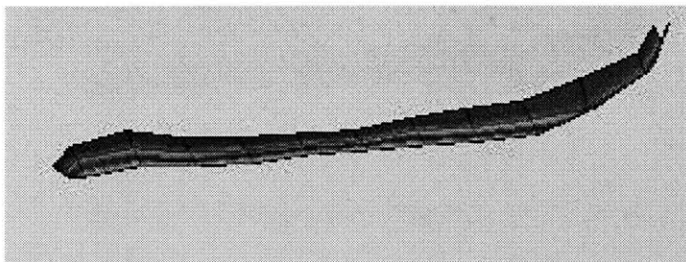Figure 3-17: Transverse Vibration at Time 4
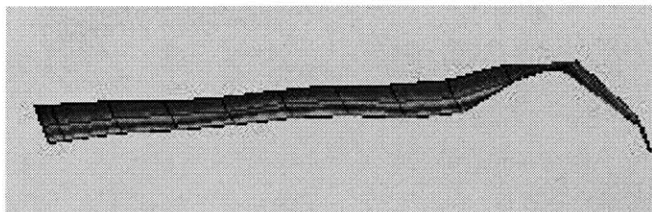

Figure 3-18: Transverse Vibration at Time 5

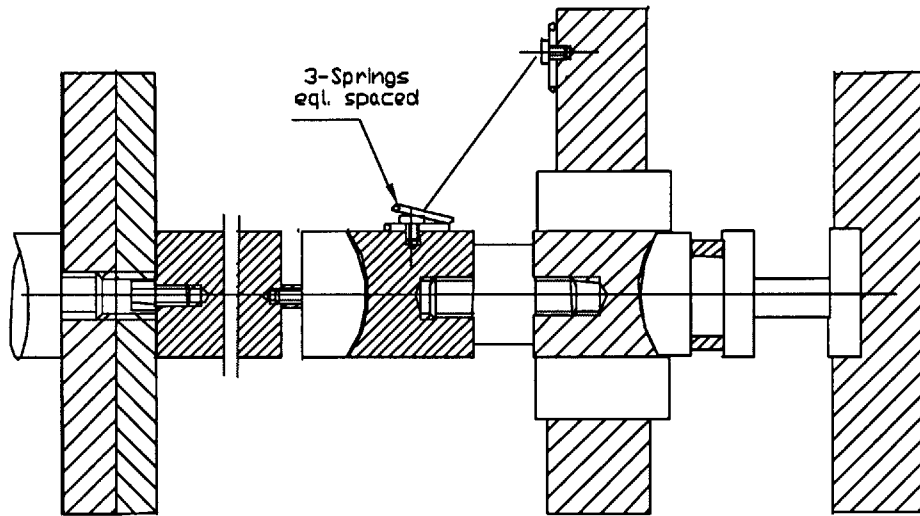Figure 3-19: Transverse Vibration at Time 6

Figure 3-20: Improvement on the New Design by Providing Springs for Preload

very effective because the transverse vibration was suppressed.

3.5 Validation of the New Design

The validation tests were conducted to verify the correct measurement of displacement, force voltage and current or charge. The current and voltage validation is done by capacitance measurement of standard capacitor, and the force and displacement validation was done by stiffness measurement.

3.5.1 Stiffness Measurement

To measure the stiffness of sample correctly, the load cells, which measure force, and the Fotonic sensors, which measure displacement were calibrated first.

Load Cell Calibration

The load cells, Kistler 9212 and Entran miniature, were compared with the standard load cell of the Instron testing machine, Kistler 9300. The results showed a very good match while the calibration of the kistler load cell was adjusted to be 100 N/V and that of the Entran load
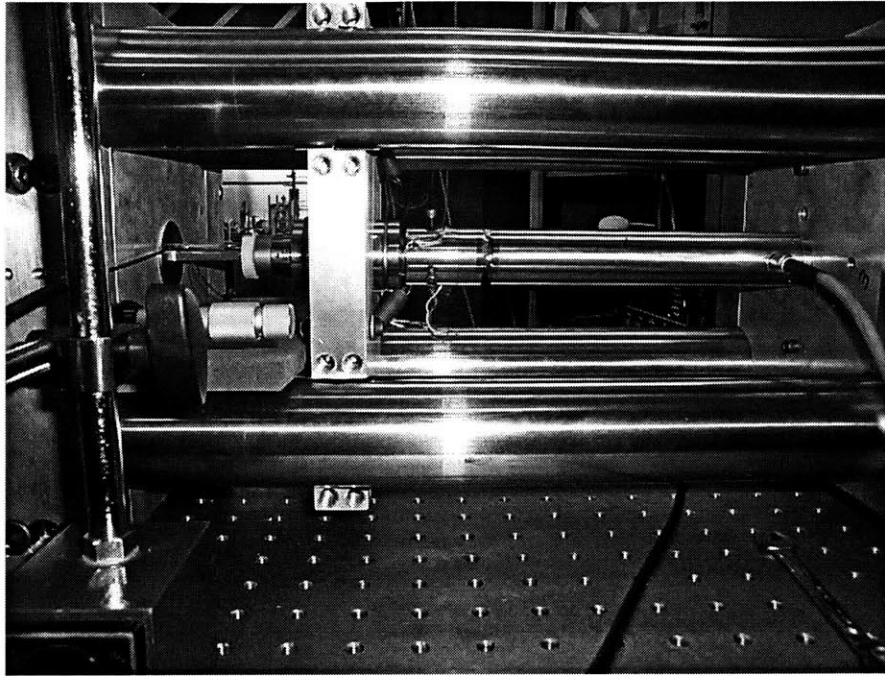
Figure 3-21: New Design of the Load Transfer Systems1
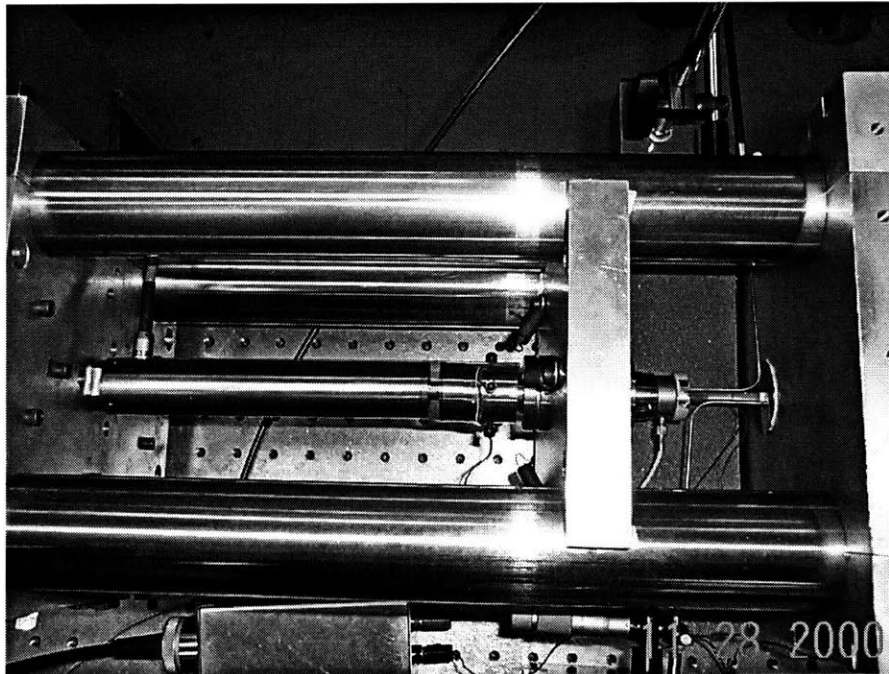

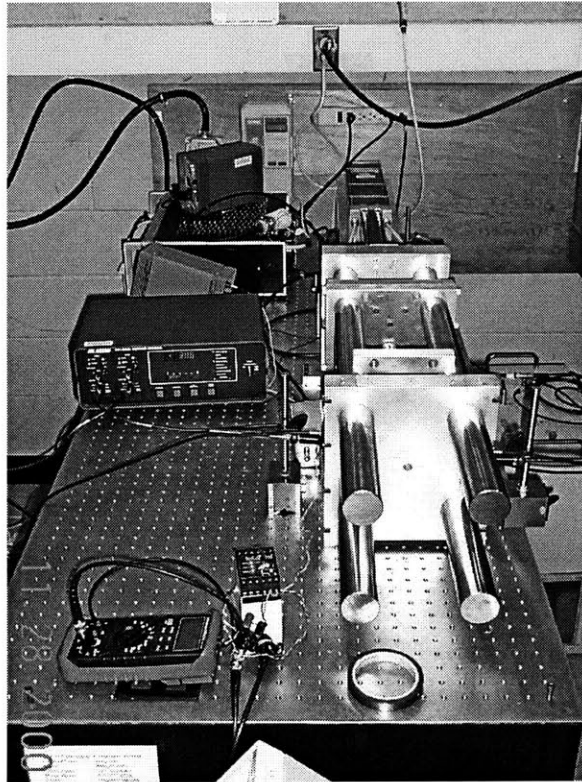Figure 3-22: New Design of the Load Transfer System 2

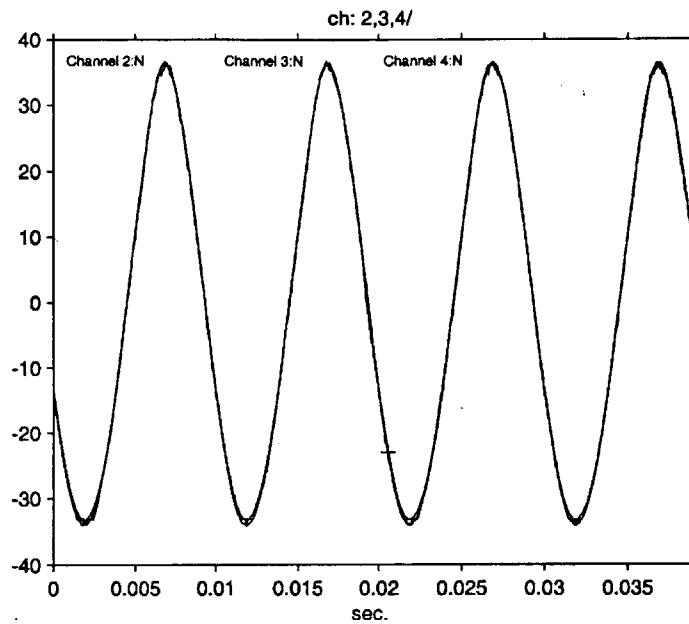Figure 3-23: Overall View of the New Tester

Figure 3-24: Force Calibration for the New Design

cell was 1570 N/V. The comparison is shown in Fig. 3-24. In this figure, channel 2,3 and 4 represents Kistler 9300, Kistler 9212 and Entran miniature respectively.

Fotonic Sensor Calibration

The displacement of the two Fotonic sensors, also called MTI probes, were compared with each other first. Then the displacement of a sample measured by the two Fotonic sensors (differential displacement) and strain gauges was compared. The results were comparable as seen in Fig. 3-25 and Fig. 3-26.

Stiffness Measurement

The sample used for the stiffness test was a steel tube: $\phi 12.65$ mm $\times$ 0.15 mm $\times$ 101.55 mm. Three equally spaced strain gages were bonded on the outer surface of the sample. The measured stiffness by the strain gages and the Fotonic sensors was compared in Fig. 3-27. The Kistler load cell was used to measure force.

The stiffness measured by strain gages and Fotonic sensors are very close as can be seen
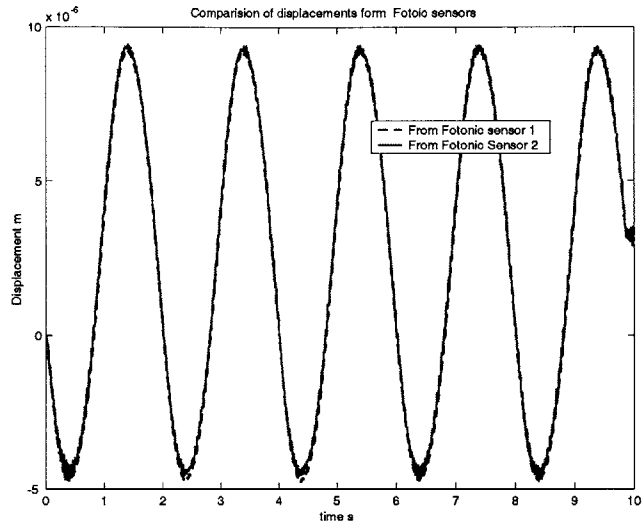
Figure 3-25: Comparison of Displacement measured by Two MTI Probes
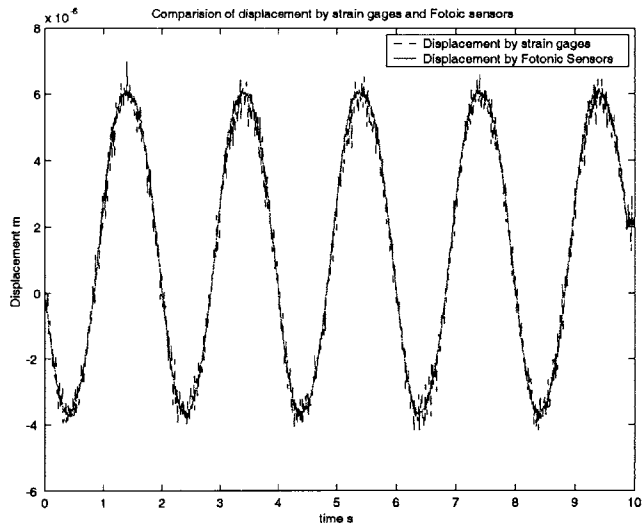
Figure 3-26: Comparison of Displacement Measured by MTI Probes and Strain Gages

64
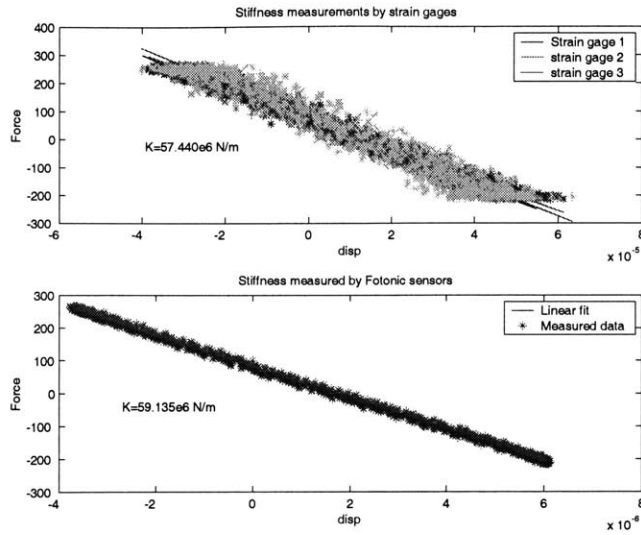
Figure 3-27: Stiffness Measured from MTI probes and Strain Gages

from the figure: 57.440×10^6 N/m and 59.135×10^6 N/m respectively.

3.5.2 Capacitance Measurement

The capacitor used for this test was a standard capacitor with a nominal capacitance of 800 nF, which was close to the capacitance of the Sumitomo piezo stack. The capacitance was determined by

$$Q = CV \tag{3.3}$$

Where Q was determined by integrating current monitored by the Trek amplifier over time, and V directly came from the voltage monitor of the Trek amplifier. A set of representative curves have been shown in Fig. 3-28.

As can be seen from the figure, the measured capacitance 791.39 nF has very good correlation with the nominal value 800 nF (1% error). The test was conducted at a frequency of 10 Hz. At this frequency and an applied voltage of 225 V, it is possible to compute the magnitude of
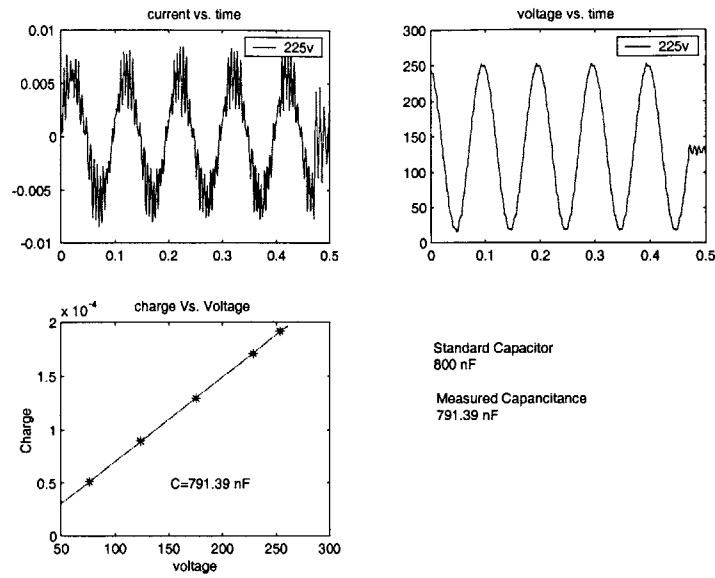
Figure 3-28: Capacitance Measurement for Standard Capacitor

the current in the circuit using equation 3.1 as following:

$$
\begin{aligned}
I &= 2\pi f V F \\
&= 2 \times 3.14 \times 10 \times 225 \times 800 \times 10^{-9} \\
&= 11.30 \text{ mA}
\end{aligned}
$$

This magnitude of current is well within the range of an accurate measurement as can be seen from the figure. This proved out our suggestion made early about increasing the test frequency for linear and non-linear tests.

3.6 Summary

The renovation and validation of the component tester has been presented. The status of the existing component tester and the test results from it have been discussed. Both the electrical work and mechanical work could not be measured accurately in those tests. The poor electrical work measurement is caused by the low test frequency. The current magnitude computed for a typical linear test done before is about 0.025 mA, which is far below the

lowest value of an accurate measurement. The current monitor of the Trek amplifier is capable of measuring a current as low as about 0.1 mA. The current measurement problem has been solved by increasing the test frequency so that the current magnitude is high enough for accurate measurements. This has been demonstrated by a capacitance test. When the test frequency is raised to 10 Hz for a standard capacitor with a similar capacitance as the sample stack, the computed magnitude of current is 11.30 mA, and the current signal is very clean. Capacitance measurement of a standard capacitor (800 nF) has been used as a validation of the voltage and current measurement method. The actual measured capacitance of this capacitor is 791.39 nF.

The poor mechanical work measured is caused by the load transfer systems, and the misalignment during the tests. The cage assembly has been replaced by a linear bearing system, while the alignment mechanism has been replaced by spherical joint connectors. A laser vibrometer has been used to monitor the transverse vibration due to misalignment. An adjustment mechanism has been applied for fine adjustment of the position of the sample stack. Stiffness measurement of a steel tube has been chosen as the validation method for the force and displacement measurement. Displacement has been measured using both the MTI probes and 3 strain gages on the tube, while the force is measured by the Kistler load cell. The stiffness of which measured by the strain gages and MTI probes are very close which are 57.440$\times 10^6$ N/m, and 59.135$\times 10^6$ N/m respectively.

As a conclusion, the renovation of the component tester is validated, and the measurement methods for displacement, force, current and voltage are reliable.

Chapter 4

One Dimensional Linear and Non-linear Tests

In order to verify the theoretical prediction made in chapter 2, linear and non-linear tests were to be conducted. In this chapter, the linear and non-linear test approach and test results will be presented. The original feedback approach which was used by Lutz [Malinda1, 1999] will be examined and the problems of this approach will be discussed, then a new test approach proposed. The linear and non-linear test results will be compared and contrasted at the end of this chapter.

4.1 FeedBack Test Approach

A feedback closed loop control method was originally chosen for the linear and non-linear tests. The idea was to provide the capability of testing a sample against a programmable impedance, either linear or non-linear. The input to this control loop is the displacement and force information from the Fotonic sensors and the load cells. The output from this control loop is the voltage level to supply to the driving stacks. For an assumed structure stiffness or impedance, the voltage level to the driving stacks is determined first by detecting what the desired change of force in the system is, then finding the corresponding change in electrical field to satisfy this requirement. This is analogous to finding a root of an equation using iteration method.
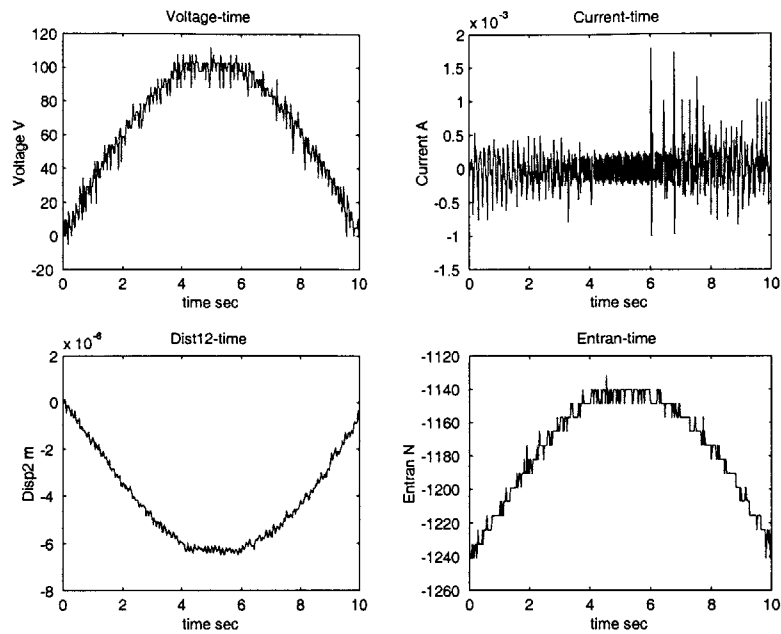
Figure 4-1: Time Trace for Linear Test at 0.05 Hz, Assumed Stiffness 3000 lbs/in

To do the linear and non-linear tests planned successfully, it is important to determine whether to use feedback close loop control or other methods. From the discussion in the last chapter, it has been demonstrated that increasing the test frequency could solve the problem of a noisy current signal. To verify this assumption for linear or non-linear tests, some tests have been done on the component tester before it was renovated. The renovation on the tester was mainly for improving force and displacement measurement. Renovation did not influence the current and voltage measurement at all since these two parameters were obtained from the current and voltage monitors of the Trek amplifier. Therefore, the linear tests should still be valid for checking current and voltage measurement. Some of the test results have been shown in the following figures. The test frequency has been increased form 0.05 Hz to 10 Hz.

The input signal for these tests was half a sine wave. From Fig.4-1, Fig4-2 and Fig.4-3 we can see that at 0.05 Hz and 1 Hz the current signal is noisy as predicted, however, the system becomes unsteady at 10 Hz, thereby making the situation worse.

A MATLAB simulation of the process for the feedback controller to determine the voltage level for the driving stacks according to the applied voltage to the sample stack has been
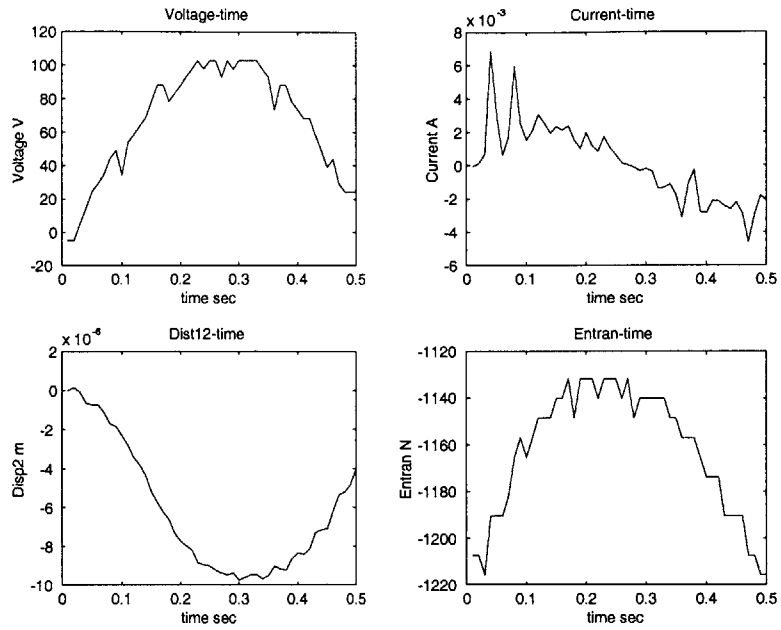
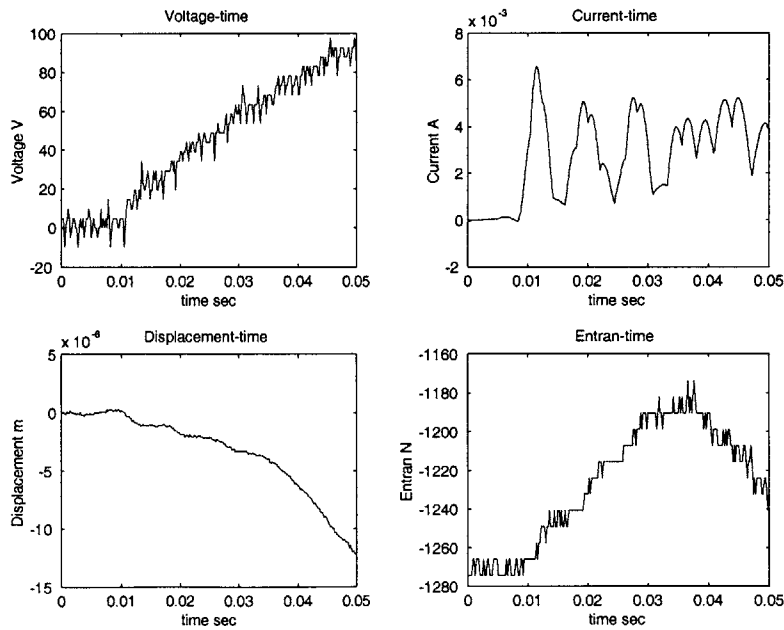Figure 4-2: Time Trace for Linear Test at 1 Hz, Assumed Stiffness 3000 lbs/in

Figure 4-3: Time Trace for Linear Test at 10 Hz, Assumed stiffness 3000 lbs/in

conducted. A given sine wave was applied to the sample stack for an assumed structure stiffness. The input sine wave signal (one cycle) was represented by 2000 points for accuracy. The objective was to find the sine wave signal to the driving stacks represented by another set of 2000 corresponding points using iteration method. The simulation has shown that the computer requires about 25 minutes to find the 2000 corresponding voltage value. If reducing the points to 100, it still need about 150 seconds. However, to drive the test at 10 Hz, for example, requires the computer to find the 100 points or 2000 points within 0.1 seconds. This is a probable cause for why the system goes unsteady when testing at 10 Hz. A different method should be considered for successful linear and non-linear tests.

4.2 FeedForward Test Approach

From the discussion of the last section, it is unlikely to determine the drive voltage for the driving stacks using feed back controller. A possible solution is to solve for the driving voltage in advance, which leads to the feed forward open loop control method. The principle of this method has been shown by the block diagram in Fig. 4-4.

From Fig.4-4, it was seen that a Voltage-Force model is required to compute the voltage to the driving stacks. The material properties of the test sample Sumitomo stack are also needed. The non-linear functions shown in this figure could also be linear functions. An easier way to perform the linear tests will be shown later in this chapter.

4.3 Material Properties of Test sample

The material properties of the test sample Sumitomo stack is required not only in theoretical prediction, but also in defining the linear and non-linear functions, determining the voltage-displacement relation and establishing the Voltage-Force model. The methods used to measure the material properties in this section are those methods validated in Chapter 3.

4.3.1 Test Sample Physical Parameters

The test sample chosen is the Sumitomo stack MLA-20B for comparison with the data obtained by Malinda. The physical parameters are shown in Table 4.1

Open Loop Test Approach

Figure 4-4: Feedforward Open Loop Test Approach
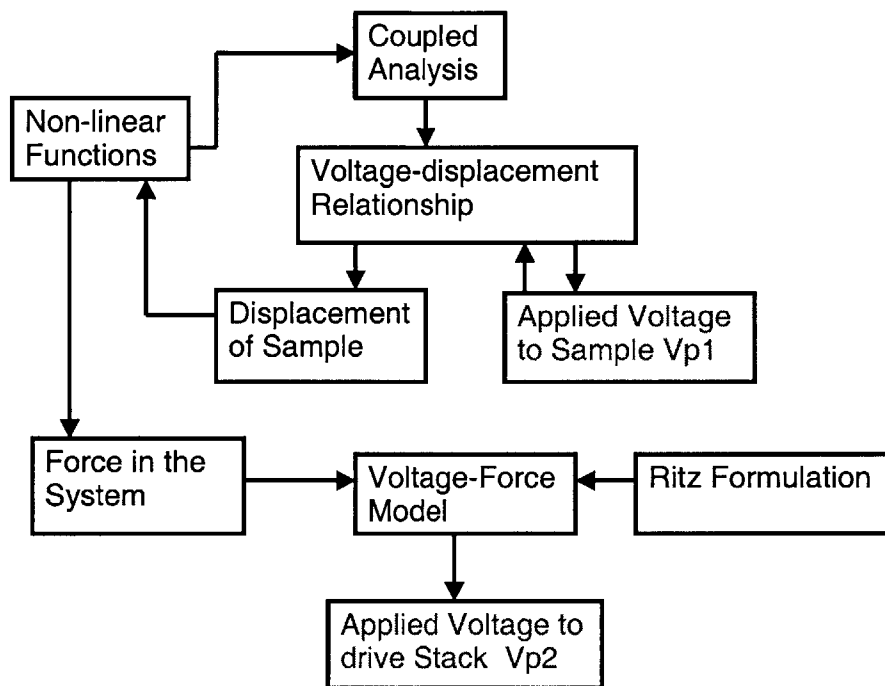
Total Length mm	41
Active Length mm	37
Section Area mm^2	23.4
Layer Thickness mm	0.18
Number of Layers	200
Max. Applied Voltage V	250

Table 4.1: Sumitomo Stack Physical Parameters

4.3.2   Stiffness and Elastic Constants

The stack stiffness test were performed on the component tester. The sample was placed on the clamping plate, then pressed and held by the three springs. The position of the stack was carefully adjusted to make sure it had a good contact with the clamping plates. After that, a preload was applied to the stack gradually while the Entran load cell was used to monitor the increase of the preload. The preload was maintained to be around 150 N and this preload was used for all of the tests including both the linear and nonlinear tests for the Sumitomo stack. It was found that preload had some influence on the test results and it was necessary to minimize it.

The tests were done through the actuation of one long stack in the loading systems. This configuration was kept through out all the tests including linear and non-linear tests. The driving signal to the driving stack was a sine wave with a frequency of 10 Hz and voltage level of 160 V, 200 V or 240 V. The Sumitomo stack was tested at both open circuit and short circuit conditions. k^D and k^E were found through the ratio of force to displacement measured, while s_{33}^D and s_{33}^E were found from the following equations:

$$s_{33}^D = \frac{A}{k^D l} \qquad\qquad (4.1)$$

and

$$s_{33}^E = \frac{A}{k^E l} \qquad\qquad (4.2)$$

The measured value for $k_{p1}^D 10^6$ N/m have been shown in Table 4.2, where Test 1, 2 , 3 indict that the driving voltage of the driving stack is 160 V, 200V and 240 V respectively, and it was the same in the tables for S_{33}^D, K^E and S_{33}^E. Measured Value for S_{33}^D 10^{-12} m^2/N, k_{p1}^E 10^{-12} N/m and S_{33}^E 10^{-12} m^2/N has been listed in Table 4.3, Table 4.4 and Table 4.5 respectively.

Typical time trace and force-displacement relation curves are shown in Fig.4-5 and Fig. 4-6.

4.3.3   Capacitance and Dielectric Constant

The capacitance of the Sumitomo stack was measured in the same way as the standard capacitor was measured in Chapter 3. Here the Sumitomo stack was placed on a support to restrain it

	k_{p1}^{D} 10^6 N/m							
Test1	39.983	39.996	40.024	40.039	40.051	39.974	40.086	39.865
Test2	41.107	40.988	41.049	41.058	41.077	41.094	41.015	41.125
Test3	41.749	41.635	41.654	41.708	41.712	41.727	41.747	41.763
Average	40.924							

Table 4.2: Sumitomo Measured Stiffness at open Circuit,

	S_{33}^{D} 10^{-12} m^2/N							
Test1	15.865	15.835	15.812	15.801	15.795	15.791	15.821	15.777
Test2	15.385	15.430	15.407	15.403	15.396	15.390	15.378	15.420
Test3	15.148	15.190	15.183	15.163	15.162	15.157	15.149	15,143
Average	15.458							

Table 4.3: Sumitomo Stack Measured Compliance st Open Circuit

	k_{p1}^{E} 10^{-12} N/m							
Test1	20.872	20.904	20.914	20.930	20.949	20.955	20.935	20.972
Test2	20.865	20.885	20.899	20.913	20.931	20.932	20.950	20.953
Test3	20.884	20.932	20.970	20.968	21.007	21.027	21.037	21.052
Average	20.943							

Table 4.4: Sumitomo Stack Measured Stiffness at Short Circuit

	S_{33}^{E} 10^{-12} m^2/N							
Test1	30.301	30.255	30.239	30.216	30.188	30.180	30.210	30.155
Test2	30.311	30.282	30.261	30.242	30.216	30.214	30.188	30.183
Test3	30.282	30.214	30.158	30.162	30.106	30.078	30.063	30.041
Average	30.198							

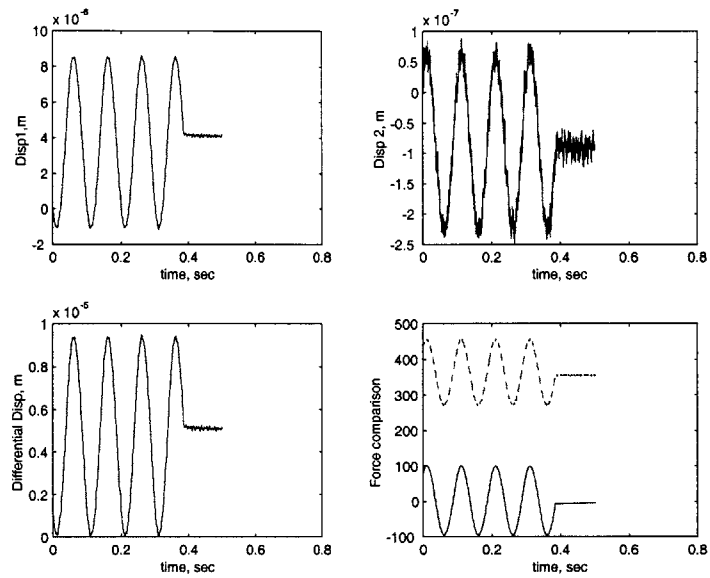Table 4.5: Sumitomo Stack Measured Compliance at Short Ciucuit

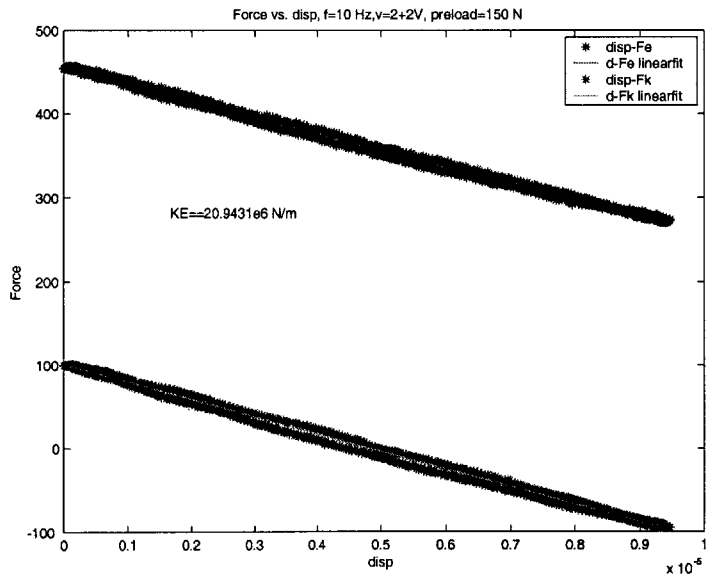Figure 4-5: Time Trace of Displacement and Force for Stack Stiffness Measurement

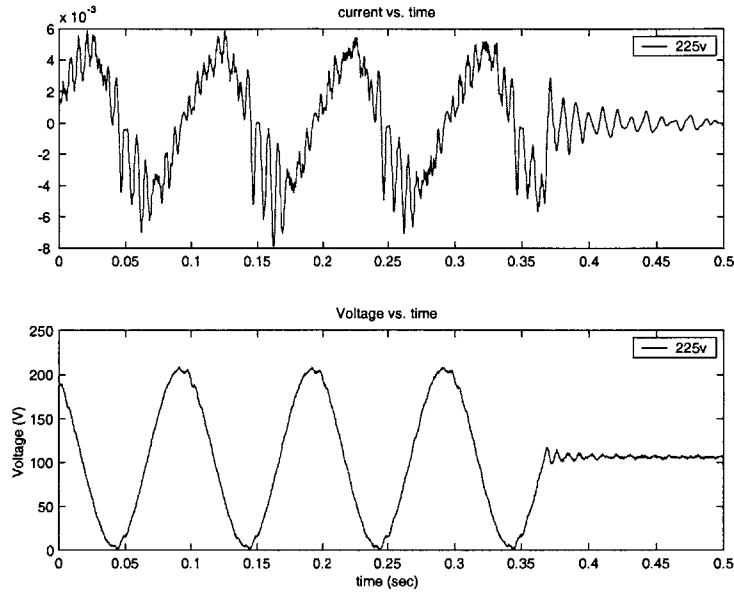Figure 4-6: Force vs. Displacement for Stack Stiffness Measurement

Figure 4-7: Time Trace of Current and Voltage for Capacitance Measurement

at either ends, while different levels of voltage were applied to it, while the current signal going to the stack was measured. The current measured was integrated over time to find the charge value which was then used to find capacitance as described by 3.3. The driving frequency was 10 Hz and the signal used as input to the Trek amplifier was

$$V_{appl} = \frac{1}{2}V_{\max}\sin(20\pi t) + \frac{1}{2}V_{\max} \tag{4.3}$$

Where $V_{\max}$ ranges from 25 V to 225 V.

The dielectric constant under constant stress can be found from the measured capacitance for the stack. The equation used to determine ε_{33}^T is

$$\varepsilon_{33}^T = \frac{C^T t_l}{AN} \tag{4.4}$$

The measured capacitance and dielectric constant have been shown in Table 4.6. and the typical representative time trace curve and voltage-charge relation is shown in Fig. 4-7 and 4-8.
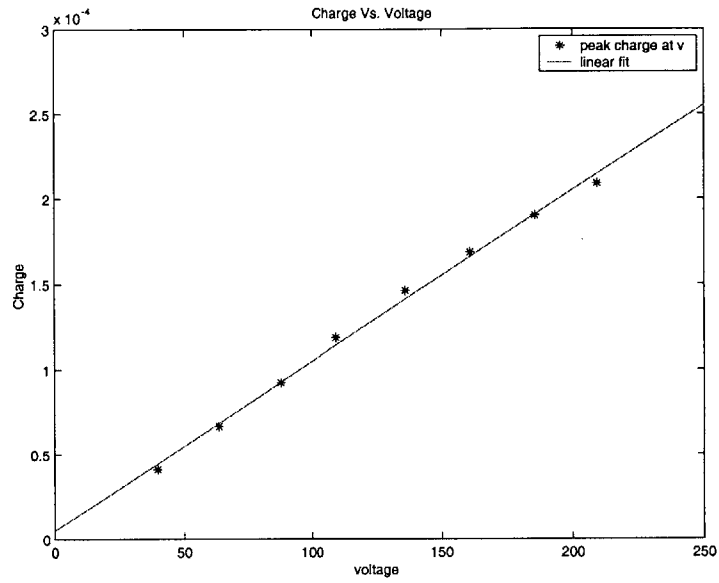
Figure 4-8: Charge vs. Volatge for Capacitance Measurement

C nF	1004.0	1008.0	999.79	999.37	1022.7	1013.8	1001.2
C Ave.	1006.98 nF						
ε_{33}^T	38730 F/m						
$\varepsilon_{33}^T/\varepsilon_0$	4376.3						

Table 4.6: Measured Capacitance and Dielectric Constant for Sumitomo Stack
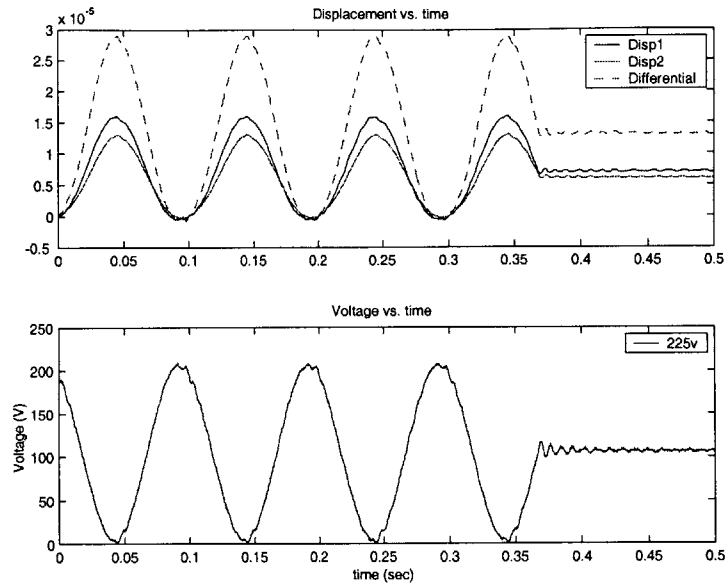
77

Figure 4-9: Time Trace of Displacement and Voltage for Stack d_{33} Measurement

4.3.4 Electromechanical Coupling Term

The test for measuring the electromechanical coupling term was similar to the capacitance measurement test. The driving frequency used was 10 Hz and the applied voltage to the driving stack was the same as shown in 4.3. Current and voltage was monitored in the same manner. The difference between the two tests was that the actuator was placed on the support and held in a horizontal position, while two Fotonic sensors were used to measure the displacement of the Sumitomo stack during actuation. The electromechanical coupling term was found using the following equation.

$$d_{33} = \frac{(\frac{x}{V})t_l}{l} \tag{4.5}$$

The measured electromechanical coupling term was shown in Table 4.7. and the typical representative time trace curve and voltage-displacement relation is shown in Fig. 4-9 and 4-10.
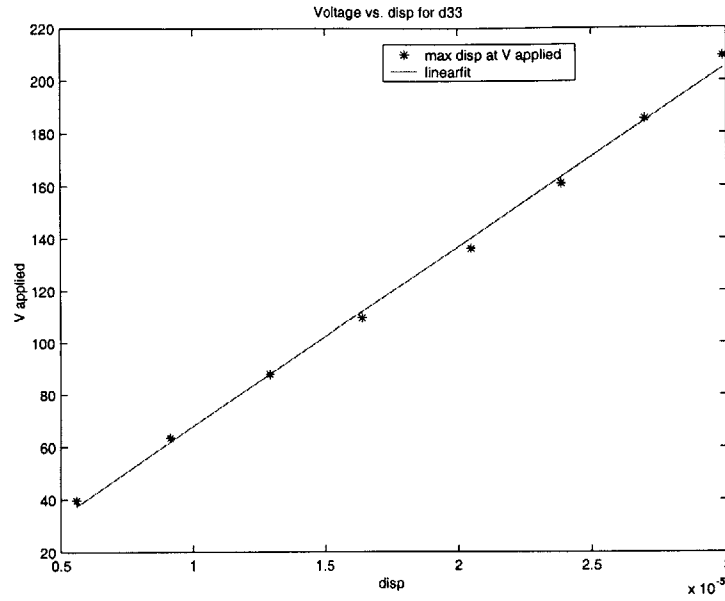
78

Figure 4-10: Displacement vs. Voltage for Stack d_{33} Measurement

4.3.5 Material Coupling Coefficient

The material coupling coefficient can be determined based on the material properties which have be measured using equation 1.1. The computed the material coupling coefficient k_{33} for Sumitomo stack was 0.6928.

4.3.6 Material Properties Summary

The measured material properties are summarized in Table 4.7. The accuracy of the measured material properties of the Sumitomo stack can be examined through the equation which related s^D and s^E:

$$s^D = s^E - d_t(\varepsilon)^{-1}d \tag{4.6}$$

For one dimensional systems, equation 4.6 can be simplified as

$$s_{33}^D = s_{33}^E - d_{33}(\varepsilon_{33}^T)^{-1}d_{33} \tag{4.7}$$

79

	Specification	Measured Value
Stiffness k^E 10^6 N/m		20.934
Stiffness k^D 10^6 N/m		40.924
Elastic Constant s_{33}^E 10^{-12} m^2/N		30.198
Elastic Constant s_{33}^D 10^{-12} m^2/N		15.458
Capacitance nF	800±20%	1006.98
Dielectric Constant $\varepsilon_{33}^T/\varepsilon_0$	3570	4376.3
Electromechanical Coupling d_{33} 10^{-12} m/V	778	728.987
Material Coupling Coefficient k_{33}		0.6928

Table 4.7: The Measured Material Properties for Sumitomo Stack

Substitute the material properties listed in Table 4.7, we can find S_{33}^D:

$$\begin{aligned} s_{33}^D &= 30.198 \times 10^{-12} - \frac{(728.987 \times 10^{-12})^2}{4376.3 \times 8.85 \times 10^{-12}} \\ &= 16.477 \times 10^{-12} \end{aligned}$$

There is only a 6% error between the computed s_{33}^D and the measured s_{33}^D in the table.

4.4 Actuating Voltage for Test Sample

4.4.1 Linear and non-linear Functions

With the material properties of the Sumitomo stack measured, it is possible to rewrite equations 2.6, 2.7 and 2.8 for the convenience of analysis. The three loading functions can be written in the form of equation 2.48:

$$f_{lin} = \alpha k_{p1}^E x \tag{4.8}$$

$$f_{non1} = \alpha k_{p1}^E \cdot 41x \cdot \exp\left(-5.45\left(\frac{x}{x_{free}}\right)^{0.5}\right) \tag{4.9}$$

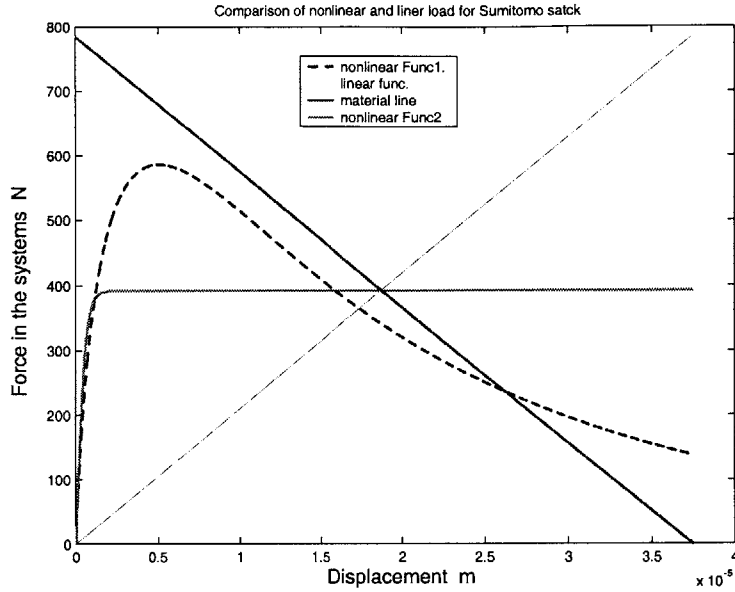$$f_{non2} = \alpha k_{p1}^E \cdot 0.5x_{free} \tanh\left(66\frac{x}{x_{free}}\right) \tag{4.10}$$

Figure 4-11: Linear and Non-linear Functions in terms of Displacement of the Actuator

And the material load line can be written as:

$$f_{material} = k_{p1}^E x_{free} - \alpha k_{p1}^E x \tag{4.11}$$

Where α is the stiffness ratio,which is the same as in equation 2.44 and 2.63. x_{free} is the maximum free displacement of the Sumitomo Stack, which can be expressed as

$$x_{free} = V_{\max} d_{33} \frac{l}{t_t} \tag{4.12}$$

The new linear and non-linear loading functions in terms of displacement have been shown in Fig. 4-11.

4.4.2 Actuating Voltage for Sumitomo Stack

The actuating voltage is not an important parameter for linear tests as long as the voltage is high enough for accurate current measurement. However, from the Fig. 4-11, we can see that the initial stiffness of the non-linear functions shown is very high. In order to allow the Sumitomo

81

stack to do more work under non-linear conditions than it could under linear conditions, the actuator should overcome this initial stiffness, and approach the maximum displacement or the displacement at balanced conditions, which are at the intersections of the material line and linear or non-linear loading lines. From the coupled analysis, however, we have found that the maximum displacement the actuator could approach is determined by the actuating voltage of the actuator.

To determine the actuating voltage for the test sample actuator, voltage-displacement relation from the coupled analysis as expressed by equation 2.15 was to be written in a convenient form. k_s for the linear and non-linear functions can be found by dividing the right hand side of equation 4.8, 4.9 and 4.10. Substitute these stiffness terms and the coefficients terms in K_{p1}^E and θ_1 expressed by equation 2.33 and 2.34, the new expression of the voltage-displacement relation for the linear and non-linear cases becomes:

Linear function:

$$V = \frac{1 + \alpha}{d_{33}l} t_l \tag{4.13}$$

Non-linear 1:

$$V = \frac{1 + 41\alpha \exp\left(-5.45\left(\frac{x}{x_{free}}\right)^{0.5}\right)}{d_{33}l} x t_l \tag{4.14}$$

Non-linear 2:

$$V = \frac{x + \frac{1}{2}\alpha x_{free} \tanh\left(66\frac{x}{x_{free}}\right)}{d_{33}l} t_l \tag{4.15}$$

For $\alpha = 1$, the voltage-displacement relations for different loading functions are shown in Fig. 4-12.

A close check of the voltage-displacement curve of non-linear function 1 has shown that the voltage should be higher than 235 V for the actuator to overcome the initial stiffness and generate large enough displacement. A higher voltage, however, is too close to the maximum allowed voltage of the actuator and could destroy the actuator. For non-linear function 2 this voltage can go lower, while for linear functions, it could go even lower. However, for the purpose of comparison of the linear and non-linear systems, we should drive the actuator at the same magnitude of voltage. 235 V has been chosen as the magnitude of test sample actuating voltage for all of the actuation tests in this research. As discussed in the stack material properties
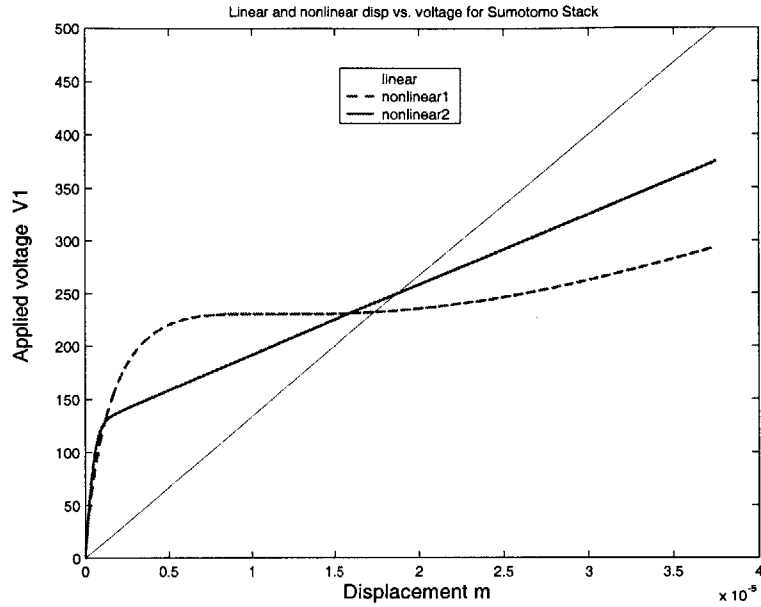
Figure 4-12: Voltage vs. Displacement from Coupled Analysis

measurement, an offset voltage was applied to the actuator to prevent the driving voltage from being negative, which may depolarize the sample. The applied voltage to the test sample, the Sumitomo stack, has been determined as

$$V_1 = 235 \left(\frac{1}{2} \sin \left(20\pi t + \frac{3}{2}\pi \right) + \frac{1}{2} \right)$$
(4.16)

4.5 Voltage-Force Model

From the feed forward approach diagram shown in Fig. 4-4, it is obvious that an accurate Voltage-Force Model is critical in determining the driving voltage for driving stacks from the required force in the system. The model has been developed in the same way as that of the coupled analysis was develpoed in chapter 2. However, here there are three components instead of two: the test sample piezo stack, the structure (connectors and load cells), and the driving piezo stacks. The system is shown as in Fig. 4-13.
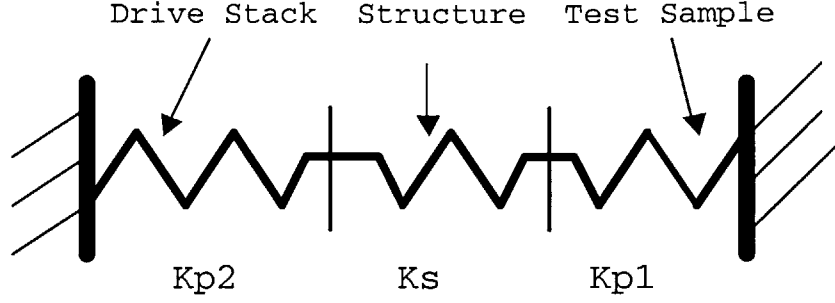
83

Drive Stack   Structure   Test Sample

Kp2   Ks   Kp1

Figure 4-13: Three Component System for Voltage-Force Model

4.5.1   Model Development

The method used for the model development is the same as that used for the coupled analysis derived in Chapter 2. The governing equations for the piezo active materials are the simplified actuator equation and sensor equation for quasi-static cases as in Chapter 2.

For the sample stack, the equations are exactly the same as equation 2.10. For the convenience of discussion, they are listed here again:

$$\begin{bmatrix} K_{p1}^E & -\theta_1 \\ \theta_1 & C_{p1}^S \end{bmatrix} \begin{Bmatrix} x_1 \\ V_1 \end{Bmatrix} = \begin{Bmatrix} f_1 \\ Q_1 \end{Bmatrix} \tag{4.17}$$

For the driving stack, they can be expressed as

$$\begin{bmatrix} K_{p2}^E & -\theta_2 \\ \theta_2 & C_{p2}^S \end{bmatrix} \begin{Bmatrix} x_2 \\ V_2 \end{Bmatrix} = \begin{Bmatrix} f_2 \\ Q_2 \end{Bmatrix} \tag{4.18}$$

For the structure, it can be expressed as

$$k_s x_s = f_s \tag{4.19}$$

The force balance equation in the system is given by:

$$f_1 = f_2 = f_s \tag{4.20a}$$

84

The compatibility equation is given by:

$$x_1 = -(x_2 + x_s) \tag{4.21}$$

From equation 4.17, 4.18, 4.19, 4.20a and 4.21, we can find out that

$$f = \frac{\frac{\theta_1 V1}{K_{p1}^E} + \frac{\theta_2 V2}{K_{p2}^E}}{\frac{1}{K_{p1}^E} + \frac{1}{K_{p2}^E} + \frac{1}{K_s}} \tag{4.22}$$

Assuming the same mechanical and electrical mode shapes as described by equation 2.31 and 2.32, we can find the coefficients in equation 4.22 using the same equations as shown in 2.33 and 2.34. Then the force model can be written as

$$f = \frac{d_{33p1} V1 + d_{33p2} V_2}{\frac{1}{K_{p1}^E} + \frac{1}{K_{p2}^E} + \frac{1}{K_s}} \tag{4.23}$$

Where $d_{33p1} = d_{33} \frac{l}{t_l}$ is the effective electromechanical coupling terms for the Sumitomo stack and d_{33p2} is that of the driving stack. From this equation we can see that if all the stiffness terms and the d_{33p2} are determined, we can find the driving voltage V_2 according to the sample voltage V_1 and the force in the system f. However, there are two problems which make it difficult to for us predict the driving voltage accurately using equation 4.23. First, this model is developed based on a simplified three component systems, assuming the system is clamped at both ends. Actually this is not true and there will be some displacement at both ends. An accurate model should include a few more springs in series or in parallel. Second, the three unknown coefficients in equation 4.23 should be measured accurately. Even if this has been done, the developed model still needs to be verified experimentally. For these considerations, we will determine the model in the form of this equation directly from experiments. This has been proven to be a very effective way.

85

4.5.2 Experimental Determination of model coefficients

The Voltage-Force expressed in equation 4.23 can be written as

$$f = aV_1 + bV_2 \qquad (4.24)$$

where a and b are undetermined.

The two coefficients were determined in two steps. First, the test sample was actuated, while the driving stack was at constant electrical field, i.e. $V_2 = 0$. The magnitude of the applied voltage to the test sample varied from a small voltage to its maximum, while the force in the system was recorded. The coefficient a was found from the linear fit of the peak V_1 vs. peak f relation. Second, both the sample stack and the driving stack were actuated to find coefficient b using the determined a. Since it was determined that the magnitude of test sample actuating voltage would be 235 V for all tests, the voltage expressed by equation 4.16 has been applied to test sample. The voltage applied to the driving stack is in the same form as expressed by equation 4.16, while the magnitude of the voltage varied from the lowest to the highest. The phase and frequency of the applied voltage to sample stack and driving stack were all the same. The frequency was 10 Hz with a phase difference of zero.

The experimental voltage-force relations are shown in Fig. 4-14 and Fig. 4-15. The experimental determined Voltage-Force Model can be expressed as

$$f = 2.1394V_1 + 1.3859V_2 \qquad (4.25)$$

4.6 Theoretical Predictions for systems driven by Sumitomo Stack

With the material properties measured, actuating voltage and frequency chosen and the Voltage-Force Model determined, it is possible toperform the linear and non-linear tests. The theoretical prediction of the electrical and mechanical work and actuation efficiency of the systems driven by the Sumitomo stack can provide some information for comparison. The linear and non-linear functions used are the same as those expressed in equation 4.8, 4.9 and 4.10. The driving
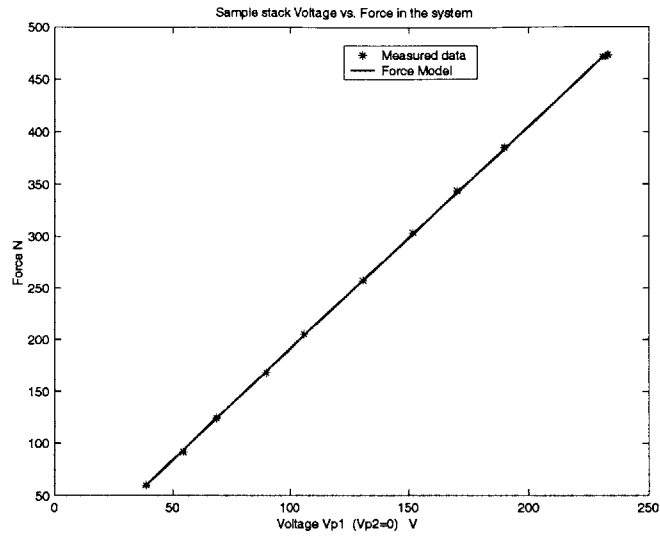
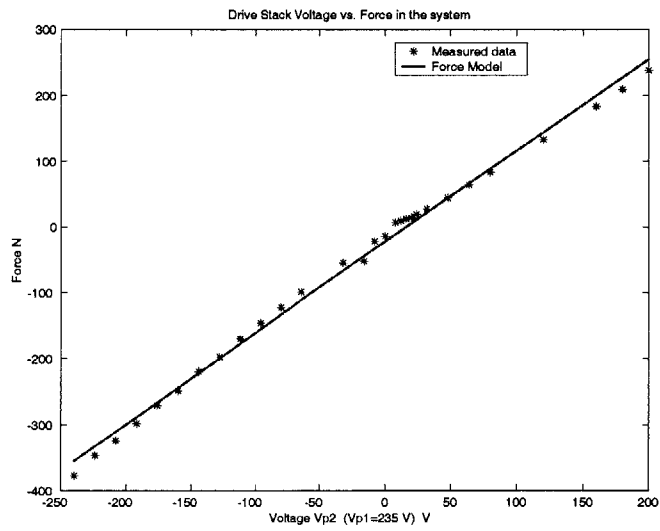Figure 4-14: Force vs. Voltage V1 for Voltage-Force Model

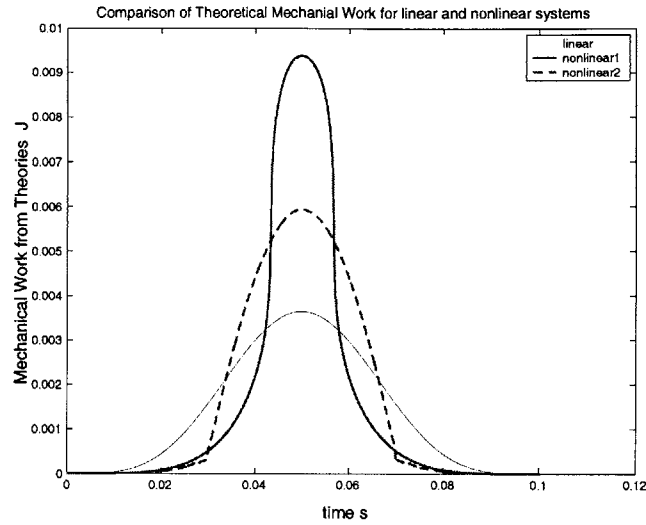Figure 4-15: Force vs. Voltage V1 and V2 for Voltage-Force Model

Figure 4-16: Prediction of Mechanical Work for Systems Driven by Sumitomom Satck

frequency for both the sample stack and the driving stack was 10 Hz and the actuating voltage of the sample stack was the same as expressed in equation 4.16. The stiffness ratio α is assumed to be 1. The results have been shown in Fig. 4-16, Fig. 4-17 and Fig. 4-18.

From these figures, we can obtain the similar information as was done in chapter 2. However, the system discussed here is real and the material properties used are measured. The mechanical work out of non-linear system1 is about 254% that of linear system, while the actuation efficiency of non-linear 1 is about 200% that of linear systems.

4.7 Linear Tests

As mentioned early, the linear tests have been done in a relatively easier way than the non-linear tests. Voltage was applied to both the sample stack, the Sumitomo stack, and the driving stack. The phase and the frequency of the applied voltage for the two stacks was all the same. The frequency chosen was 10 Hz and the phase difference was zero. The applied voltage to the sample stack was expressed by equation 4.16, while the voltage to the driving stack was either increased from zero to a higher magnitude gradually, simulating a higher structure stiffness or decreased from zero to a lower magnitude gradually, simulating a lower structure
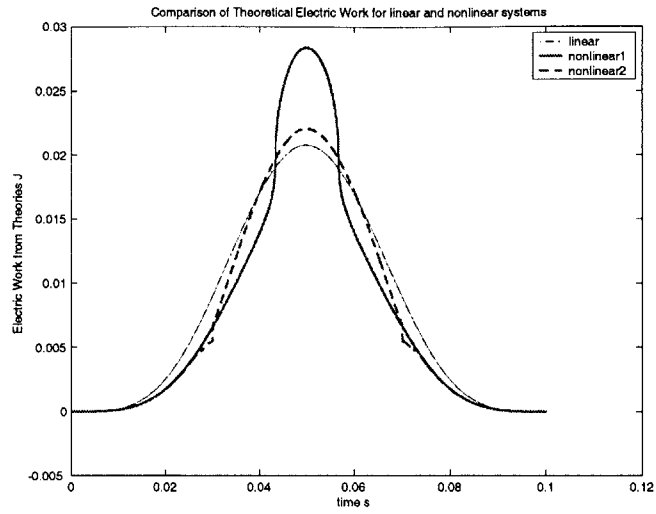
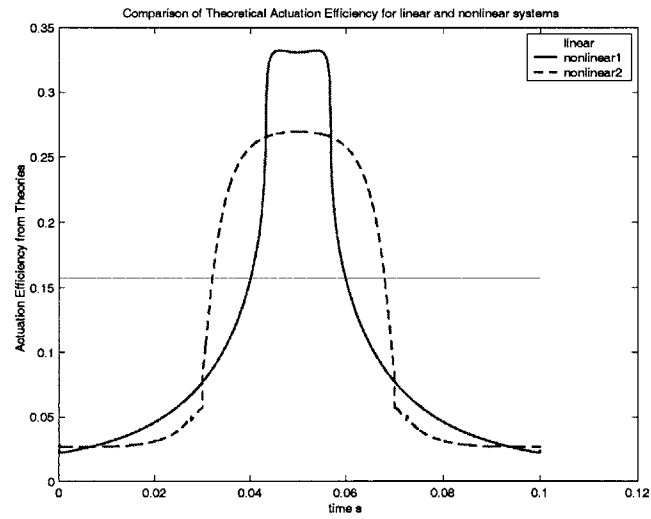Figure 4-17: Prediction of Electrical Work for Systems Driven by Sumitomo Satck

Figure 4-18: Prediction of Actuation Efficiency for Systems Driven by Sumitomo Satck

89

stiffness. During the voltage increasing or decreasing process, the displacement of the sample stack and the force in the systems was monitored carefully to prevent the sample stack from being over compressed by the driving stack or the sample stack dropping off. Effective stiffness of the structure was determined from the measured displacement and force data because the displacement of the structure was assumed to be the negative of that of the sample stack as expressed the compatibility equation 4.21.

The current and voltage in the circuit was obtained from the current and voltage monitor of the Trek amplifier, while the displacement and force data were taken from the Fotonic sensors, Kistler and Entran load cells.

The test results have been shown in the following figures. Fig. 4-19, Fig. 4-21 and Fig. 4-20 shows the measurement of the basic parameters. Fig. 4-22 shows the representative cycle for determining the effective stiffness, mechanical work, electrical work and actuation efficiency. These results have been shown in Fig. 4-23, 4-25, 4-24 and 4-26 where the experimental data were compared with the theoretical predications. The actuation efficiency was shown as a function of the stiffness ratio α.

The experimental mechanical and electrical work have been obtained from the following equations

$$W_M = \int_{x_0}^{x_f} F dx \tag{4.26}$$

$$W_E = \int_{t_0}^{t_f} V I dt \tag{4.27}$$

The experimental actuation efficiency was obtained from the ratio of the peak mechanical work to that of the electrical work.

The theoretical prediction for the mechanical work and electrical work was obtained from the following equations:

$$W_M = \frac{1}{2} N^2 \frac{A}{l} V_1^2 \varepsilon_{33}^T k_{33}^2 \frac{\alpha}{(1+\alpha)^2} \tag{4.28}$$

$$W_E = \frac{1}{2} N^2 \frac{A}{l} V_1^2 \varepsilon_{33}^T \left(1 - \frac{\alpha}{1+\alpha} k_{33}^2\right) \tag{4.29}$$
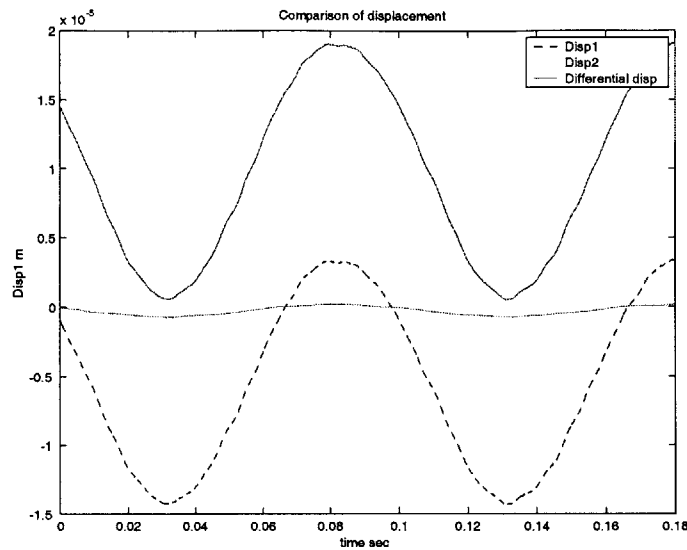
90

Comparison of displacement

Figure 4-19: Typical Displacement Measurement for Linear Tests

And the actuation efficiency was from the ratio of the two equations as expressed by equation 2.45.

From these figures, we can see that the experimental data of the mechanical work, electrical work and actuation efficiency correlate with the theoretical prediction very well.

4.8 Non-linear Tests

The test approach of non-linear tests was exactly as shown in Fig. 4-4. Voltage with the same frequency and the same phase were applied to both the sample stack and the driving stack. However, unlike in linear tests, the applied voltage to the driving stack was determined according to the Voltage-Force Model, while force was determined from the chosen non-linear loading functions and voltage applied to the sample stack was the same as expressed by equation 4.16. The frequency chosen was still 10 Hz and the phase difference of the two applied voltage was zero. The current and voltage in the circuit was obtained from the current and voltage monitor of the Trek amplifier, while the displacement and force data was taken from the Fotonic sensors and Kistler and Entran load cells.

The experimental mechanical and electrical work has been obtained using equation 4.26 and
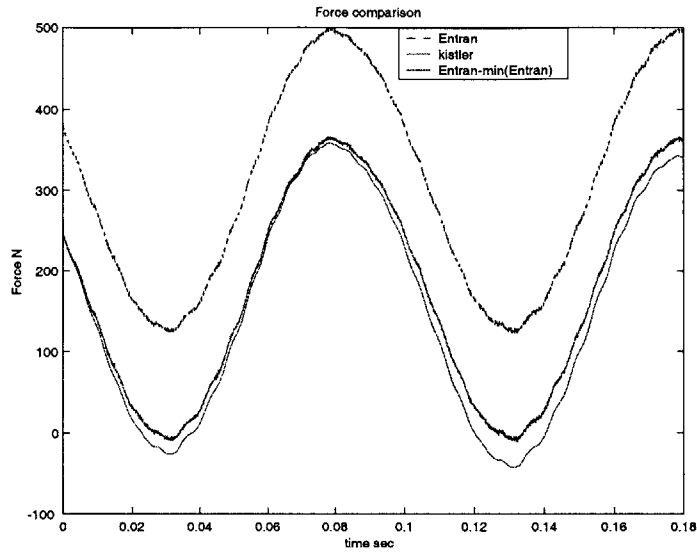
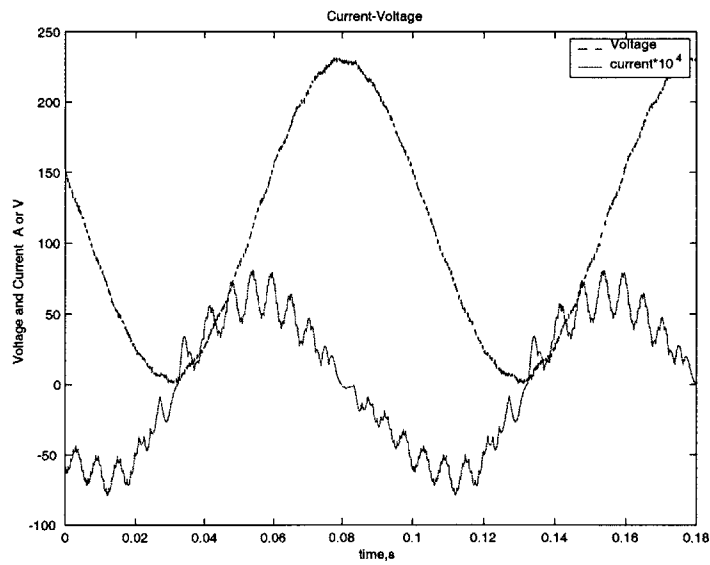Figure 4-20: Typical Force Measurement for Linear Tests

Figure 4-21: Typical Current and Voltage Measurement for Linear Tests
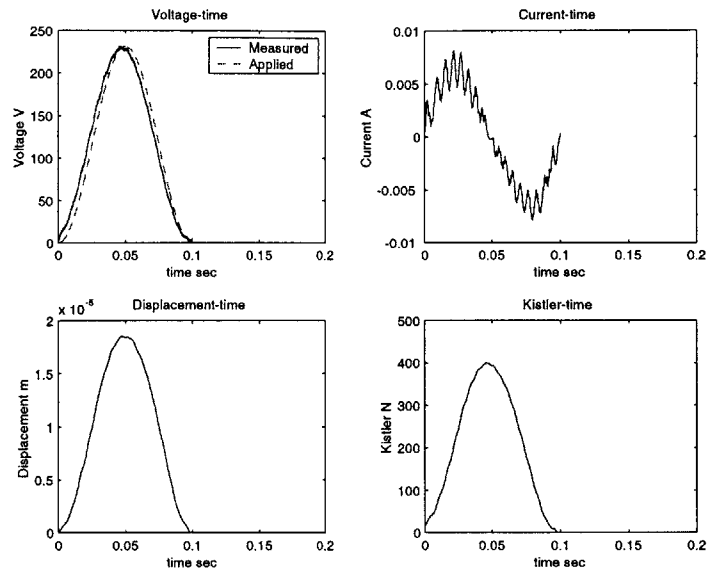
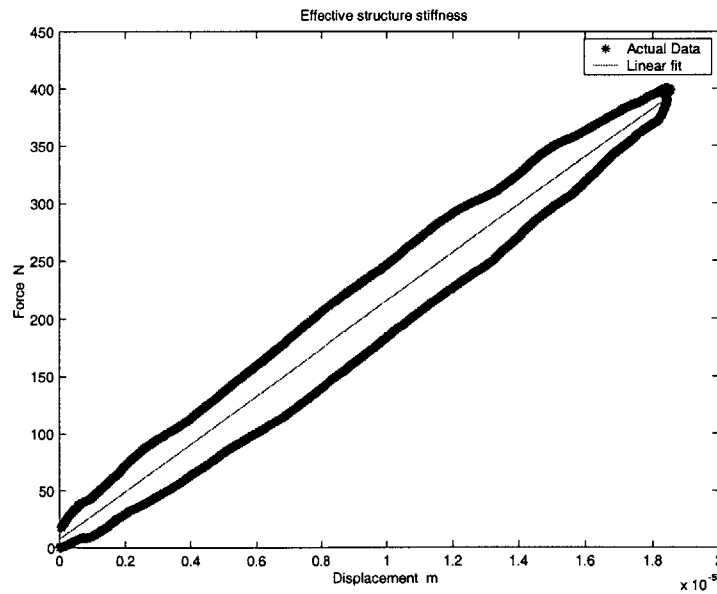Figure 4-22: The Resentative Cycle for Computing Work Terms

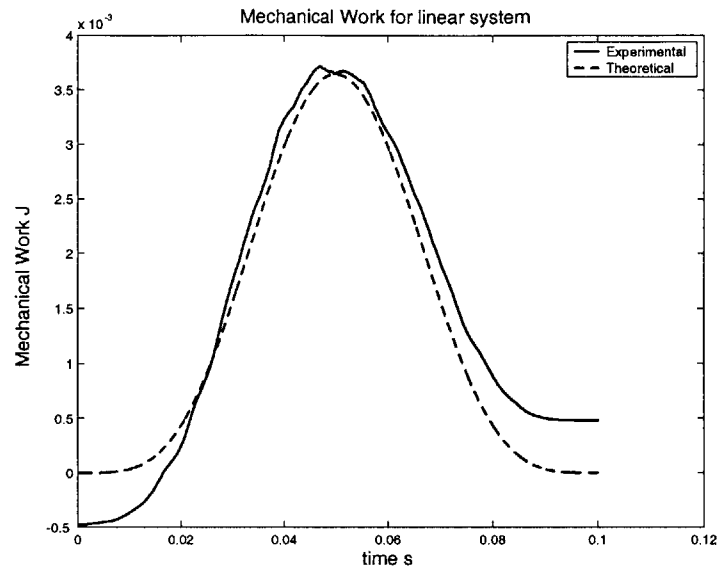Figure 4-23: Typical Effective Stiffness Determined from Actaul Data

93

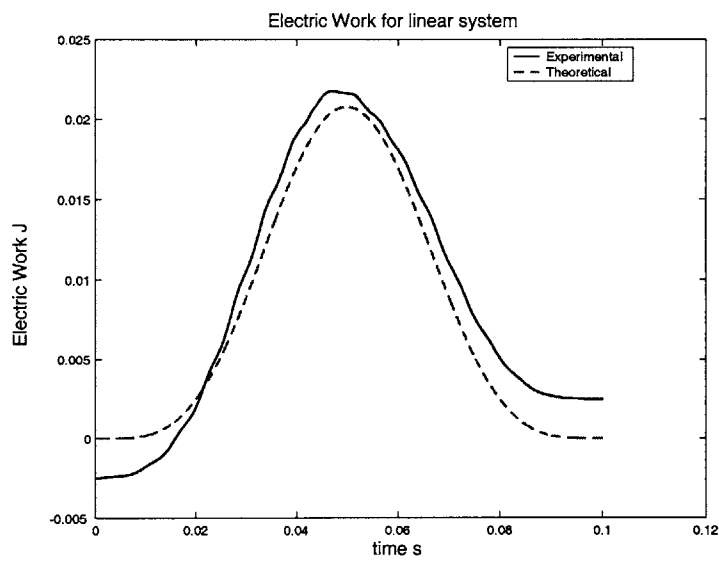Figure 4-24: Typical Mechanical Work from Theory and Experiment for Linear Test

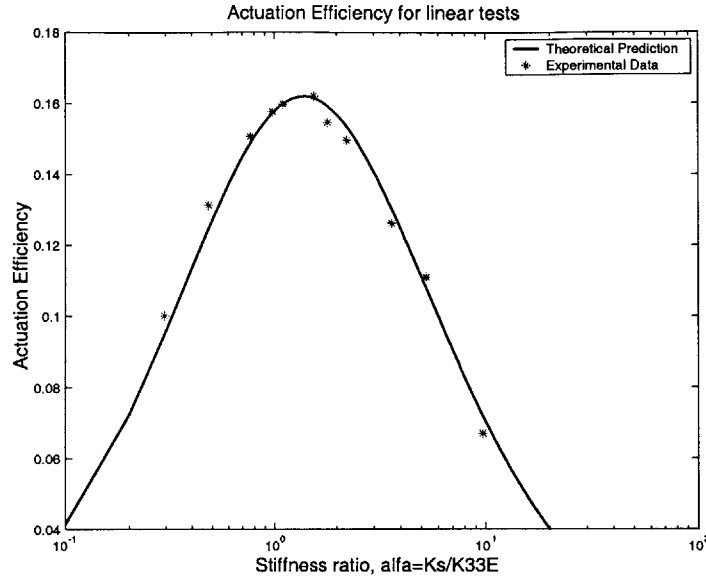Figure 4-25: Typical Electrical Work from Theory and Experiment for Linear Tests

Figure 4-26: Actuation Efficiency as a Function of Stiffness Rato Ks/K_{33}^E for Linear Tests

equation 4.27. Similarly the actuation efficiency was determined by the ratio of peak mechanical work to peak electrical work.

The theoretical mechanical work and electrical work has been determined by the following equations which is the same as expressed in Chapter 2 and are listed here for convenience. α was chosen to be 0.96 for safety consideration.

$$W_M = \frac{c_{33}^E A}{l} \alpha \int_{x_0}^{x_f} c_x x \, dx \tag{4.30}$$

$$W_E = \frac{c_{33}^E A}{l} \int_{x_0}^{x_f} (1 + \alpha c_x) x \, dx + \frac{c_{33}^E A}{l} \left(\frac{1}{k_{33}^2} - 1 \right) \int_{x_0}^{x_f} (1 + \alpha c_x)^2 x \, dx + \tag{4.31}$$

$$+ \frac{c_{33}^E A}{l} \alpha \left(\frac{1}{k_{33}^2} - 1 \right) \int_{x_0}^{x_f} (1 + \alpha c_x) x^2 \frac{dc_x}{dx} \, dx \tag{4.32}$$

The actuation efficiency was determined by the ratio of equation 4.30 and equation 4.31. For non-linear system 1 and 2, the non-linear part of the stiffness is expressed by equation 2.49 and equation 2.50 respectively.
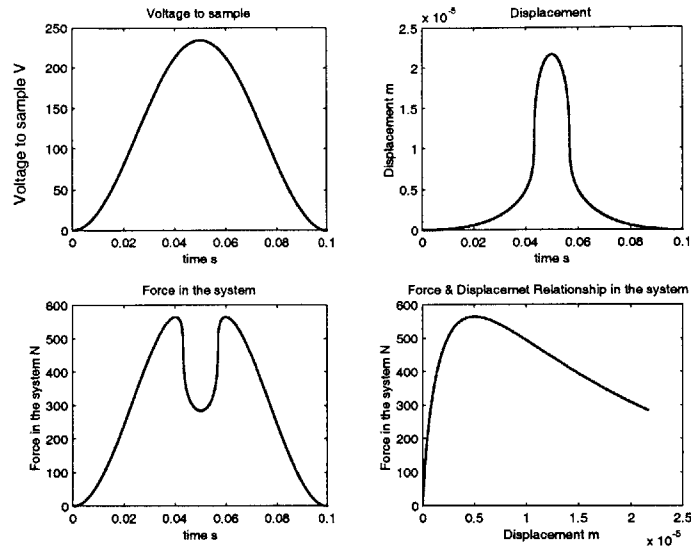
95

Figure 4-27: Predicted Displacement and Force for Non-linear Test 1

4.8.1 Non-linear system 1

Determination of Voltage to Drive Stack

As mentioned above, voltage to the driving stack was determined from the Voltage-Force model. The theoretically predicted displacement of the sample stack and the force in the system as well as the driving voltage to driving stack have been shown in Fig. 4-27 and 4-28.

Test Results

Test results have been shown in the following figures. Fig. 4-29, Fig. 4-30 and Fig. 4-31 show the measurement of basic parameters. Fig. 4-32 shows the representative cycle which was used to determine the experimental mechanical and electrical work and the actually simulated force-displacement relationship. Fig. 4-33, Fig. 4-34 and Fig. 4-35 shows the simulated force-displacement relationship, the mechanical work out and the electrical work in.
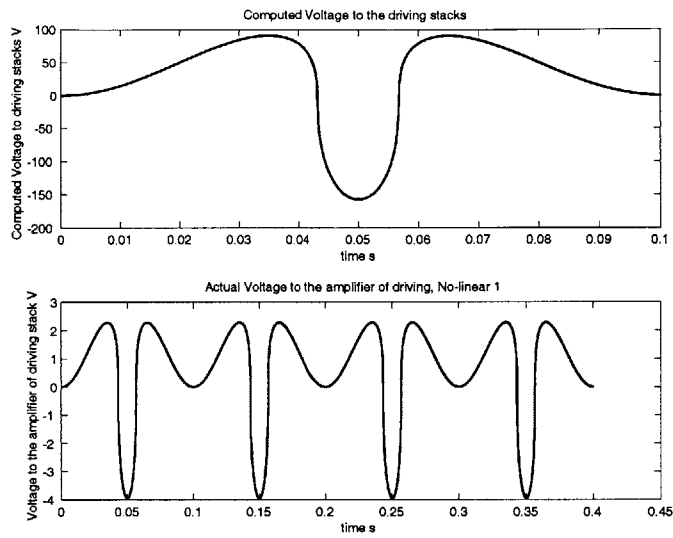
96

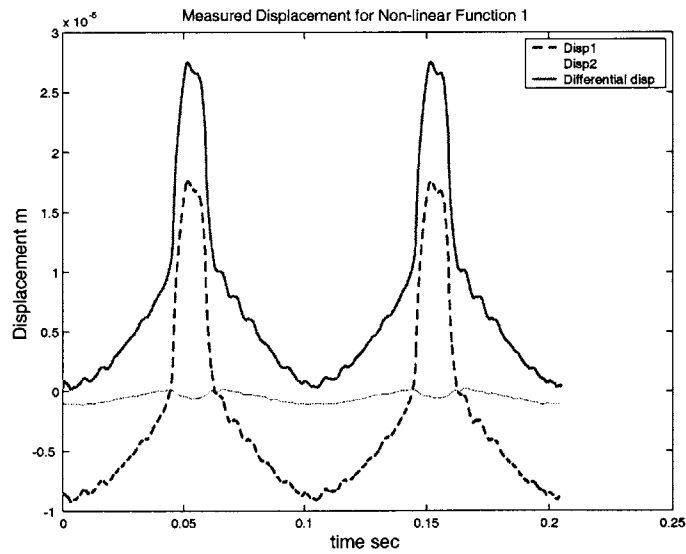Figure 4-28: Predicted Voltage to the Driving Stack for Non-linear Test 1

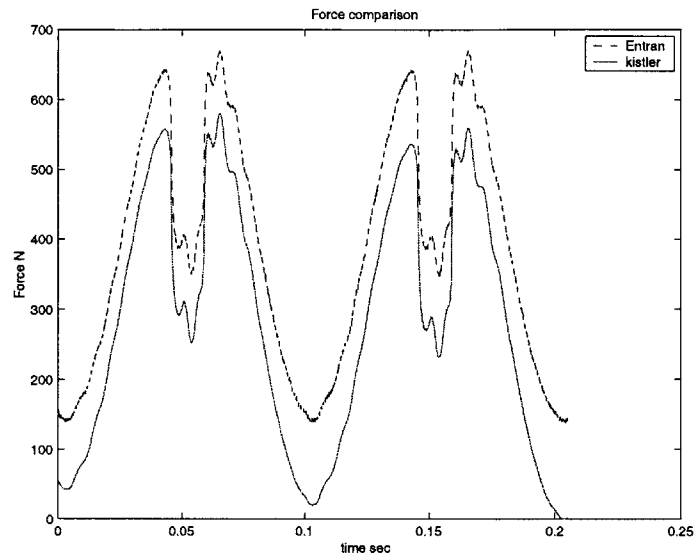Figure 4-29: Measured Displacement of Sample for Non-linear System 1

97

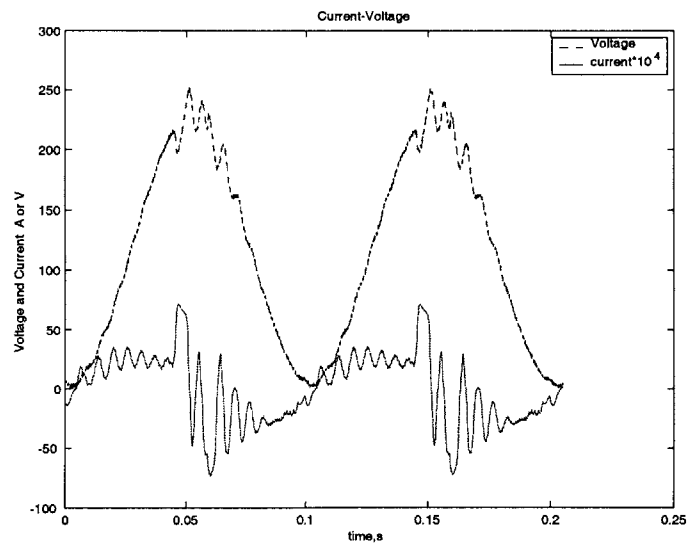Figure 4-30: Measured Force in the System for Non-linear System 1

Figure 4-31: Measured Volatge and Current for Non-linear Test 1
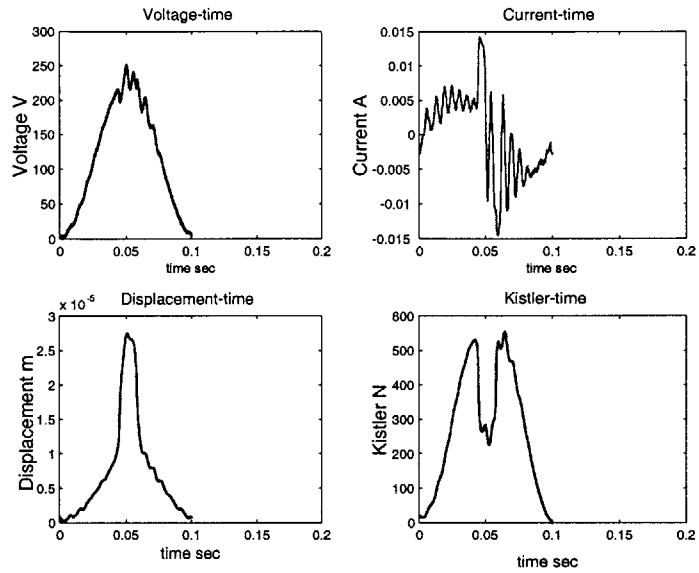
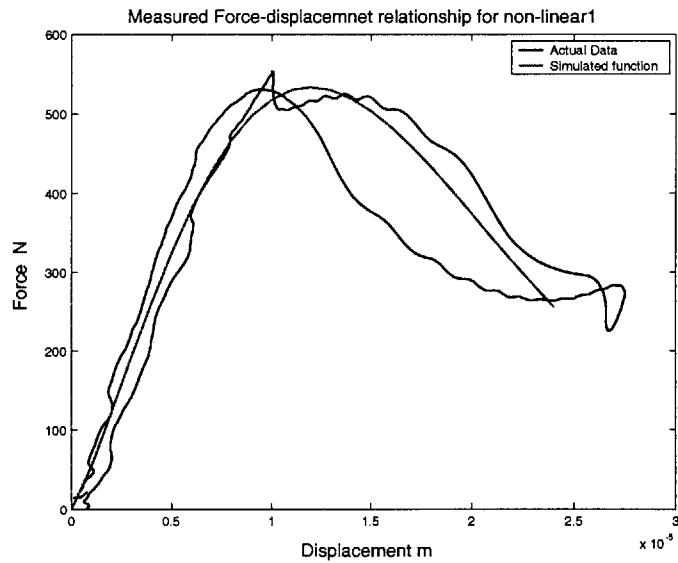Figure 4-32: Representative Cycle for Work terms for Non-linear 1

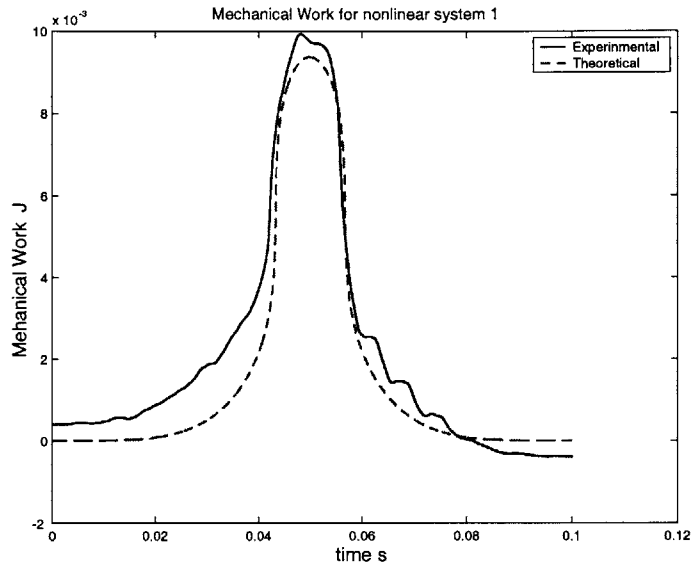Figure 4-33: Simulated Force vs. Displacement for Non-linear1

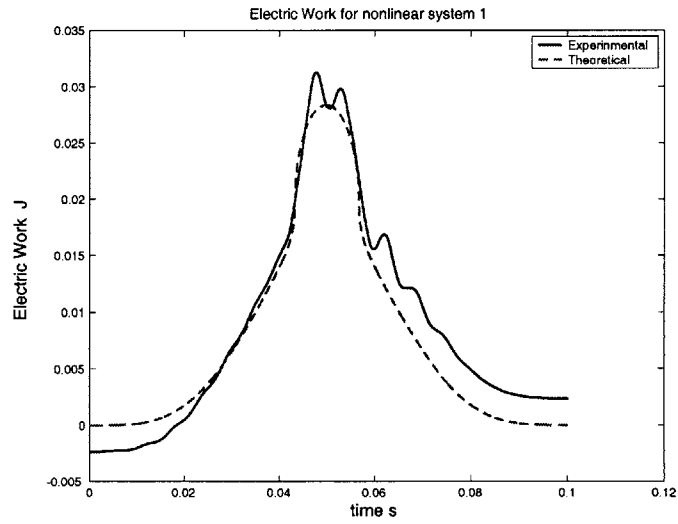Figure 4-34: Mechanical Work out Comparison for Non-linear System 1

Figure 4-35: Electrical Work in Comparison for Non-linear System 1
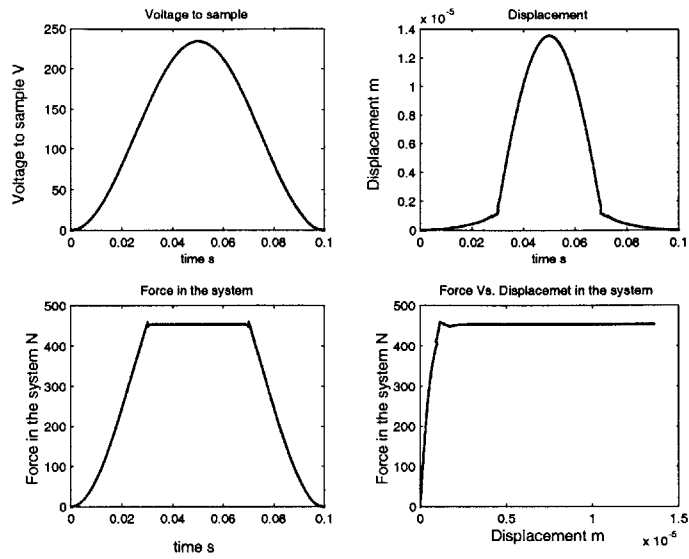
100

Figure 4-36: Predicted Force and Displacement for Non-linear 2

4.8.2 Non-linear system 2

Determination of Voltage to Drive Stack

Similar to non-linear systems 1, voltage to the driving stack for non-linear system 2 was also determined from the Voltage-Force model. The theoretically predicted displacement of the sample stack, the force in the system, as well as the driving voltage to driving stack, have been shown in Fig. 4-36 and 4-37.

Test Results

Test results have been shown in the following figures. Fig. 4-38, Fig. 4-39 and Fig. 4-40 shows the measurement of the basic parameters. Fig. 4-41 shows the representative cycle which was used to determine the experimental mechanical and electrical work and the simulated force-displacement relationship. Fig. 4-42, Fig. 4-43 and Fig. 4-44 shows the simulated force-displacement relationship, the mechanical work out and electrical work in.

101
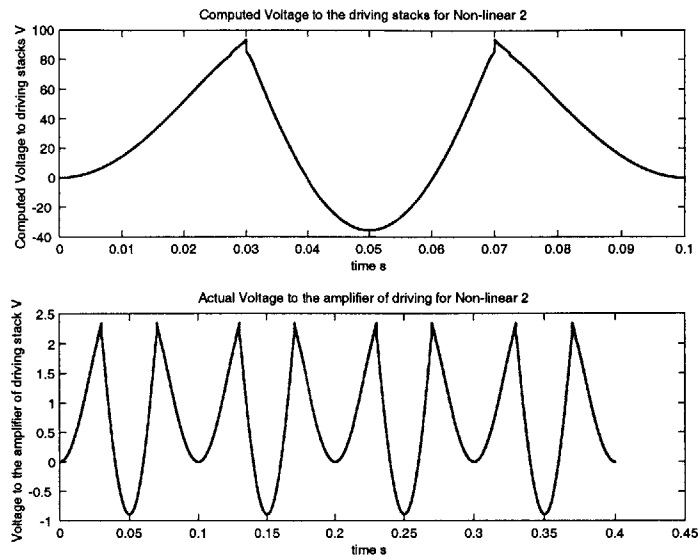
Figure 4-37: Computed Voltage to Driving Stack for Non-liner 2
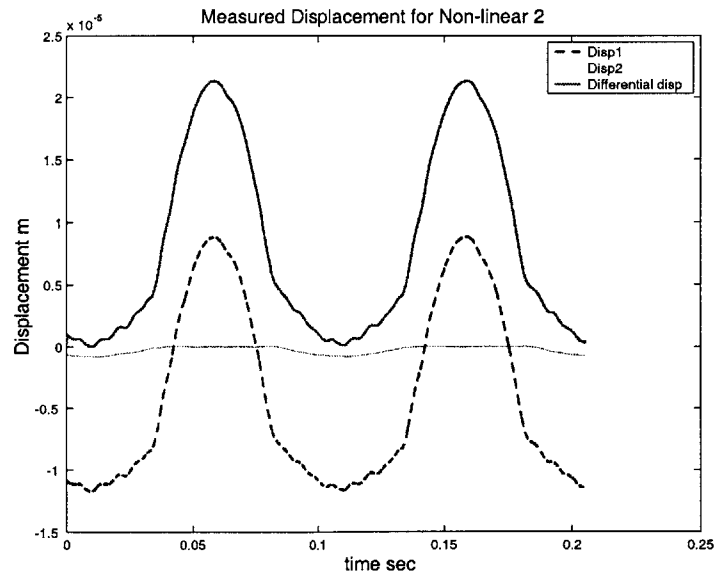
Figure 4-38: Measured Displacement of Sample for Non-linear System 2

Figure 4-39: Measured Force in the system for Non-linear System 2

Figure 4-40: Measured Current and Voltage for Non-linear System 2

Figure 4-41: Representative Cycle for determining Work Terms for non-linear 2

Figure 4-42: Simulated Force vs. Displacement for Non-linear System 2

104
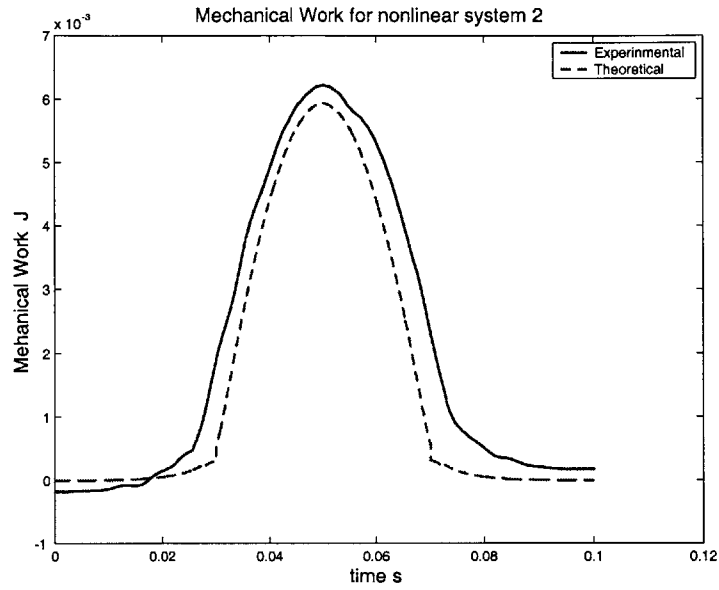
Figure 4-43: Mechanical Work out Comparison for Non-linear system 2
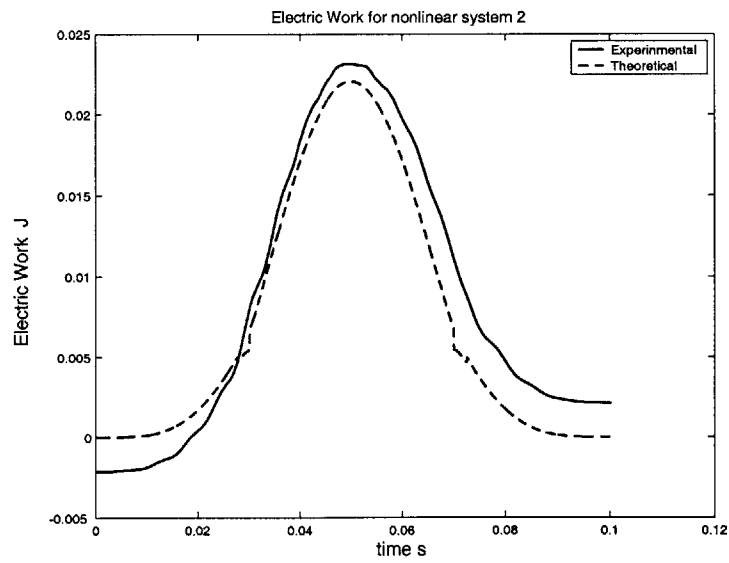
Figure 4-44: Electrical Work in Comparison for Non-linear system 2

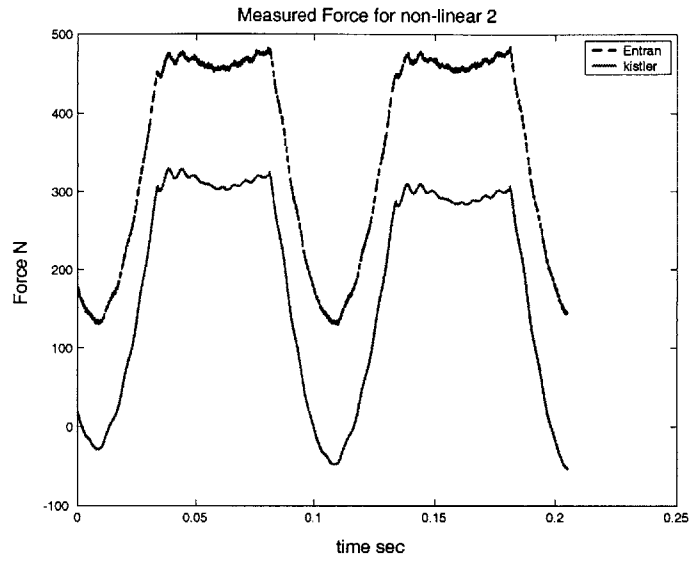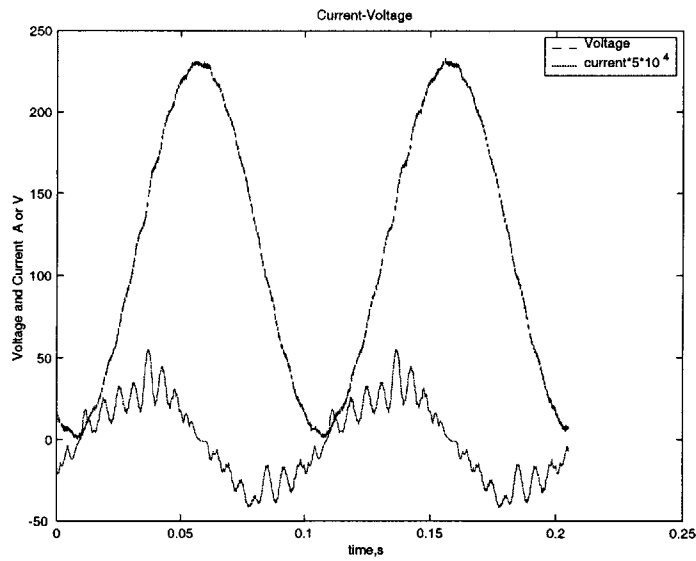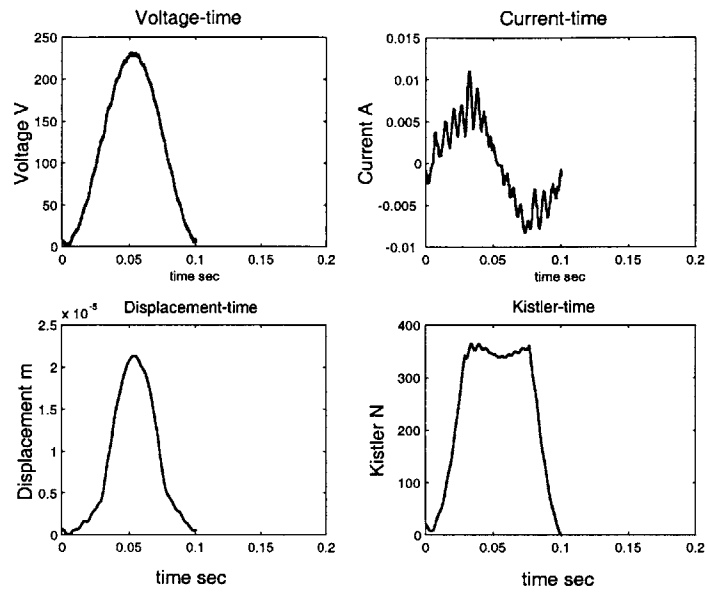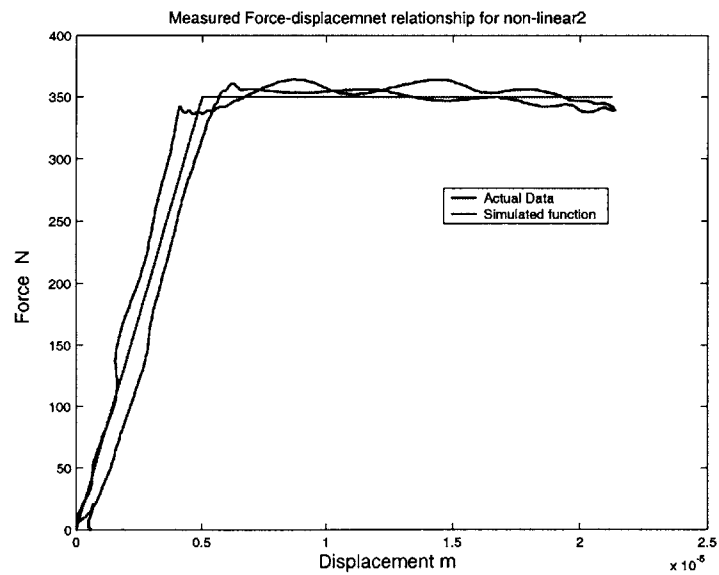|	Linear System	Non-linear System 1	Non-linear System 2
Predicted	0.1578	0.3321	0.2693
Measured	0.1496	0.3181	0.2596

Table 4.8: Comparison of Actuation Efficiency for Linear and Non-linear Systems
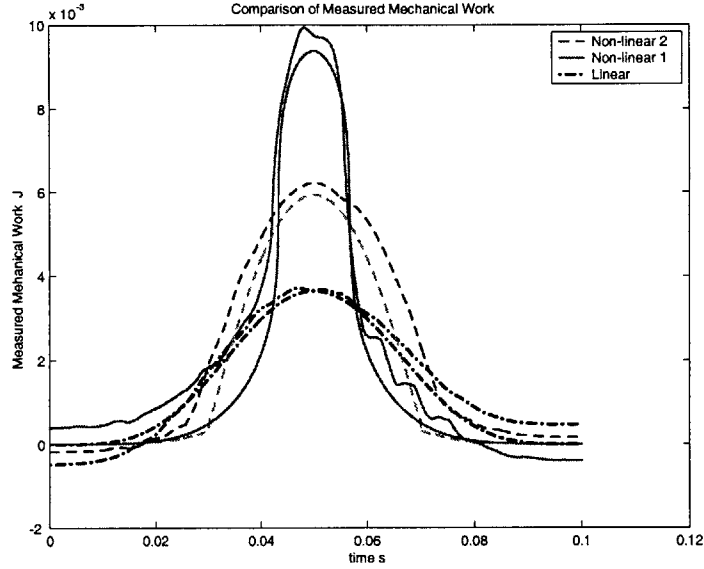
Figure 4-45: Comparison of Mechanical Work for Linear and Non-linear Systems

4.9   Comparison and Discussion

The experimental and theoretical mechanical work and electrical work for both linear and non-linear systems has been compared in Fig. 4-45 and Fig. 4-46. The actuation efficiency of the linear and non-linear systems was listed in Table 4.8. The stiffness ratio α is 0.96.

From the table we can see that actuation efficiency of the non-linear systems is about 200% that of the linear systems. From the figures of mechanical work of the linear and nonlinear systems, we can see that the mechanical work out of the non-linear system is about 250% that of the linear systems. The theoretical predictions correlate with experimental results very well. This has verified theoretical prediction made in Chapter 2.

106
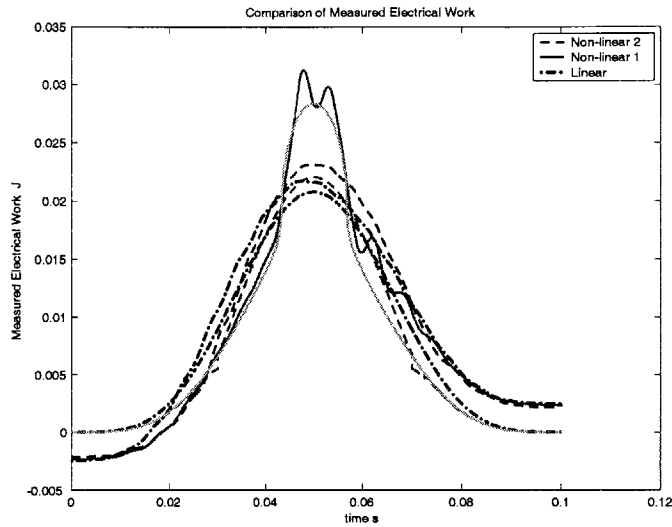
Figure 4-46: Comparison of Electrical Work for Linear and Non-linear Systems

4.10 Summary

All the linear and non-linear test results and their correlation with theoretical prediction have been discussed. The feedback control methodology used previously and have been replaced by a feedforward approach. The Voltage-Force model needed for the simulated actuator-structure-actuator system has been derived using the Rayleigh-Ritz formulation, and the related coefficient in its expression have been determined by experiment. The magnitude of the voltage to the sample stack is 235 V for all the linear and the non-linear tests, while the frequency of all the test is 10 Hz. For the linear systems, the test results have shown that the actuation efficiency is the highest when the stiffness ratio is larger than one, and this maximum value is much higher than that of the uncoupled analysis. For non-linear systems, the actuation efficiency of systems simulated by non-linear function 1 is about 200% that of the linear systems, while the work output of this system is about 250% that of the linear systems. The test results have exactly proved out the theoretical predictions.

Chapter 5

Non-Conservative Systems

5.1 Net Work in Conservative Systems

Up to now, all the systems discussed are conservative systems. The net electrical work input to the systems and the net mechanical work out of the systems is all zero. This can be seen from Fig. 4-45 and Fig. 4-46. To do actual work on the environment, we need to choose non-conservative thermodynamic cycles.

5.2 Non-Conservative System and Its Efficiency

5.2.1 Non-Conservative Cycles

Highly non-linear functions can be used as thermodynamic cycles to do work on the environment. Such a cycle could be a circle or an elliptical circle or any other functions. The comparison of such a thermodynamic cycle with the non-linear function 1 analyzed in the previous chapters has been shown in. Fig. 5-1. A few more different such cycles have been shown in Fig. 5-2.

The general equation of the non-conservative cycles shown in 5-2 can be expressed as

$$x = d_1 \cos(\theta) + d_2 \sin(\theta) + d_{0x} \tag{5.1}$$
$$f = d_3 \cos(\theta) + d_4 \sin(\theta) + d_{0f}$$

Where $\theta = 0 - 2\pi$ is an independent variable. $d_1, d_2, d_3, d_4, d_{0x}$ and d_{0f} are all constants.
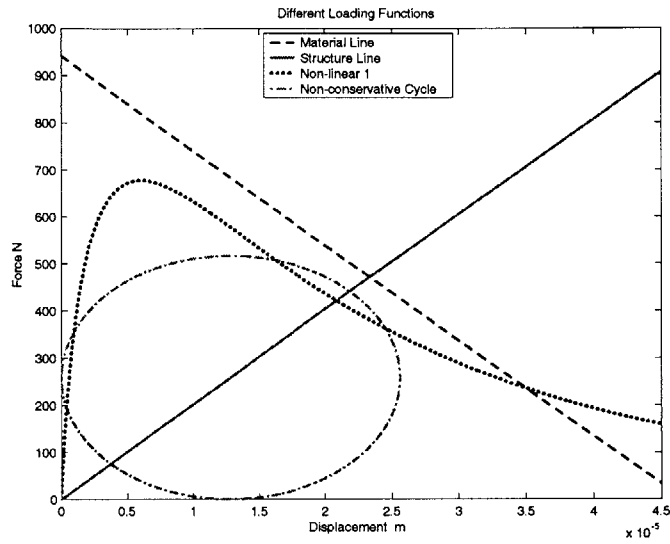
Figure 5-1: Comparison of non-linear function 1 with a Non-conservative Cycle
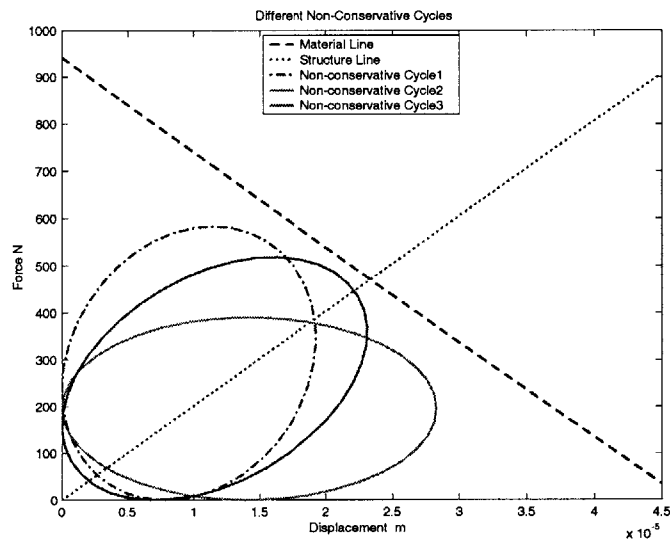

Figure 5-2: Different Non-Conservative Thermodynamic Cycles

5.2.2 Efficiency

For these non-conservative systems, The net work into the systems and net work out of the systems is not zero. The efficiency of the cycles can be defined as the ratio of net mechanical work out to net electrical work in expressed as

$$\eta = \frac{Net\_Wm\_out}{Net\_We\_in} \tag{5.2}$$

Where Net_Wm_out is net the mechanical work done on the environment, and Net_We_in is the net electrical work into the systems.

5.3 Experimental Demonstration

5.3.1 Simulation Methods

The non-conservative cycles shown in Fig. 5-2 can be simulated by driving the sample stack and the driving stack simultaneously, and maintaining a constant phase difference between the voltage to the sample and the voltage to the driving stack. For the purpose of demonstration, non-conservative cycle 1 shown in Fig. 5-2 has been chosen as an example. The test frequency and the driving voltage to the sample stack is the same as in the linear and the non-linear tests in Chapter 4. The driving voltage to the driving stack has been increased gradually to find out its influence on mechanical and electrical work as well as efficiency of the cycles simulated. The phase shift of the voltage to the driving stack is $\pi/2$.

Fig. 5-3 has shown the voltage to the sample and the driving stack for such an example.

5.3.2 Test Results

The test results have been shown in the following figures. Fig. 5-4, Fig. 5-5 and Fig. 5-6 show the measurement of basic parameters such as displacement, force, current and voltage. Fig. 5-7 shows the representative cycle which has be used to determine the experimental mechanical and electrical work and the simulated force-displacement relationship. Fig. 5-8, Fig. 5-10 and Fig. 5-9 show the simulated force-displacement relationship, the net mechanical work out and net electrical work in. for this cycle.

110
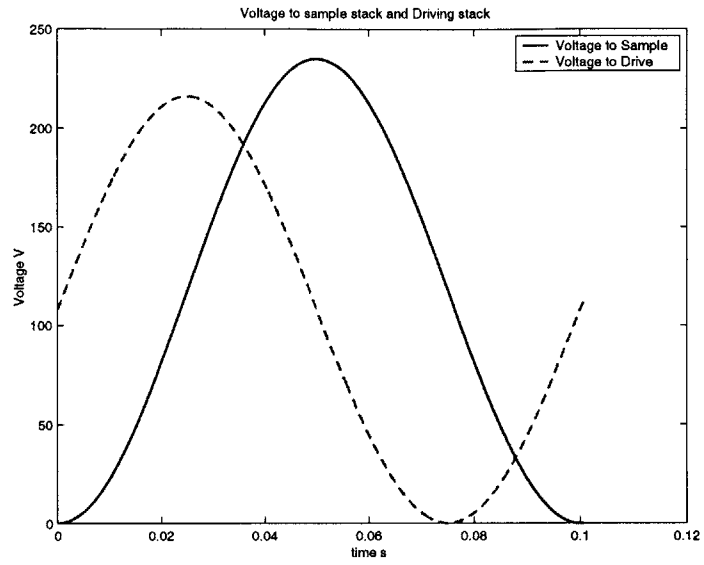
Figure 5-3: Voltage to the Sample and Driving Stacks
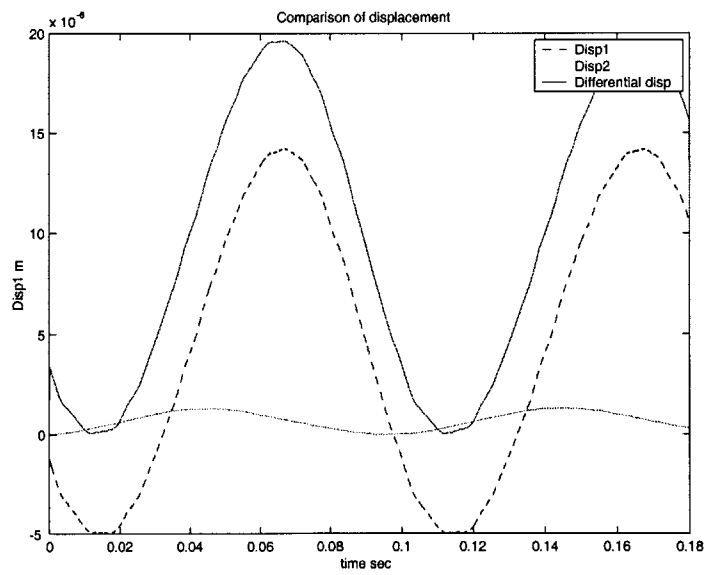
Figure 5-4: Displacement Measurement for a Non-Conservative Cycle

111
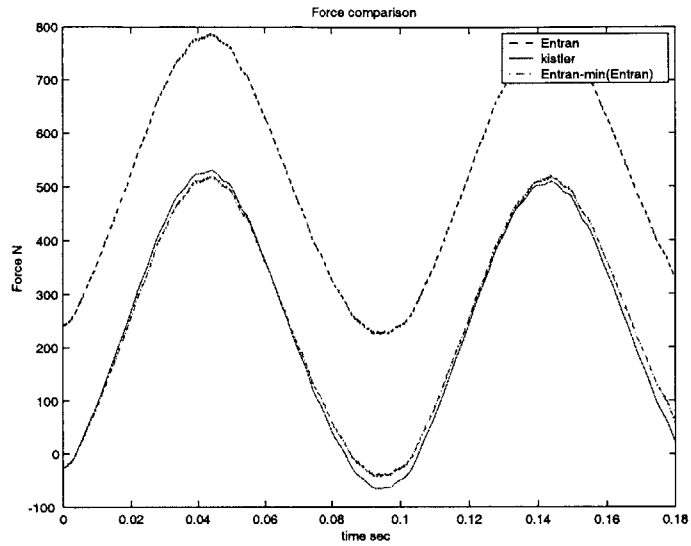
Figure 5-5: Force Measurement for a Non-Conservative Cycle
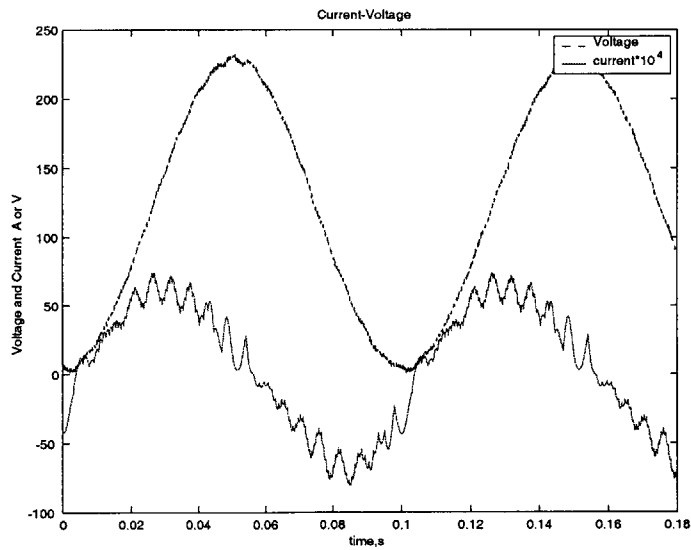
Figure 5-6: Current and Voltage Measurement for a Non-Conservative Cycle

112
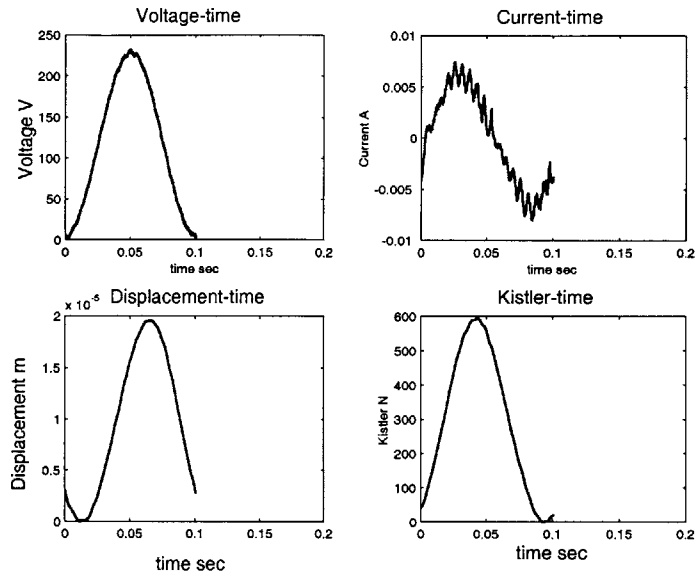
Figure 5-7: Representative Cycle for Determining Work and Efficiency
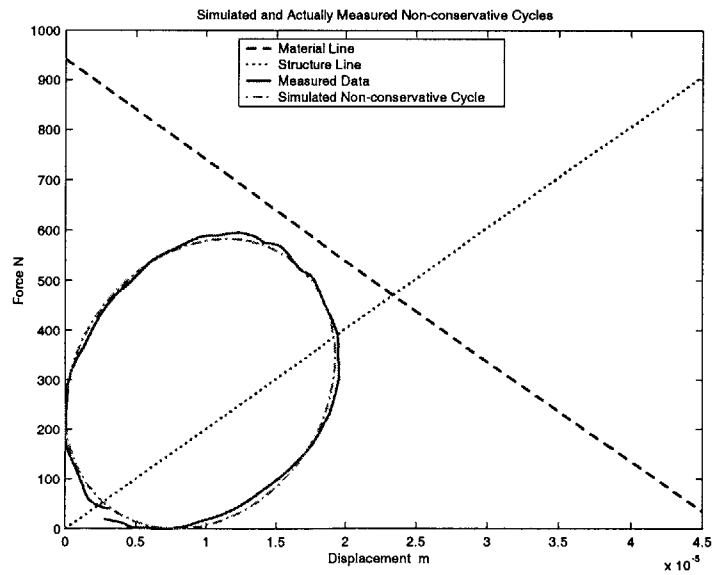
Figure 5-8: Comparison of the Non-Conservative Cycle 1 and the Actually Simulated Cycle
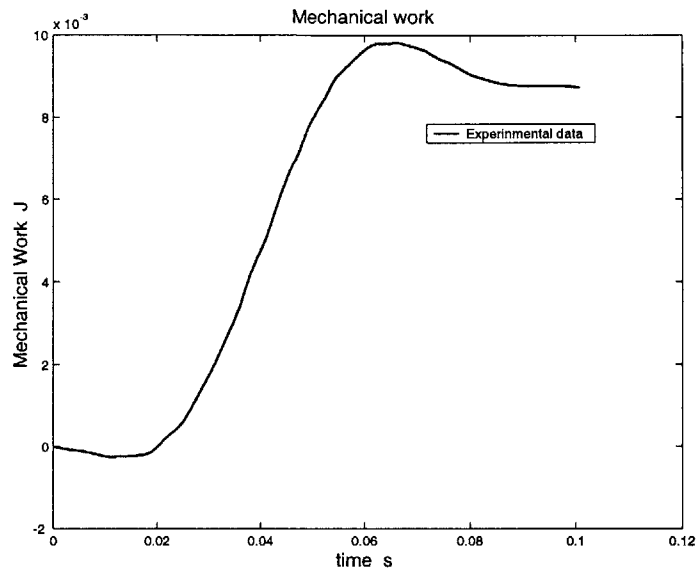
Figure 5-9: Net Mechanical Work Done by a Non-Conservative Cycle
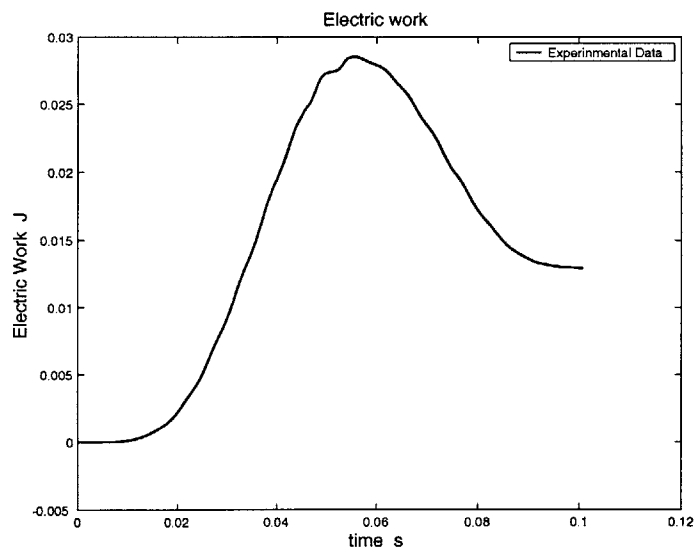
Figure 5-10: Net Electrical Work into a Non-Conservative Cycle

114

Mechanical and Electric Work in one Thermodynanic Cycle
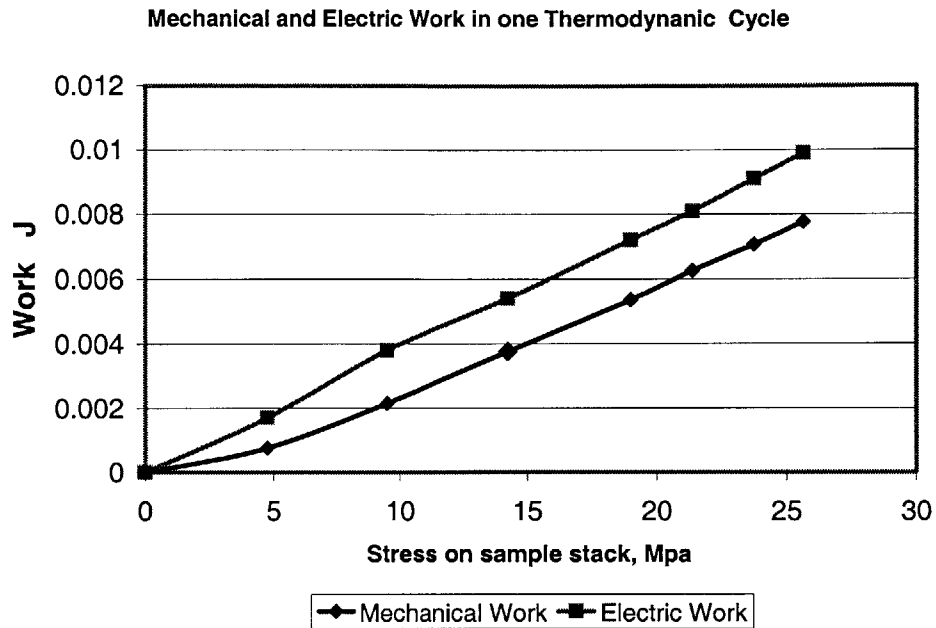
Figure 5-11: Mechanical work and electric work vs. Sstress on the sample stack

The influence of driving voltage to the driving stack on the mechanical work, electrical work and efficiency of the cycles have been shown in Fig. 5-12 and 5-11.

5.4 Summary

It has been shown that for the thermodynamic cycles chosen here the net work out of the systems is not zero. The non-conservative cycle 1 has been successfully simulated by driving the test sample and the driving stack simultaneously but maintaining a phase shift between the two driving voltages. The efficiency of the cycles increases with the increasing of the magnitude of voltage to the driving stack.

Efficiency of thermodynanic cycle vs. driving level (phase difference pi/2)

Figure 5-12: Efficiency of non-conservative cycles vs. stress on the sample stack

Chapter 6

Conclusions and Recommendations for Future Work

6.1 Conclusions on the Linear and the Non-linear Tests

The work presented has demonstrated that actuation efficiency viable metric coupled systems. Different expressions such as material coupling coefficient, device coupling coefficient and actuation efficiency, which have been used to describe and evaluate the energy flow and efficiency of coupled systems, have been compared and contrasted. It has been found that load coupling effects the performance for both linear and non-linear systems. The true thermodynamic actuation efficiency expressed as the ratio of work output to work input of a system can incorporate the coupling effects better than material coupling coefficient. Thus, actuation efficiency is more efficient and more accurate in evaluating the performance and behavior of a system.

Through the coupled analysis and tests of piezoelectrically driven systems, the performance of linear systems have been better understood. For a linear system in which a piezoelectrically active material working against a linear load, it is believed traditionally that the maximum efficiency of systems is a quarter of the material coupling coefficient squared. This maximum is reached when the stiffness ratio of structure and piezo active material equals one. However, the coupled analysis and tests in this research have shown that actuation efficiency is the highest when the stiffness ratio is larger than one, and this maximum value is much higher than that of the uncoupled analysis, although the efficiency of the uncoupled analysis does increase when

material coupling coefficient increases. These results agree very well with those found from the literature, and have been verified by the linear tests in this research. The test results correlate with theoretical prediction very well.

For a non-linear system in which a piezoelectrically active material working against a non-linear load, the coupled analysis has found out that it is possible to significantly increase the work output and actuation efficiency of the system. Two non-linear functions have been chosen for the demonstration. The test results have shown that the actuation efficiency of non-linear systems is much higher than that of linear systems. The actuation efficiency of systems simulated by non-linear function 1 is about 200% of that of the linear systems, while the work output of this system is about 254% of that of the linear systems. This has also been verified by tests.

The renovation of the component tester has proven to be a success. The previous tester was designed and built with programmable impedance and closed loop test capability. However, the feed back control method is not fast enough in determining the voltage for the driving stack which has limited the test frequency. Meanwhile, the original mechanical design can not guarantee the accurate measurement of mechanical work. Therefore, renovation of this tester is essential in experimental verification of the linear and non-linear theoretical predictions. The load transfer system of the tester has been redesigned and feedforward open loop test methodology has used instead of the feedback control. All the linear and non-linear tests have been conducted on the renovated test facility, and the theoretical predictions about the linear and non-linear systems have been experimentally verified.

6.2   Conclusions on Non-Conservative Systems

All the linear and non-linear tests done are for conservative systems. The net work on the environment has been shown to be zero. To do work into environment, non-conservative cycles have been chosen. Such cycles could be a circle or an elliptical circle. The efficiency of such a thermodynamic cycle can be defined as the ratio of net mechanical work out to the net electrical work in.

The net work out of the systems for non-conservative cycle 1 has been demonstrated to be

118

non-zero. The systems have been simulated by driving the test sample and the driving stack simultaneously but maintaining a phase shift between the two driving voltages. The efficiency of the cycles increases with the increasing of the magnitude of voltage to the driving stack.
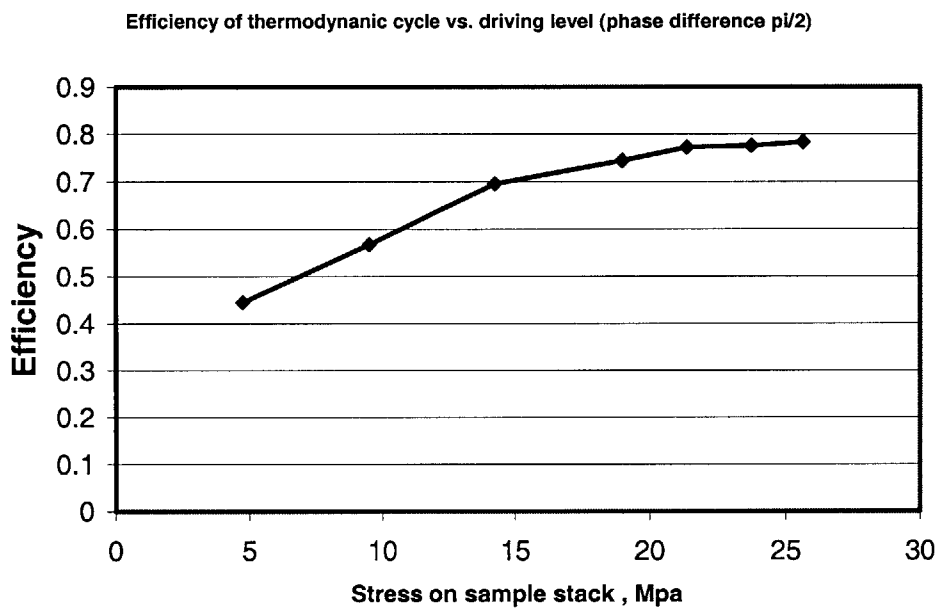
6.3   Recommendation for Future Work

This research has shown that the actuation efficiency of the non-linear systems is almost twice as high as that of the linear systems, and for the non-conservative systems, work can be done on the environment. This will highly reduce the complexity of the actuation systems for some applications such as a pump. However, the non-linear loading device and non-conservative cycle device must be designed and built first. A method of achieving such a non-linear system is to configure two springs into a triangle and looking at the behavior of the springs as they are loaded through the central platform they are connected, as explained in [Malinda1, 1999].

The analysis and tests presented here are all in quasi-static region. However, in some cases such the helicopter rotor blade and airplane wing applications, active materials undergo dynamic load. The behavior and performance of active materials and the actuation efficiency of the piezoelectrically driven systems under dynamic loads should be explored also.

Bibliography

[Bar-Cohen, 1999] Y. Bar-Cohen, X. Bao, et. al., "Rotary ultrasonic motors actuated by travelling flexural wave", *Proceedings of SPIE, Smart Structures and Materials 1999, Vol. 3668,* pp. 698-704, 1-4 March 1999, New Port Beach, California.

[Binghamand, 1999] B. S. Bingham, N. W. Hagood, M. J. Atalla, "Performance comparison of feedback and feedforward structural-acoustic control techniques", *Proceedings of SPIE, Smart Structures and Materials 1999, Vol. 3668,* pp. 698-704, 1-4 March 1999, New Port Beach, California.

[Berlincount, 1971] D. Berlincount, "Piezoelectric crystals and ceramics," *Ultrasonic Transducer Materials,* O. E. Mattiat, ed., Plenum Press, New York, 1971.

[Davis, 1999] C. L. Davis, F. T. Calkins te. al. " Predicting actuation efficiency of structurally integrated active materials" *Proceedings of SPIE, Smart Structures and Materials 1999, Vol. 3674,* pp. 476-486.

[Frank, 1999] J. E. Frank, G. H. Koopmann, et. al. "Design and performance of a high-force piezoelectric inchworm model," *Proceedings of SPIE, Smart Structures and Materials 1999, Vol. 3668,* pp. 717-723, 1-4 March 1999, New Port Beach, California.

[Giurgiutiu, 1997] "Power and energy characteristics of solid-state induced-strain actuators for static and dynamic applications," *Journal of Intelligent Material Systems and Structures,* Vol. 8, September 1997.

[Hagood, 1990]   N. Hagood, W. Chung, and A. von Flowtow, " Modeling of piezoelectric actuator dynamics for active structural control," *Journal of Intelligent Material Systems and Structures* 1[3], pp. 327-354, 1990.

[Hagood, 1991]   N. W. Hagood, A. V. Flotow, "Damping of structural vibrations with piezoelectric materials and passive electrical networks" *Journal of Sound and Vibration*, 146(2), pp243-268, 1991.

[Hall, 1996]   S. R. Hall, E. Prechtl, "Development of a piezoelectric servoflap for helicopter rotor control, " *Smart Materials and Structures*, Vol. 5, pp. 26-34, 1996.

[IEEE,1978]   *IEEE Standard on Piezoelectricity*, IEEE, inc., 1978.

[Karl, 2000]   K. Spanner, "Breakthrough in piezo actuator application," *Proceedings of the 7th International Conference on New Actuators*, B.2.0, 19-21 June 2000, Bremen, Germany.

[Lesieutre, 1997]   G. Lesieutre, C. Davis, " Can a coupling coefficient of a piezoelectric device be higher than those of its active material ?," *Journal of Intelligent Material Systems and Structures* 8[10], p. 859, 1997.

[Malinda1, 1999]   M. K. Lutz, "Study of work flow in piezoelectrically driven linear and non-linear systems," *Master Thesis,* Department of Aeronautics and Astronautics, Massachusetts Institute of Technology, 1999.

[Malinda, 1999]   M. K. Lutz, N. W. Hagood, "Actuation efficiency in piezoelectrically driven linear and non-linear systems", *Proceedings of SPIE, Smart Structures and Materials 1999, Vol. 3668,* pp. 780-796, 1-4 March 1999, New Port Beach, California.

[Mitrovic, 1999]   M. Mitrovic, G. P. Carman, et. al. "Electromechanical characterization of piezoelectric stack actuators," *Proceedings of SPIE, Smart Structures and Materials 1999, Vol. 3668,* pp. 586-601, 1-4 March 1999, New Port Beach, California.

[Roberts, 1999]   D. Roberts, "Development of a linear piezoelectric motor based upon the inchworm model," *Proceedings of SPIE, Smart Structures and Materials 1999, Vol. 3668*, pp. 705-716, 1-4 March 1999, New Port Beach, California.

[Varadan, 2000]   V. K. Varadan, V. V. Varadan, " Microsensors, microelectromechanical systems (MEMS), and electronics for smart structures and systems," *Smart Materials and Structures*, Vol. 9, pp. 953-972.,2000.

Appendix A

Component Testing Facility Drawings

The following pages contain the complete set of the mechanical drawings for the renovation of the Component Testing Facility. The materials used and the tolerances of each part have been specified on each of the drawings.
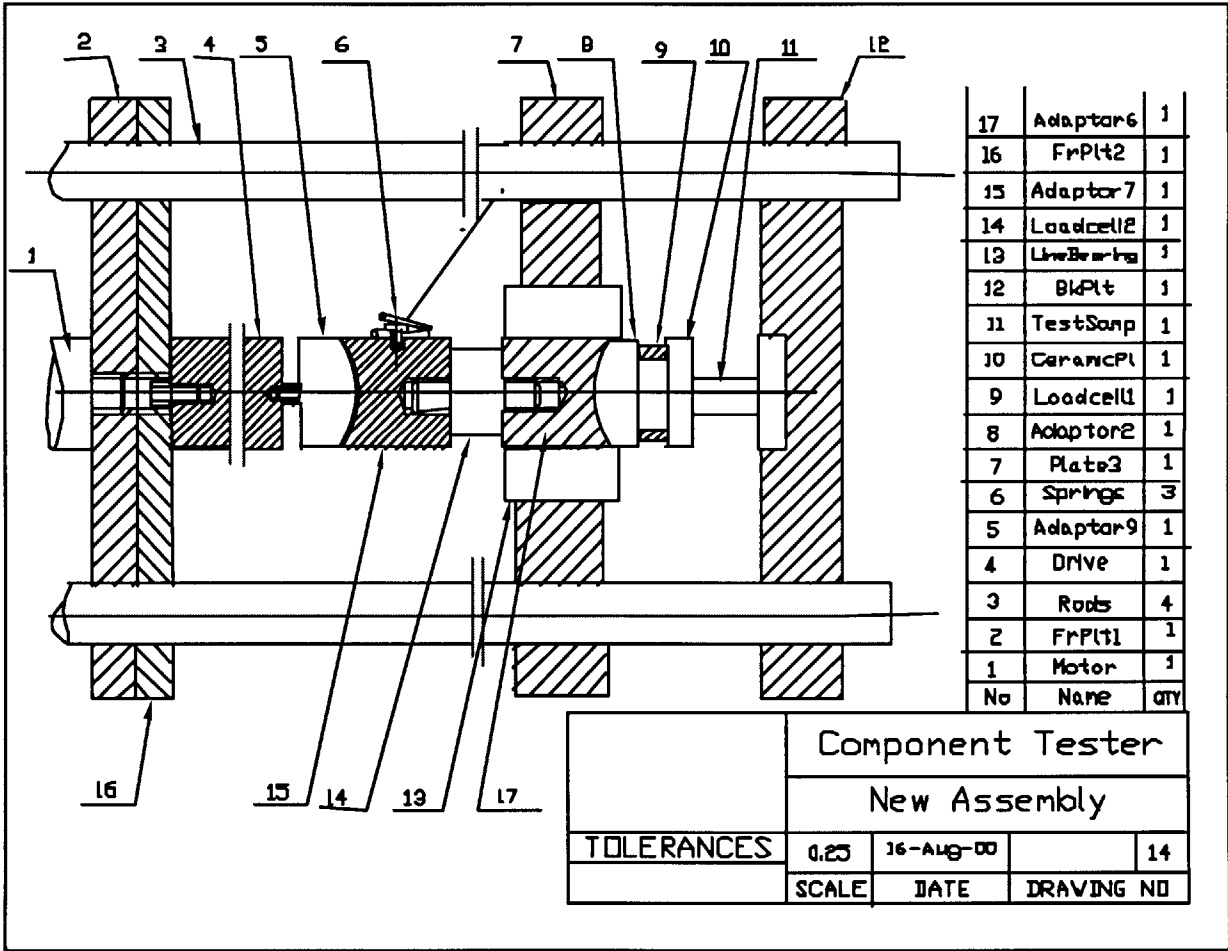
Figure A-1: Assembly Drawing of the Renovated Component Tester

No	Name	QTY
17	Adaptor6	1
16	FrPlt2	1
15	Adaptor7	1
14	Loadcell2	1
13	LinBearing	1
12	BkPlt	1
11	TestSamp	1
10	CeramicPl	1
9	Loadcell1	1
8	Adaptor2	1
7	Plate3	1
6	Springs	3
5	Adaptor9	1
4	Drive	1
3	Rods	4
2	FrPlt1	1
1	Motor	1

Component Tester

New Assembly

TOLERANCES	0.25	16-Aug-00		14
	SCALE	DATE	DRAVING NO	

124

4-40, 3 holes eql
sp on Ø1.25

SRl.50
Note

0.5

Ø 1.0

Note. Spherical surface should
mate with the spherical surface
of adaptor2 Drn. No2

	Component Tester			
	Adaptor2			
TOLERANCES	0.75	12-Aug-00		2
Steel	SCALE	DATE	DRAWING NO	

Figure A-2: Adaptor 2 Drawing

125
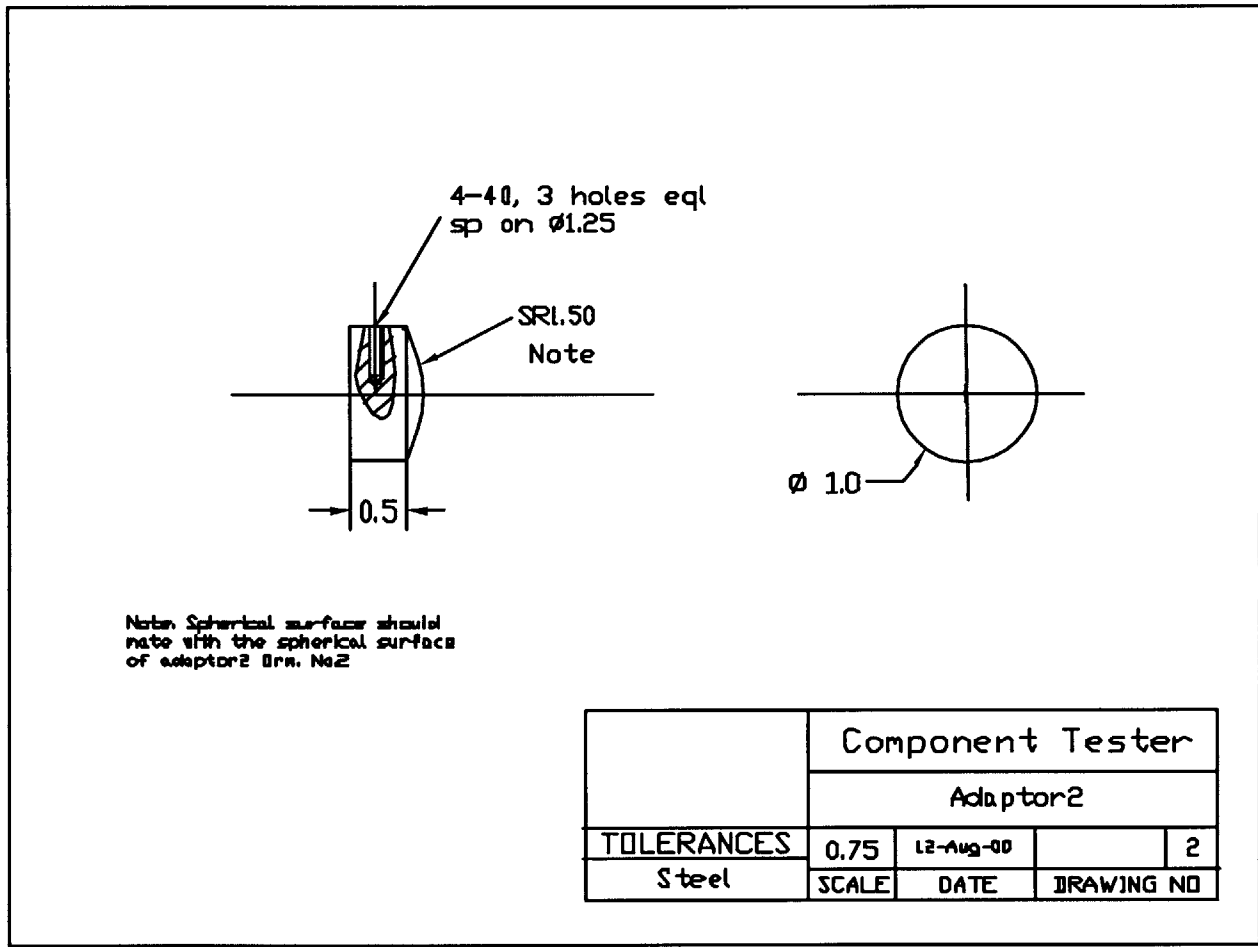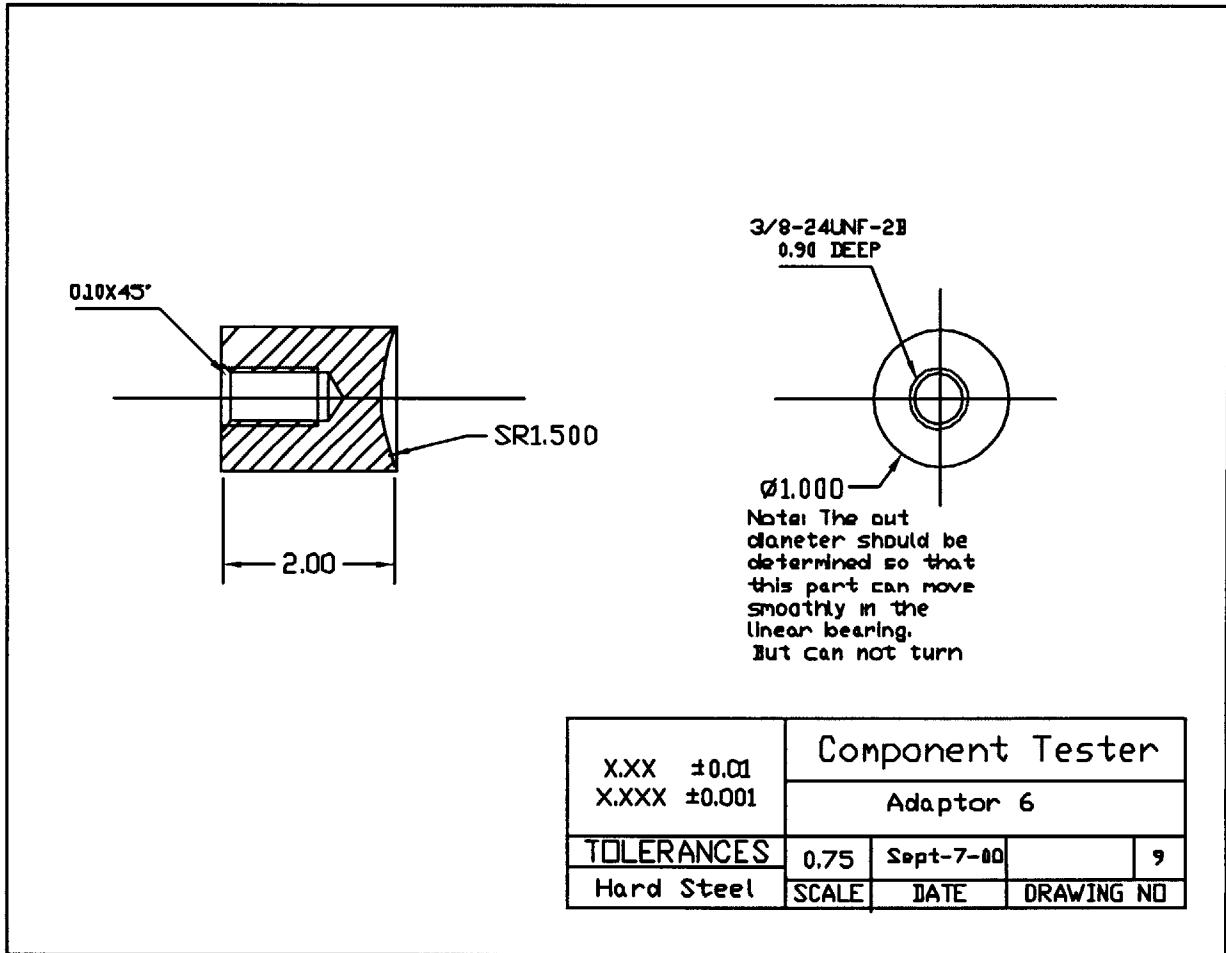
Figure A-3: Adaptor 6 Drawing

126

0.10X45°

SR1.500

2.00

3/8-24UNF-2B
0.90 DEEP

Ø1.000

Note: The out
diameter should be
determined so that
this part can move
smoothly in the
linear bearing.
But can not turn

X.XX ±0.01 X.XXX ±0.001	Component Tester		
	Adaptor 6		
TOLERANCES	0.75	Sept-7-00	9
Hard Steel	SCALE	DATE	DRAWING NO
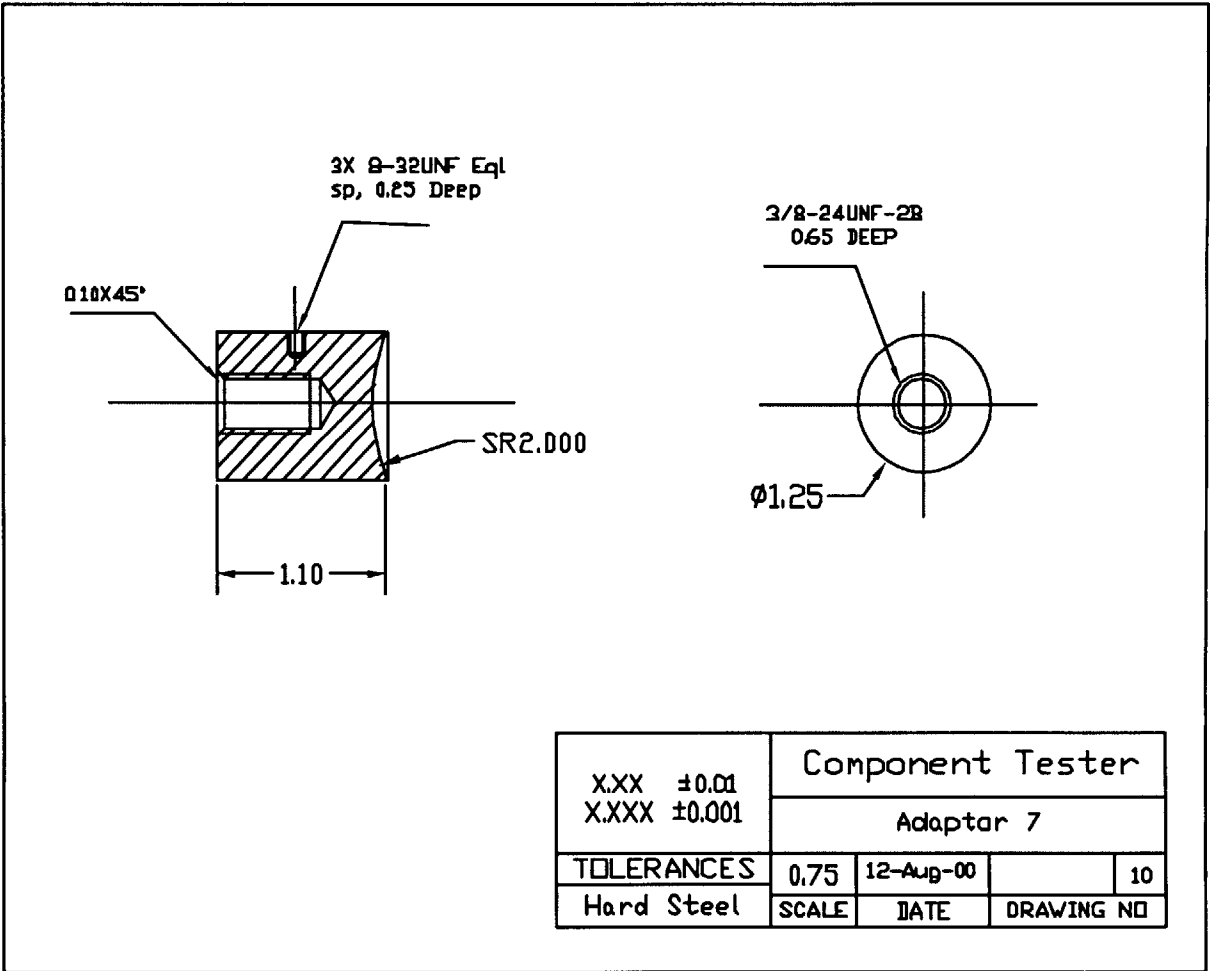
Figure A-4: Adaptor 7 Drawing

127

3X 8-32UNF Eql
sp, 0.25 Deep

0.10X45°

SR2.000

1.10

3/8-24UNF-2B
0.65 DEEP

Ø1.25

X.XX ±0.01 X.XXX ±0.001	Component Tester		
	Adaptor 7		
TOLERANCES	0.75	12-Aug-00	10
Hard Steel	SCALE	DATE	DRAWING NO

Figure A-5: Adaptor 9 Drawing

128

0.31

SR2.00

M6

0.05x45°

0.5

0.05xØ0.2

Ø1.25

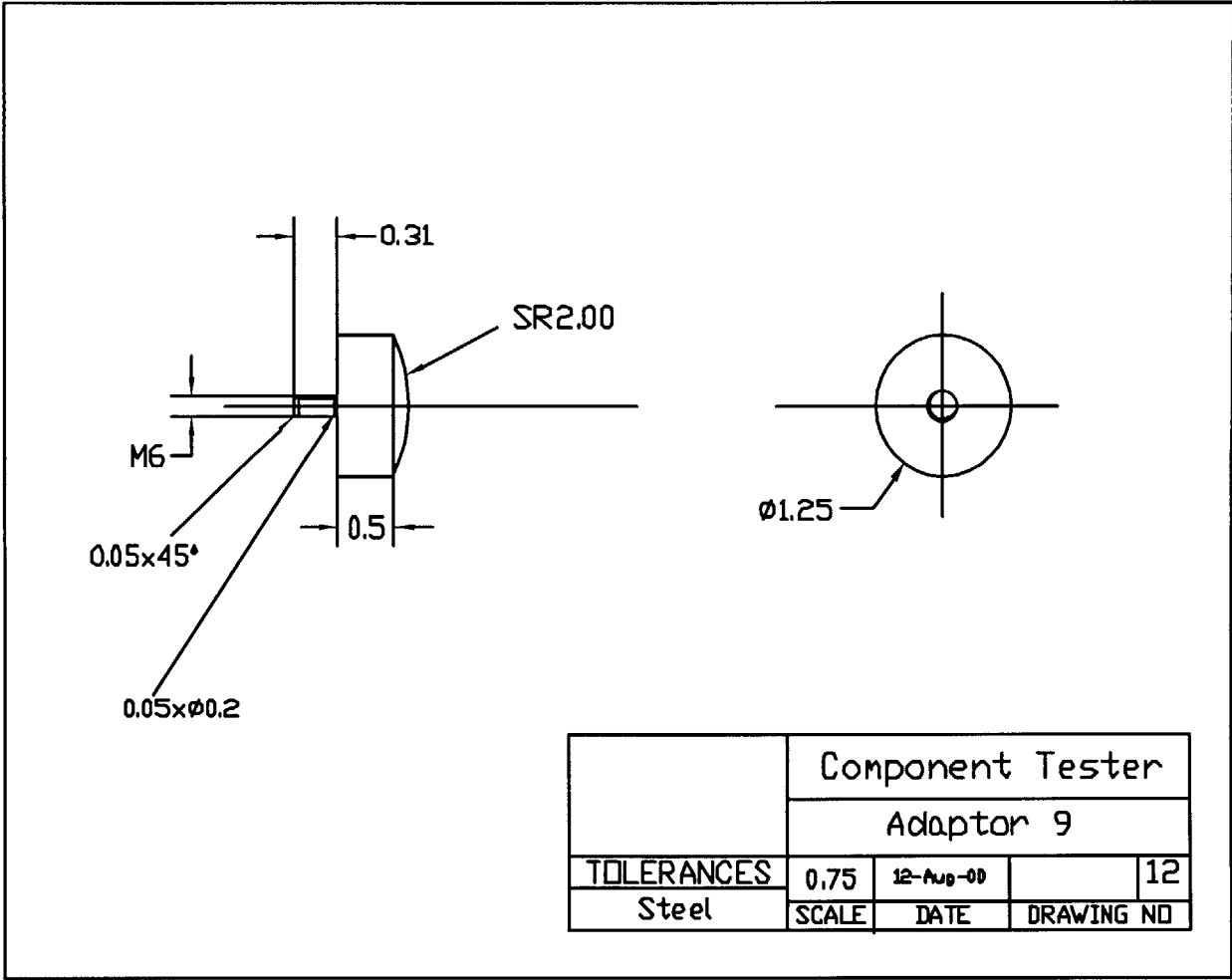|	Component Tester		
	Adaptor 9		
TOLERANCES	0.75	12-Aug-00	12
Steel	SCALE	DATE	DRAWING NO
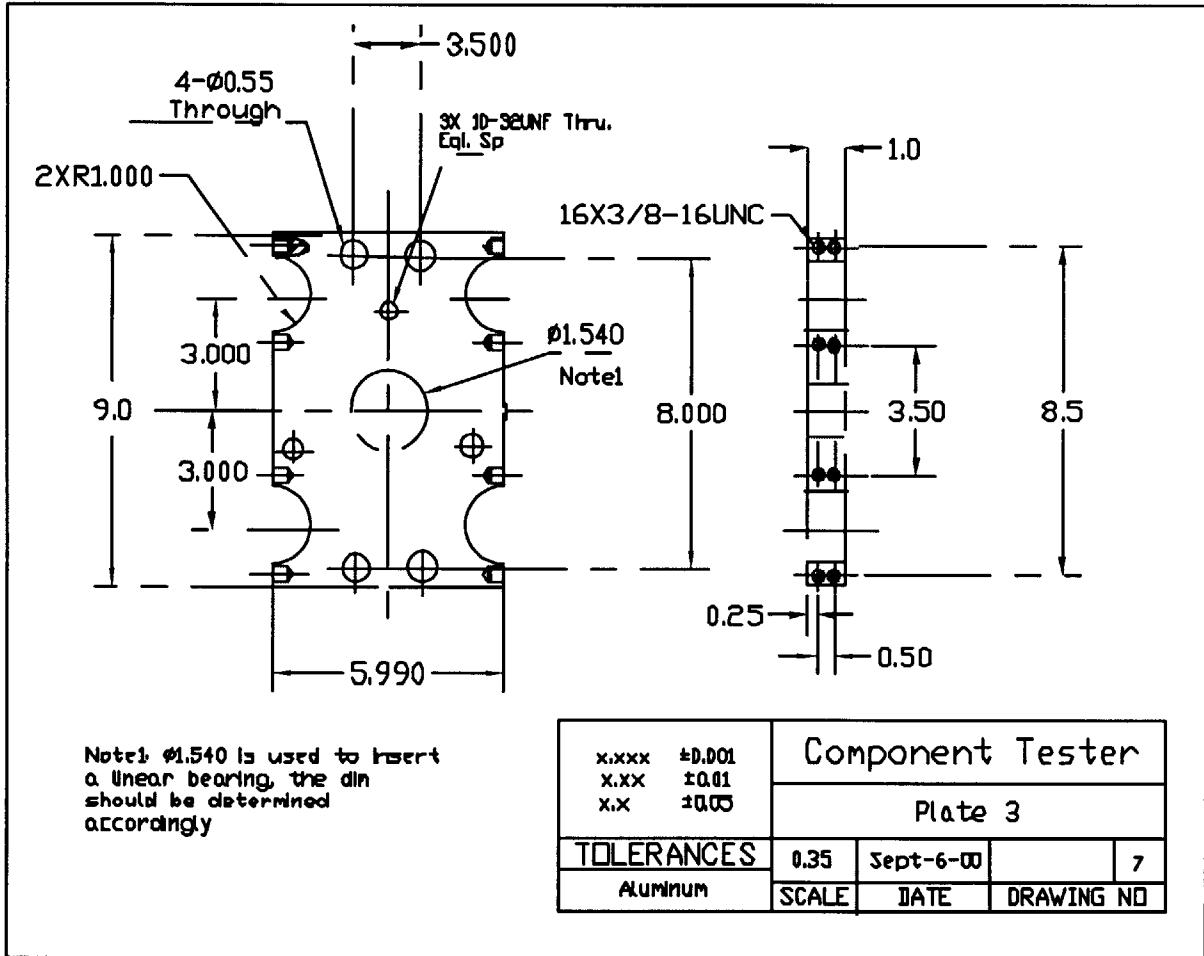
Figure A-6: Linear Bearing Mounting Plate Drwaing

129
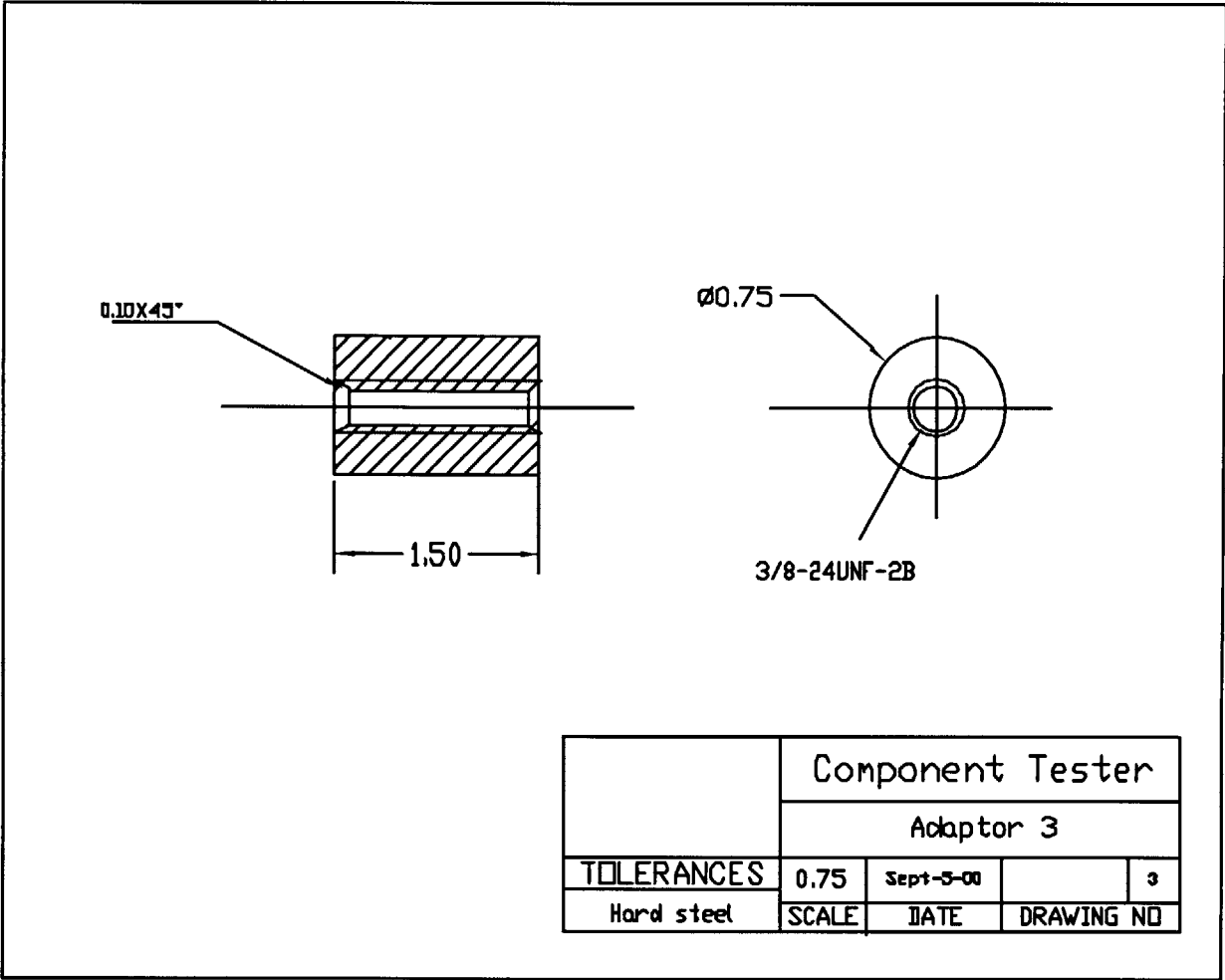
Figure A-7: Adaptor 3 Drawing

130

0.10X45°

1.50

Ø0.75

3/8-24UNF-2B

	Component Tester		
	Adaptor 3		
TOLERANCES	0.75	Sept-5-00		3
Hard steel	SCALE	DATE	DRAWING NO
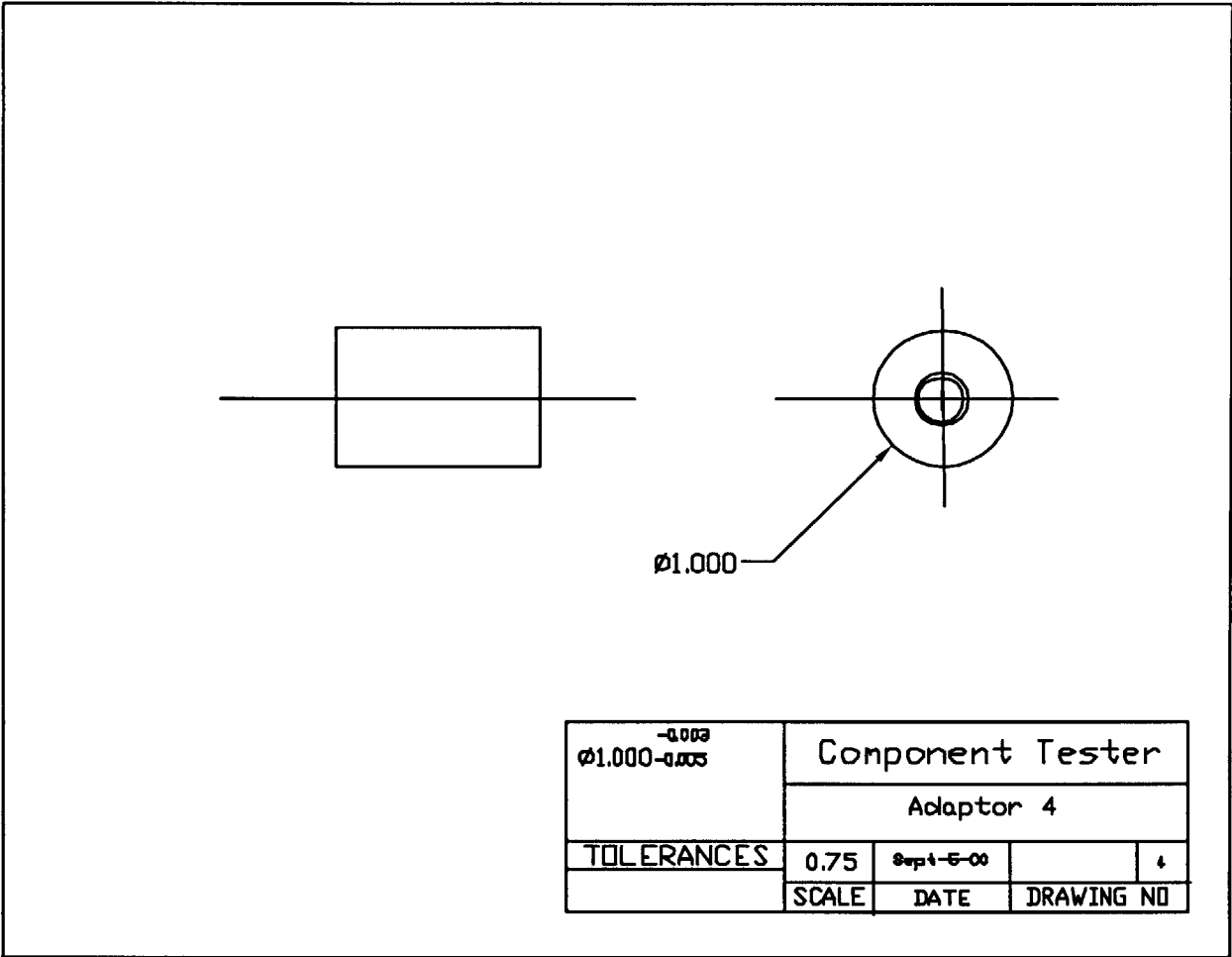
Figure A-8: Adaptor 4 Drawing

131

$\emptyset 1.000$

$\emptyset 1.000^{-0.003}_{-0.005}$	Conponent Tester		
	Adaptor 4		
TOLERANCES	0.75	Sept-5-00	4
	SCALE	DATE	DRAWING NO

Figure A-9: Adaptor 5 Drawing

132

10-32UNF
0.25 Deep

SR2.000

1.00

Ø1.25

	Component Tester		
X.XX ±0.01 X.XXX ±0.001	Adaptor 5		
TOLERANCES	0.75	Sept-7-00		0
Hard Steel	SCALE	DATE	DRAWING NO